Canadian Technical Report of

Hydrography and Ocean Sciences No. 91

September 1987

DYNAMIC MODELLING OF ICEBERG DRIFT USING CURRENT PROFILES

by

Stuart D. Smith[1] and Norman R. Donaldson[1,2]

1 Physical and Chemical Sciences Branch
Scotia-Fundy Region
Department of Fisheries and Oceans,
Bedford Institute of Oceanography,
P.O. Box 1006,
Dartmouth, N.S. B2Y 4A2

2 Now at: Atmospheric Environment Service
Department of the Environment,
4905 Dufferin Street,
Downsview, Ontario M3H 5T4

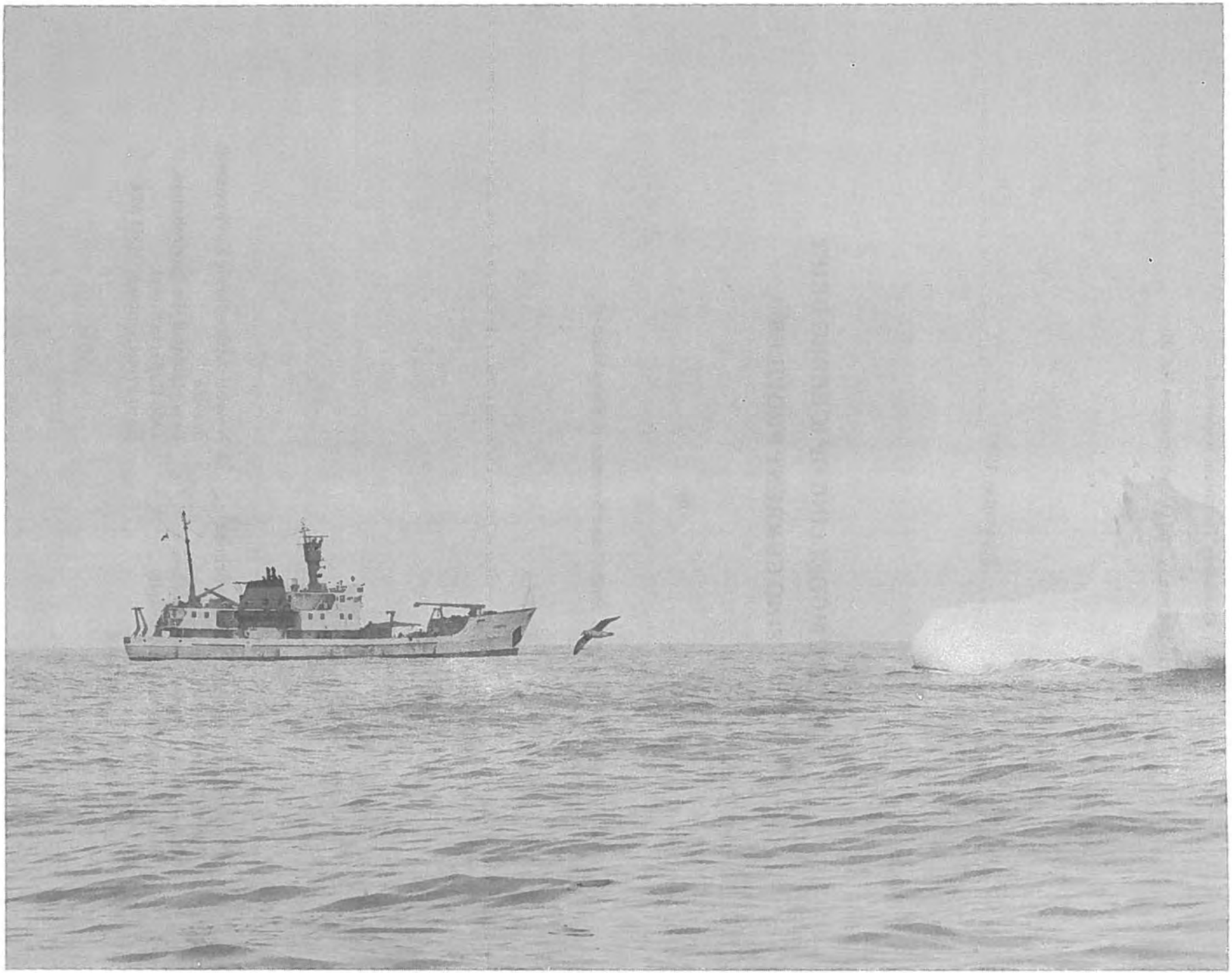

Frontispiece. C.S.S. Dawson tracking Iceberg 85-4 (Photograph by D. Diemand, Memorial University).

ACKNOWLEDGEMENTS

Captains J. Mein, J. Lewis and R. Dickinson and the crew of CSS Dawson made possible the success of the three iceberg tracking cruises. The Doppler current profiler application was developed by N.A. Cochrane and J.W.E. Whitman. The authors thank Leslie Mantin of Evans Computer Applications for carrying out the computer analysis reported here. This project was funded by the Programme on Energy Research and Development, Department of Energy, Mines and Resources.

Cat. No. FS 97-18/91E ISSN 0711-6764

Correct citation for this publication:

Smith, S.D. and Donaldson, N.R., 1987 Dynamic modelling of iceberg drift using current profiles. Can. Tech. Rep. Hydrogr. Ocean Sci. No. 91: viii + 125 p.

ABSTRACT

Smith, S.D. and Donaldson, N.R., 1987. Dynamic Modelling of Iceberg Drift using Current Profiles. Can. Tech. Rep. Hydrogr. Ocean Science No. 91: viii + 125 p.

Dynamic models of iceberg drift tracks require as input the currents and winds which drive the iceberg motion, but in the past it has not been possible to obtain adequate data on currents. Three cruises of CSS Dawson have collected data for the testing and development of a dynamic iceberg drift model, with current profiles continuously monitored by a hull-mounted acoustic Doppler current profiler, usually within 1 to 2 km range of an iceberg. Winds were measured by a propellor anemometer on a bow mast. The iceberg tracks were logged by radar ranges and bearings, while the ship was positioned by LORAN C. Sonar profiles and photographs were analyzed to estimate the mass and the cross-sectional areas in air and in water.

The 12 track segments of 7 icebergs reported have been compiled at 10 min intervals for periods of 12 hours to 3 days. A dynamic model with quadratic air and water drag, Coriolis, and pressure gradient forces reproduces the tracks of nearby icebergs (mean range < 10 km) with an average rms position error of only 5% of the distance travelled. Errors are larger for more distant icebergs where the measured currents are less representative. A kinematic model which represented the drift velocity as a sum of multiples of the current and wind achieved similar accuracy.

RÉSUMÉ

Smith, S.D. and Donaldson, N.R., 1987. Dynamic Modelling of Iceberg Drift using Current Profiles. Can. Tech. Rep. Hydrogr. Ocean Science No. 91: viii + 125 p.

Les modèles dynamiques de trajectoires de dérive d'icebergs exigent comme données d'entrée les courants et les vents qui causent le déplacement des icebergs, mais par les passé il a été impossible d'obtenir des données convenables sur les courants. Lors de trois croisières du CSS Dawson on a recueilli des données pour la mise à l'épreuve et le perfectionnement d'un modèle dynamique de la dérive des icebergs; des profils du courant étaient surveillés de manière ininterrompue au moyen d'un profileur Doppler de courant installé sur la coque du navire, et ce habituellement à une distance de moins de 1 à 2 km d'un iceberg. Les vents étaient mesurés au moyen d'un anémomètre à hélice sur un mât à l'avant. Les trajectoires des icebergs étaient enregistrées d'après des relèvements et des distances obtenus au moyen du radar, tandis que le navire était positionné à l'aide du LORAN C. Des profils obtenus au sonar et des photographies ont été analysés afin d'estimer la masse et les superficies en coupe transversale dans l'air et dans l'eau des icebergs.

Les 12 trajectoires de 7 icebergs signalées ont été compilées à des intervalles de 10 minutes pour des périodes variant de 12 heures à 3 jours. Un modèle dynamique basé sur des traînées aéro et hydrodynamiques quadratiques, sur la force de Coriolis et sur les gradients de pression reproduit les trajectoires d'icebergs à proximité (distance moyenne < 10 km) avec une erreur quadratique moyenne de position de seulement 5% de la distance parcourrue. Les erreurs sont plus importantes pour des icebergs plus éloignés puisque les courants mesurés sont alors moins représentatifs. Un modèle cinématique représentant la vitesse de dérive sous forme d'une somme de multiples du courant et du vent donnait une précision analogue.

TABLE OF CONTENTS

TABLES

FIGURES

A. INTRODUCTION

In the proposed development of petroleum resources off the east coast of Canada, the presence of icebergs is the one environmental factor which has not been encountered in other production regions. In managing an iceberg hazard, either by towing the iceberg or by shutting down operations and moving a drilling rig or other facility, it is important to know the probability that the iceberg will collide with and damage the facility, or will drift harmlessly away. Even if iceberg-resistant production platforms are installed, plans call for towing icebergs to minimize the number of impacts.

A number of models have been developed in an attempt to forecast or hindcast iceberg drift tracks. Dynamic models (e.g. Mountain, 1980; Smith and Banke, 1983; Banke and Smith, 1984; Sodhi and El-Tahan, 1980) evaluate the various forces acting on an iceberg and integrate acceler-ation twice to obtain velocity and position as a function of time. In general, these models depend on a detailed specification of the winds and currents, of iceberg mass and cross-sectional area, and on a representation of how these influence the drift. In most studies to date, major deficiencies in the available data (particularly in the currents) have prevented meaningful evaluation of the models themselves.

Statistical models (e.g. Garrett, 1984, 1985, Garrett *et al.*, 1985a,b, Gaskill and Rochester, 1984) use the last known positions, together with statistical properties of previous trajectories, to estimate a probability distribution of the iceberg's position and velocity as a function of time. This has the advantage of quantifying the effects of uncertain ties. Some of these models incorporate deterministic effects by the direct use of environmental information such as tides and winds. However, if the drift rate is small compared to the uncertainties, the error limits may become ever larger circles surrounding the initial position. Lack of knowledge of the currents and other factors still leads to uncertainty in forecasting the paths of icebergs. Improvements in the knowledge of iceberg dynamics and in the forecasting of ocean currents may allow an improvement in the performance of combined models by allowing the user to transfer some phenomena from the probabilistic to the deterministic portion of the model.

Models which represent the drift track by empirical relationships with other phenomena can be referred to as kinematic models. A simple example is the common knowledge that icebergs drift relative to the current at about 2% of the wind speed. Gaskill and Rochester (1984) and Garrett *et al.* (1985a,b) use this kinematic model to infer currents from observed drift rates. Kinematic aspects can be added to statistical models, as mentioned above, or to dynamic models. In our model we shall select air and water drag coefficients which optimize the fit of the dynamically modelled drift track to the observed track. We will

test this kinematic criterion as an alternative to arbitrarily selecting values for the drag coefficients. A brief overview of the present work is given by Smith and Donaldson (1987).

B. A DYNAMIC MODEL OF ICEBERG DRIFT

An iceberg is assumed to drift under the influence of the vector sum of air drag F_a and water drag F_w, pressure gradient force F_p in the water, Coriolis, and possibly towing force F_T. With these forces, the equation of motion in the rotating coordinates of the earth is

$$M(a+f\times V)=F_a+F_w+F_p+F_T \tag{1}$$

where M is the iceberg's mass, a its acceleration, and V its velocity. Our model simulates each of the terms in Equation 1 based on available data.

The Coriolis parameter $f=2\Omega \sin\phi$ is directed vertically upward, where Ω is the earth's rate of rotation and ϕ the latitude. We do not specifically include forces exerted by surface waves, which in stormy conditions can become comparable to the wind drag. If the waves travel in the same direction as the wind an increase in the wind drag coefficient could in effect compensate for the missing wave forces.

1. Wind drag

The wind drag is taken to be proportional to the square of the relative wind velocity, u=U-V, where U and V are the wind and iceberg velocity vectors,

$$F_a=\frac{1}{2}\rho_a C_A A_a |u|u \tag{2}$$

where A_a is the cross-sectional area of the iceberg above the waterline in a vertical plane normal to the wind, ρ_a is the density of air. The air drag coefficient C_A is typically about 1 for irregularly shaped objects at high Reynolds numbers. In the applications to follow we will try both an arbitrarily selected value $C_A=1.0$ and an "optimized" value selected to best fit the modelled track to the observed track of a particular iceberg. We also allow the possibility of arbitrarily rotating the wind force by a fixed angle in the belief that icebergs with "fin" or "sail" shapes above the waterline may produce a component of "lift" perpendicular to the wind direction. Wind direction typically is constant within 10° over the height of an iceberg. Winds were measured at a height of 13 m above the water, and we have not allowed for variation of wind speed with height. Typical wind profiles vary from 20% less at 2 m to 10% more at 40 m, as compared to winds at the height of measurements..

2. Water drag

The water drag force F_w is modelled in the same way as the wind drag, but the iceberg's underwater area is subdivided into a number of depth layers. For each layer i we

take the water velocity relative to the iceberg, $w_i = W_i - V$, and again use a quadratic drag law. Summing over the layers, the total drag force is

$$F_w = \frac{1}{2} \rho C_W \left[\sum_i A_i |w_i| w_i \right] \tag{3}$$

where ρ is the density of water and A_i is the cross-sectional area in a vertical plane of the i^{th} layer below the waterline. In the applications to follow we shall again try both an arbitrarily selected value $C_w = 1.0$ and an "optimized" value selected to best fit the modelled track to the observed track of a particular iceberg. We will not attempt to model variability of C_w with depth, although such variability may in fact exist.

3. *Coriolis and pressure forces*

Coriolis acceleration is the influence of the earth's rotation on a moving object. In the rotating coordinates of the earth's surface, and in the absence of applied forces, a moving object accelerates to the right (in the northern hemisphere) of its velocity,

$$A_c = -f \times V \tag{4}$$

as in the left-hand side of Eq. 1. The motion of water parcels is also governed by Coriolis acceleration and pressure gradient in the water. The equation of motion for the water moving with a velocity v_W and having an acceleration a_W may thus be written as,

$$a_w - f \times v_w = -\frac{1}{\rho} \nabla p \tag{5}$$

The pressure force F_p exerted on a fixed volume - i.e. an iceberg - is a surface integral which may according to Green's Theorem be written as a volume integral,

$$F_p = \int \int_A p \, dA = - \int \int \int_{Vol} \nabla p \, dx \, dy \, dz \tag{6}$$

Assuming that the pressure gradient ∇p is uniform horizontally in the neighbourhood of the iceberg, and replacing the vertical integration by a sum over a series of layers of volume B_i,

$$F_p = \sum_i \nabla p_i B_i \tag{7}$$

Taking Eq. 5 to apply to each layer, the pressure force may be estimated from the measured current profile and its acceleration.

$$F_p = \rho_w \sum (a_{wi} + f \times W_i) \tag{8}$$

For computational simplicity we define a volume-averaged current

$$W = \sum_i B_i W_i / \sum_i B_i \simeq \sum_i A_i^2 W_i / \sum_i A_i^2 \tag{9}$$

(The volume of each layer will be assumed to be proportional to the square of its measured cross-sectional area A_i in a vertical plane, since we will not have direct measurements of underwater volume B_i nor of cross-sectional area in a horizontal plane.) The sum of the

Coriolis and pressure forces is

$$F_p - Mf \times V = M[f \times (W - V) + dW/dt] \tag{10}$$

This differs from Smith and Banke's (1983) model, which did not include the last term is Eq. 10, i.e. the water column acceleration, but in practice the influence of this term is found to be very small. An intuitive understanding of this term is that pressure forces influence the iceberg in the same way that they would influence the water mass which it displaces; therefore in the absence of other applied forces the iceberg would accelerate in the same way as the water column.

4. Towing force

To simulate the effect of towing an iceberg, an arbitrary force F_T can be added in Eq. 1. Simulation of towing is relatively simple in a dynamic model, provided that the other forces-have been correctly simulated. Modelling the trajectory of a towed iceberg will be the subject of a later report.

5. Integration

At each time step $t_j = t_{j-1} + \Delta t$ the acceleration is calculated using the velocities from the previous time step,

$$a = a_c + a_w + (F_a + F_w + F_t)/M \tag{11}$$

where

$$a_c = f \times (W - V),\ a_w = (W_j - W_{j-1})/\Delta t \tag{12}$$

The velocity and position are then updated,

$$V_j = V_{j-1} + a\Delta t,\ X_j = X_{j-1} + V_j \Delta t \tag{13}$$

In the modelling to be described below, V_0 was set equal to the observed iceberg velocity over the first 20 or 30 minutes of observation. In practice, we have found that the choice of the initial velocity has a negligible influence on the modelled track.

We have normally set the time step $\Delta t = 24$s. Calculations with shorter time steps were found to result in entirely negligible differences in the modelled tracks, while at much longer time steps (e.g. > 100s) computational instabilities and overflows can occur.

The wind vector and the current profile at 10 m depth intervals are specified initially, and thereafter given at arbitrary time intervals. The ship's position and the range and bearing to the iceberg are specified with each observation. Winds and currents at each time step of the integration are linearly interpolated between the previous and following observation; the wind and currents remain at the last observed value. In the present application the data are given at regular 10 min intervals. In a few cases we have replaced missing

or obviously incorrect values with interpolated ones; there is no provision in the model itself to accept incomplete data.

C. DATA COLLECTION AND QUALITY CONTROL

Three cruises of CSS Dawson obtained data for the testing and development of iceberg drift models. Cruise 83-018, from June 21 - July 4, 1983, was in the eastern Strait of Belle Isle and on the southern Labrador shelf. Cruise 84-023 from June 5-20, 1984, obtained data on the inner Grand Banks northeast of St. John's. Cruise 85-008, April 22 - May 6, 1985, tracked icebergs on the outer Grand Banks. In each case the location was determined by the positions of drifting icebergs at the time of the cruise. The Cruise Reports (Smith, 1983, 1984, 1985) give details of the stations, itineraries and equipment deployed. The times and locations of the iceberg tracks are listed in Table 1, and a photograph of each iceberg is in Appendix 1.

1. Iceberg surveys

Each iceberg was surveyed to determine its mass and its cross-sectional areas in air and in 10 m layers below the waterline. The dimensions of the icebergs are listed in Table 2. The height h above the waterline was measured by vertical sextant angles above the horizon at known radar ranges. Four photographs, nominally of the north, south, east and west faces of the iceberg, were scaled with the height above the waterline to calculate the cross-section in air. A modified Klein sidescan sonar was lowered to obtain a profile of the iceberg, with the ship holding station off each of the four faces photographed. (The icebergs rotated slowly, so that the orientation of the faces generally did not remain the same through the two to three hours required to complete a survey.) The profiles were scaled and matched at the waterline to the scaled above-water photographic cross-sections (e.g. east and west profiles with north face) to obtain a cross-sectional view of the iceberg. Two such views were obtained in each survey (Appendix 2; Ice Engineering, 1983, 1984, 1985) and all of the cross-sectional areas for each layer were averaged for input to the drift model (Table 3). The estimated accuracy of determining cross-sectional area above water is $\pm 5\%$, and below water $\pm 10\%$.

The mass of each iceberg was estimated by sculpting a styrofoam model (density ρ_m, height h_m) to match the photographs of the above-water portion. The iceberg mass M was calculated from the model mass M_m assuming the density of iceberg ice to be $\rho_i = 0.899$ tonne /m^3 (density of pure ice 0.917 tonne/m^3, and 2% porosity), and the density of sea water to be $\rho_w = 1.028$ tonne/m^3.

$$M = M_m \left(\frac{\rho_i}{\rho_m} \right) \left(\frac{h}{h_m} \right)^3 \left(\frac{\rho_w}{\rho_w - \rho_i} \right) \tag{14}$$

Table 1. Iceberg tracking and modelling periods.

Iceberg No	Data period Start hour	day	End hour	day	Modelling period Start hour	day	End hour	day	mo	Duration t hours	Origin of plots N Lat. deg	min	W Long. deg	min
83-1	0500	24	1910	24	0600	24	1700	24	6	11.0	51	42	56	04
83-2	0430	25	0600	28	0430	25	0550	28	6	73.3	51	55	55	10
83-3	0450	29	2050	01	0450	29	2050	01	7	64.0	51	52	54	52
83-5	0450	29	1130	01	0450	29	0450	30	6	54.7	51	49	54	54
84-5D	0130	14	1230	14	0130	14	1230	14	6	11.0	48	15	52	12
E	1450	14	0750	17	1450	14	0750	17	6	65.0	48	00	52	30
F	2300	17	0650	19	2300	17	0650	19	6	31.8	47	58	52	20
84-6E	1450	14	0750	17	1450	14	1500	16	6	24.0	48	00	52	30
F	1330	17	0650	19	1330	17	0650	19	6	41.3	47	55.5	52	19
84-7D	0130	14	1230	14	0130	14	1230	14	6	11.0	48	20	52	15
E	1820	14	0750	17	1820	14	0750	17	6	61.5	48	03	52	30
F	1330	17	0650	19	1330	17	0650	19	6	41.3	48	04	52	21
85-1	1900	27	0700	30					4	60.0				
85-4	0100	03	0100	04					5	24.0				

The accuracy of mass estimates is ±10%, based on duplicate surveys of three icebergs. In each case the estimated mass decreased in time, which is compatible with melting and ablation, but we are not confident that mass differences are resolved.

2. Current profiles

The greatest impediment to the testing and application of iceberg drift models has been a lack of current data in the immediate vicinity of icebergs. The acoustic Doppler current profiler has made it possible to continuously monitor the current profile from a moving ship. An Ametek Straza model DCP 4400/300 current profiler with a hull-mounted 300 kHz four-beam transducer was installed on CSS Dawson. Four diagonal acoustic beams were transmitted simultaneously at 3.6 s intervals. Backscattered signals from impurities in the water were gated in time to create successive depth "bins" of 3.2 m, starting at 9 m. The Doppler shifts between fore and aft beams, and between port and starboard, were converted to orthogonal components of current relative to the ship in each depth bin, and resolved into north and east components using a signal from the ship's gyrocompass. The ship's velocity relative to the seabed was deduced from the Doppler shift of bottom echoes and was used to compute current profiles relative to the seabed. Ten minute averages were computed using approximately 166 pings of profile data. The rms noise level in this mode is expected to be 1 cm/s and tests of integrated bottom velocity against Loran navigation showed the calibration to be between 0 and 2% high (Cochrane, 1985).

Just before Cruise 85-008 a more powerful model DCP 4400A/300 profiler was installed, approximately doubling the profiling range (from 100 to 200 m), the bottom tracking range (from 200 to 400 m), and the capability to compensate for ship motion (from 6 to 14 knots) (Smith, 1985).

No profile data are obtained at depths shallower than about 7 to 9 m, a deficiency which is inherent in the transducer location and in the need to distinguish backscattered echoes near the surface from surface echoes. During Cruise 84-023 a failure of the system resulted in a lack of data for depths shallower than 27 m, and we have in these cases assumed that the current at 27 m extended up to the surface.

The current profiles were reliable when the ship was drifting or steaming at low speed, but during manoeuvering bubbles under the hull contaminated the signal, particularly during iceberg surveys. Time series of the calculated currents were examined and compared to plots of the ship's speed and track. Typically a period of bad data contains large erratic jumps in the current at one or more depths. Dubious profiles for periods of up to one hour were replaced by interpolated values. Time series plots of depth-averaged currents after these corrections are reproduced in Appendix 3, and currents are listed in the input data files (Appendix 8).

Table 2. Iceberg dimensions

Iceberg	Date	Shape	N Lat.	W Long.	Height m	Length m	Width m	Draft m	Mass kilotonnes
83-1	June 24	Pinnacle	51°46'	55°55'	19	66	37	54	85
83-2	June 25	Drydock	52°08'	55°01'	32	146	86	96	800
	June 27	Drydock	52°01'	55°06'	33	137	86	83	860
83-3	June 29	Domed	52°00'	54°48'	25	129	71	84	620
	July 1	Domed	52°00'	54°39'	27	99	67	89	530
83-5	June 30	Drydock	52°00'	54°40'	20	77	56	67	147
84-5	June 14	Drydock	48°16'	52°08'	43	198	181	120	2100
	June 17	Drydock	48°02'	52°20'	44	204	136	110	1700
84-6	June 17	Domed	48°01'	52°11'	19	90	70	70	320
	June 18	Domed	48°05'	52°00'	20	86	73	75	270
84-7	June 17	Domed	48°09'	52°17'	32	178	137	110	1700
85-1	Apr 28	Blocky	48°00'	49°07'	23	118	92	110	570
85-4	May 3	Drydock	46°00'	48°16'	16	61	41	40	33

Table 3. Mean vertical cross-sectional areas of icebergs, m^2.

Iceberg	Above water	0-10m	10-20m	20-30m	30-40m	40-50m	50-60m	60-70m	70-80m	80-90m	>90
83-1	445	546	500	427	403	348	51	-	-	-	-
83-2	2578	1477	1760	1848	1848	1775	1602	1333	963	369	73
83-3	1709	1074	1198	1220	1219	1196	1112	915	572	146	-
83-5	624	565	633	650	521	363	299	121	-	-	-
84-5	4147	1736	1924	2059	2235	2278	2247	2177	2072	1860	2395
84-6	1112	826	895	940	960	974	944	702	77	-	-
84-7	4055	1893	2117	2185	2203	2225	2160	2064	1860	1577	2242
85-1	1820	1025	1067	1084	1118	1146	1149	1104	991	798	851
85-4	387	595	594	449	299	-	-	-	-	-	-

3. Winds

A propeller anemometer was mounted at a height of 13 m above the water on a mast on the bow of CSS Dawson. For winds blowing on the bow $\pm 45°$, as was generally the case during iceberg tracking periods, this location is believed to be relatively free of flow distortion. (Errors of -50% to + 35% in wind speed as indicated by the ship's bridge-mounted anemometer, depending on wind direction were reported by Elliott, 1981.)

Wind speed and direction relative to the ship were logged continuously to a strip chart recorder, and were read at 10 min intervals. True wind directions were obtained by adding the ship's heading to the measured relative direction. No attempt was made to correct the winds for the ship's velocity, since the vector mean was the same as the vector mean iceberg velocity during the tracking periods. Time series of wind vectors were plotted and suspicious values (e.g. due to errors in direction when the ship was turning, or to human errors in reading the data) were replaced and occasional gaps were filled, both by interpolation.

Time series plots of wind speed and direction after editing are shown in Appendix 3. During cruise 85-008 there was a period from 000Z to 1120Z on April 28, when low winds and freezing mist led to ice buildup on the Gill anemometer. The propellor seems to have remained free but the ice fixed the anemometer direction at a bearing of -45° relative to the ship. For this period wind direction was taken from the ship's anemometer. The measured wind speeds from the bow were adjust ed by dividing the measured values by the cosine of the angle between the anemometer axis and the wind. Bowen and Teunissen (1986) show that the Gill anemometer does not quite follow a cosine response in direction, but we do not believe that a more complicated correction is justified.

4. Navigation

The ship's position during iceberg tracking periods was fixed by LORAN C and logged at intervals of two minutes. During Cruise 83-018 we were out of range of regular LORAN C chains in service at the time, but were able to use cross-chain fixing with Caribou and Cape Race of the Canadian East Coast chain, and Cape Race and Angissoq, Greenland, of the North Atlantic chain. By 1984 a new chain 7930 (Caribou-Cape Race-Angissoq) had been established but a problem remained with occasional loss of signal from the most distant station, Angissoq, resulting in jumps in the computed position. In addition, the fixing geometry is only marginally acceptable on the southern Grand Banks. Since our principal concern is iceberg drift, a small offset in absolute position is of no concern. By listing and plotting the ship's position and velocity we have been able to identify abnormally high velocities and edit the LORAN C time delays to remove the jumps. Although only a few corrections were needed,

considerable time was required to check and edit out the jumps, which were found to be an integer number of cycles (i.e. multiples of 10μs). A computer program was written to remove these jumps, and the corrected LORAN C data were used to calculate the ship's position. Ship positions at 10 minute observation times for use in our drift model were produced by linear interpolation between the immediately preceding and following LORAN C fixes. The edited ship's tracks during iceberg tracking periods are plotted in Appendix 4 as dotted lines.

5. *Radar range and bearing*

CSS Dawson is equipped with Decca 1230 S-Band and Decca 1229 X-Band marine radars, which required no special preparation beyond their regular maintenance and calibration. During iceberg tracking periods a member of the scientific party logged range and bearing to the icebergs at 10 minute intervals, usually using the S-band radar. When large icebergs were at short range (<1 km) the radar image resembled a plan view, and the centre of the image was tracked, often using the X-Band radar in these cases. The ship's heading was also logged at 10 minute intervals, for wind correction.

To quality check the radar range and bearing data, it was combined with ship's position to obtain iceberg position as a function of time. This series was differentiated and time series plots were made of the magnitude of the measured iceberg velocity. All values above 1 m/s were considered excessive and the data producing them were examined for errors. Apart from copying errors, errors in the berg positions were most frequently found to be due to a lack of synchronization of the hand-logged radar data and the computer-logged LORAN C data during periods when the ship was steaming. Further, as the ship-to-iceberg range increased there was an increase in position error, with the 1° resolution in bearing corresponding to a spatial resolution of tens or even hundreds of metres. Missing and suspect ranges and bearings were replaced by interpolating the berg position, and using this with the ship's position to produce new ranges and bearings. The iceberg velocities after editing are plotted as time series in Appendix 3, and the iceberg tracks are plotted as solid lines in Appendix 4. Table 4 summar izes the lengths of the tracks and the net distances travelled.

There remains in the data a low level of residual error due to experimental uncertainty in the LORAN C positions and the radar ranges and bearings. This is seen as small zig-zags in the track plots (Appendix 4), and is particularly noticeable where the radar ranges were relatively long. This accounts for a fair portion (4 to 45%) of the distance travelled, as compared to the distance travelled if the tracks are smoothed by a 3-point (30-minute) running mean (Table 4). The residual error is responsible for a similar proportion of the variance of the iceberg velocity calculated from differences in 10-minute positions and is seen typically as ± 0.2 m/s fluctuations in iceberg velocity (Appendix 3).

6. Other data

CTD casts were taken at approximately 4 hour intervals during iceberg tracking periods of all three cruises. While these data are not used in the model presented here, the thermal and density structure may be required in other applications of the data. Appendix 5 gives a typical profile for each of the icebergs tracked.

A current meter mooring was installed in the Strait of Belle Isle during Cruise 83-018 and a qualitative comparison with the Doppler current profiler was made through one tidal cycle (Cochrane, 1985). A mooring was placed on the Grand Banks during Cruise 84-023, and brief intercomparisons were made at the beginning and end of the cruise. The moorings were not close enough to any of the iceberg tracks for direct use in drift modelling. Both the CTD and the current meter data are available through the physical oceanography data archives of the Bedford Institute of Oceanography. During each of the cruises several other projects not directly related to iceberg drift modelling were also carried out, as described in the Cruise Reports (Smith, 1983, 1984, 1985).

D. DISCUSSION OF ICEBERG TRACKS

In this chapter each iceberg track and its associated data will be discussed in a qualitative sense and some statistical analyses will be presented. The following chapter will give the results of modelling these iceberg tracks.

Table 1 above shows the locations, tracking periods, and modelling periods of the icebergs studied, Table 2 gives the dimensions of the icebergs and Table 3 lists cross-sectional areas in air and in 10 m depth layers in the water derived from the cross-sections in Appendix 2. Table 4 shows the lengths of these tracks during the modelling periods. Throughout this chapter we will refer to time-series plots of iceberg drift speed and direction, winds, depth-averaged currents, radar range, and ship speed (Appendix 3), and to the iceberg track plots (Appendix 4). Table 5 gives the averaged current speed, wind speeds and radar ranges for each modelling period; progressive current vectors for each 10 m depth layer are plotted in Appendix 6. Finally, data files containing input information for dynamic iceberg drift model are listed in Appendix 8. The times in these listings start with the time (UT) during the first day, and the hours increase monotonically through the tracking period; thus the second day begins at hour 2400 and ends at 4750, the third day begins at 4800, etc.

The environmental data were collected from a ship following a nearby iceberg. The current data may be regarded as quasi-Lagrangian, in that the icebergs often tended to follow the depth-averaged currents. It would not be possible to collect truly Lagrangian current data from a ship for all layers, since the water in each depth layer follows a different trajectory.

Table 4. Lengths of tracks.

Iceberg	ℓ (km)	L_s(km)	t(hr)	D(km)	A(deg)
83-1	15.04	14.43	11.0	12.6	100
83-2	52.82	45.51	73.3	19.6	210
83-3	46.62	36.24	64.0	15.1	078
83-5	21.96	17.22	24.0	11.1	097
84-5D	6.92	5.77	11.0	0.4	057
84-5E	57.18	50.82	65.0	29.9	210
84-5F	37.43	29.06	31.8	20.6	049
84-6E	50.31	36.65	48.2	11.9	229
84-6F	27.92	24.97	41.3	20.8	058
84-7D	9.32	7.46	11.0	2.5	122
84-7E	74.24	51.92	61.5	24.1	203
84-7F	68.07	46.96	41.3	13.6	022

ℓ - length of unsmoothed track
L_s - length of track, smoothed with 3-point running average
D - net distance travelled
A - azimuth of net travel (degrees true)

Table 5. Average wind speed U, iceberg speed $V = L_s/t$, current speed W_3 in the 20-30 m layer, speed W of the water in the top 100 m, and range R.

Iceberg Track	U m/s	V cm/s	W_3 cm/s	W cm/s	R km
83-1	4.6	36	36	24	0.8
83-2	4.4	17	12	12	1.3
83-3	8.8	16	9	5	3.8
83-5	8.7	21	9	5	7.5
84-5D	5.4	14	18	13	1.6
84-5E	5.6	22	15	12	1.4
84-5F	9.5	25	11	8	8.7
84-6E	5.6	21	15	12	9.7
84-6F	9.0	17	11	8	1.0
84-7D	5.4	19	18	13	8.7
84-7E	5.8	23	14	12	13.6
84-7F	9.0	32	11	8	20.9

The wind data, on the other hand, are quasi-Eulerian since the ship moved at much less than the wind speed. Because more than one iceberg was tracked during some periods, there are fewer sets of environmental data than iceberg tracks.

Each iceberg studied had special features or offered some particular challenge or insight which is not fully described by the quantitative data presented above. The following narratives highlight some of the unique features of each iceberg track.

1. Iceberg 83-1

This small, pinnacled iceberg was tracked in the Strait of Belle Isle, an area initially chosen as the focus of Cruise 83-018 because of generally high iceberg populations. This area is also noted for strong tidal currents. During the tracking period the winds were light (4.6 m/s) and constant in direction while the currents were relatively strong, rotating anticlockwise and decreasing slightly with depth down to the 66 m draft of the iceberg. The berg generally followed the depth averaged current.

The first hour of tracking, at long range and high ship speeds, was not used in modelling. During the last two hours the iceberg drifted into water of depth approximately equal to its draft and slowed relative to the currents, suggestive of bottom scouring. This period was also deleted. Subsequently Iceberg 1 came to a stop and was presumed to have run aground, and so tracking was discontinued. No other suitable icebergs were observed in the Strait at this time, and so the cruise area was extended to the Labrador shelf.

2. Iceberg 83-2

This drydock iceberg was found just outside the northern end of the Strait of Belle Isle. The above-water portion consisted of tall fins, presumably formed by wave erosion at the waterline and subsequent shedding of overhanging ice masses. The berg drifted 20 km to the southeast over a 2-day tracking period. The looping track of the berg resulted from a superposition of cyclonic circular motion on the mean drift. The period of the rotary motion was in the range of 12 to 15 hours, but due to the short record it is not possible to distinguish between inertial and tidal motions.

The observed currents were also to the southeast near the surface, rotating to nearly southward with depth. The upper-layer currents were strongest and showed the most evidence of circular motion similar to that of the berg. These upper currents (above 20 m) moved much faster than the iceberg, the top layer net velocity being three times that of the berg.

The mean wind speed for the observation period was nearly the same as for Iceberg 83-1 (4.4 m/s) but was much less steady, and there is a sustained period (hours 17-25) when the wind speed was above 8 m/s from the southwest, opposing the current.

3. Iceberg 83-3

The rounded above-water contours of this dome-shaped iceberg indicated frequent overturning, the smooth surface being a result of melting below the waterline. Grooves cut by waves ran in a number of directions, marking earlier waterlines. On several occasions this iceberg spontaneously began rocking, with an initial amplitude of about 45°, dying down over a period of about one hour. This iceberg was at a relatively long range for a few hours in the middle of the 64 hour tracking period while Iceberg 83-5 was surveyed. The net drift was 15 km to the west, again with several clockwise loops.

During the tracking period the mean surface current was to the southeast, rotating clockwise to south below 40 m depth. The upper layer currents were much stronger, with a cyclonic rotary motion superimposed on the mean flow. The wind was predominantly from the southwest and much stronger than during previous tracking periods, peaking at 17 m/s around 2100UT on June 29, 1983.

4. Iceberg 83-5

This small, drydock shaped iceberg also had smooth above-water contours, indicative of overturning. It was tracked concurrently with Iceberg 83-3 but drifted to the west nearly twice as fast, even when the two bergs were relatively close together, travelling a net distance of 22 km to the southwest in 55 hours. Due to increasing range as the ship followed Iceberg 83-3, only the first 24 hours of this track were modelled.

In spite of its smaller size, Iceberg 83-5 did not differ enough in draft (67 m vs. 86 m) to fully account for the difference in drift rates given identical winds and current profiles, and it appears that horizontal gradients in the current, not accounted for in our data, may be responsible for some of the difference between the two drift tracks.

5. Icebergs 84-5, 6 and 7

During Cruise 84-023 a group of three icebergs was tracked on June 14-19, 1984. There were two interruptions while iceberg surveys were carried out, leaving three tracking periods which we label D, E and F. Figure A4.14 shows the tracks of the icebergs.

Iceberg 84-5 was the largest of this group, with a mass of 2,100,000 tonnes and a draft of 120 m on June 14. On June 17 the mass was estimated at 1,700,000 tonnes, but this cannot be taken as a measure of the melting rate since the apparent change could be

accounted for by ± 10% experimental error. Iceberg 84-7 was of similar size (1,700,000 tonnes), while Iceberg 84-6 was considerably smaller. A reduction from 320,000 to 270,000 tonnes between the first and second surveys of Iceberg 6 again lies within ± 10% , experimental error and again cannot be considered to be a reliable measure of melting rate.

Iceberg 84-5 was followed by the ship during period D, from 0130 to 1230 on June 14 and period E, from 1450 on June 14 until 0750 UT on June 17. During period D berg 84-7 was at a range of 8 to 10 km from the ship, and during period E the range was initially 7 km but gradually increased to as much as 18 km. Iceberg 84-6 was not observed during period D, was at 7 to 12 km range during period E, and was followed by the ship during period F from 1330 on June 17 until 0600 on June 19. During period F being 84-7 was at a range of 17 to 24 km, where reduced radar precision gives the observed track a zig-zag appearance.

The tracks of Icebergs 84-5 and 84-7 during period D followed short clockwise loops, with a maximum travel of about 3 km from the starting point. Icebergs 84-5 and 84-6 then followed anticlockwise loops of about 30 km diameter during periods E and F, while Iceberg 84-7 drifted to the south during period E and then irregularly to the north during period F.

We will identify these drift track segments by a number and a letter. Tracks 5D, 5E and 6F are the ones with the ship at about 1 km range, for which the measured current profiles are representative of those at the iceberg. We are not sure whether or not the measured currents are representative of those at the other icebergs; general experience on the Grand Banks and elsewhere suggests that at 5 km range the currents are probably similar; at about 10 km range the similarity of the currents is dubious, and beyond 20 km the coherence of the currents is weak (e.g. Garrett *et al.*, 1985a). A lack of spatial correlation in the currents may possibly explain the marked difference between the tracks of iceberg 84-7, which is farther north, and of Icebergs 84-5 and 84-6, which are qualitatively similar. The data at longer ranges will allow us to test the model performance with currents measured at various ranges.

Data for track 84-5E are not reported beyond 1500 on June 16, since some of the reported radar ranges and bearings logged beyond this time were found to be erratic.

Due to a hardware failure, the topmost layer of the measured current profiles in 1984 was from 27 to 30 m, and in our data files currents in the three shallowest layers (0 to 10, 10 to 20, and 20 to 30 m) have been set equal to those measured in the 27 to 30 m layer.

We now summarize the environmental data during the three observations periods of Cruise 84-023.

a. Period D

The currents during this period were toward the west northwest after an initial period of a couple of hours during which the upper layers were moving to the north. The deeper currents were more to the south, but turned to the north near the end of the period. The wind direction was steady from the southwest, decreasing slowly from moderate (6 m/s) to light (3 m/s).

Iceberg 84-5 initially moved to the northeast, apparently following the wind, then turned to the southwest under the combined influence of currents and winds, tracing a long loop with its axis running northeast and southwest (Fig. A4.6). At the end of this period the iceberg was only 3 km from its starting point. Iceberg 84-7 changed direction fairly steadily from northwards to southwards to northward again. This again corresponds roughly to the berg direction shifting from that of the wind to that of the current. The track was semicircular with radius 2.5 km, and ended SE of the initial position (Fig. A4.11).

b. Period E

During the first eight hours the currents, initially northeast, turned to the east (Figs. A3.6, A6.5). There was a considerably stronger component to the south as depth increased. The wind became very strong from the north after 4400 hours. During the first four hours the wind direction changed rapidly (coming from N then W then S) and again reversed from 3800-4400. It remained brisk from the north for the remainder of the tracking period, with speeds peaking briefly at 19 m/s at 6500. Iceberg 84-5 followed the current direction until the wind picked up, and then followed the wind.

The track of Iceberg 84-6 appears moderately noisy due to the long radar range (Fig. A4.9). Initially the berg travelled to the NNE, which resembles neither the wind nor the mean current. As the wind picked up, the berg followed it.

The track of Iceberg 84-7 is noisy due to the long radar range. During the first 24 hours it followed neither the observed winds nor the current. At the end, with strong winds, it seems to follow the wind direction.

c. Period F

The currents were initially to the east, and then proceeded to the southeast in two scallop-shaped loops (Fig. A6.6). During the first part of the tracking period the upper currents were much stronger than the deeper ones. The winds were persistently from the south and of moderate strength (5-10 m/s).

The initial portion of the track of Iceberg 84-5 was lost due to a radar tracking error. (A different iceberg was apparently tracked until the error was realized.) The berg

appeared to mainly follow the wind. Iceberg 84-6 was followed by the ship. It proceeded in a direction between those of the wind and of the mean current. Its track followed some of the "loops" that were observed in the current. Iceberg 84-7 roughly followed the wind.

6. Iceberg 85-1

Iceberg 85-1, of blocky shape and medium (570,000 tonnes) size, was tracked on the northeastern Grand Banks from 1900 on April 27 until 0650 on April 30, 1985. During the second half of this period this iceberg was towed toward the east by M. V. Chignecto Bay, under charter to Husky-Bow Valley, because it was judged to be a potential hazard to the drillling rig, Bowdrill II, some 120 km to the south. Although the towing directon was monitored by the relative positons of the iceberg and the towing vessel, only a routh estimate (80 tonnes) of the towing force is availabe because M. V. Chignecto Bay was not equipped to measure tension in its tow line. Modelling of this iceberg track, with towing forces included, will be the subject of a later report.

7. Iceberg 85-4

Iceberg 85-4, a small, decaying iceberg, was tracked, for 24 hours beginnning at 0100 May 31, 1985. This iceberg was in deep water just off the southeastern Grand Banks, and was simultaneously observed by USCG Evergreen, International Ice Patrol (D. L. Murphy, pers. comm.). With the water depth beyond the range of acoustic Doppler bottom tracking, current profiles will have to be compensated for ship motion using LORAN C navigation. Modelling studies of this iceberg track will be included in a later report.

E. MODELLING ICEBERG DRIFT TRACKS

In this chapter we will apply the dynamic model described in Chapter B to each of the iceberg track data files discussed in the preceding chapter. Initially each track will be modelled with air and water drag coefficients set to "reasonable" values for irregularly-shaped objects, $C_A = C_W = 1.0$. Next the model will be used to select values of C_A and C_W which minimize the rms deviation of the modelled track from the observed track, with both tracks starting from the same initial position. Having in this sense an "optimum" balance of wind and current influences, we will then re-run the model with the same coefficients and with the winds set to zero; the difference from the previously modelled track is one estimate of the contribution of wind drift. A larger estimate of wind drift is obtained by setting all of the currents to zero and running the model with wind forcing only, again with the same coefficients. Due to the quadratic water drag forces in the model, removal of the current shear allows the same wind force to influence the drift rate more strongly, usually by more than twice the

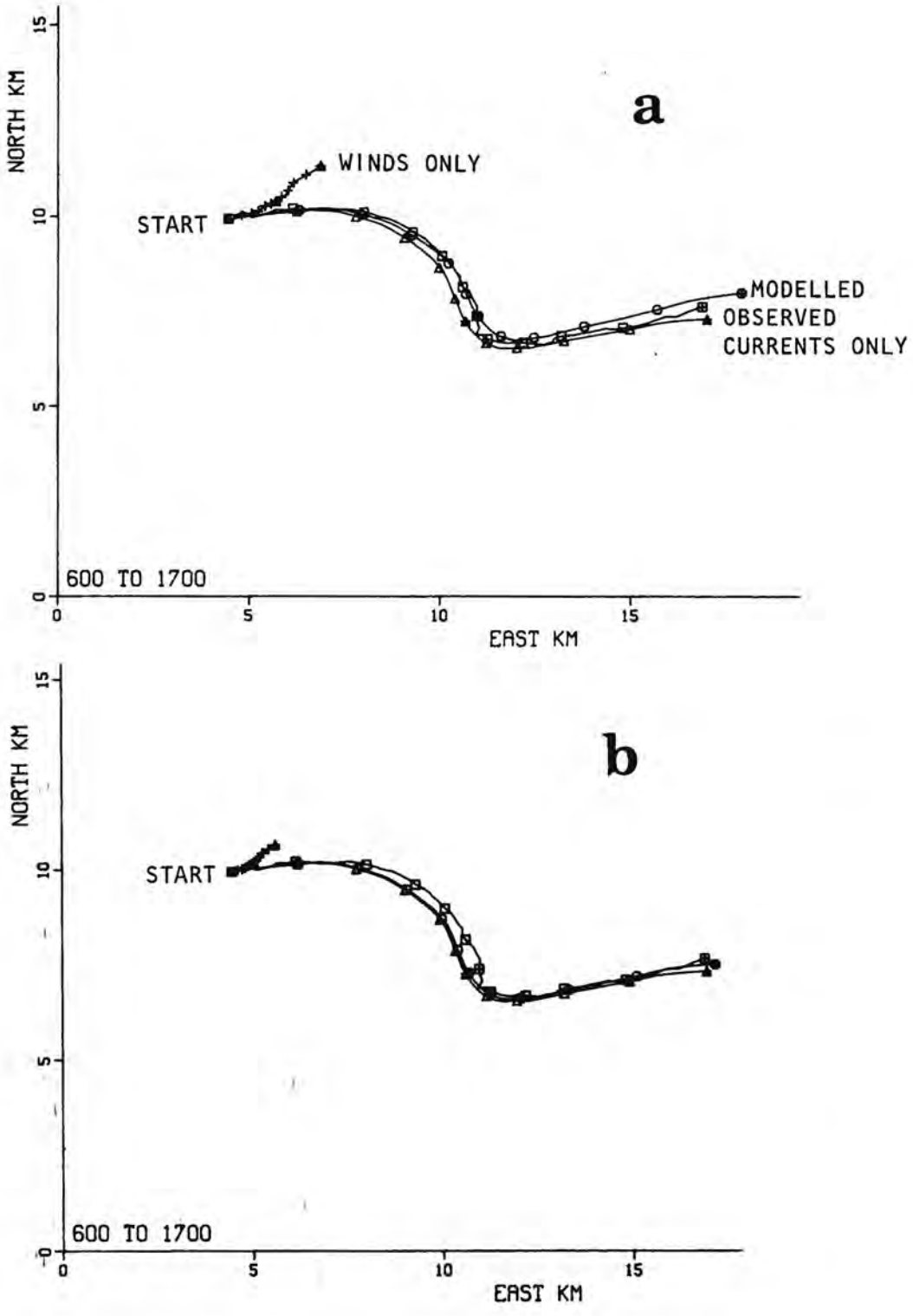

Fig. 1 Modelled (O) and observed (□) tracks of Iceberg 83-1: (a) with $C_A = C_W = 1.0$, (b) with optimized coefficients $C_A = 0.6$, $C_W = 2.6$; modelled tracks with winds only (+) and currents only (Δ).

former amount.

In several cases we shall see that the model is unable to reproduce the observed track as closely as we might have expected. In these cases the iteration selects air and water drag coefficients are both either much greater than 1 or much less than 1, which we do not consider realistic. In the absence of wind (or towing forces) the model follows a weighted mean of the currents. The selection of the coefficients mainly influences the wind-driven portion of the drift. A larger or smaller *ratio* C_A/C_W determines the rate of wind drift. The Coriolis term deflects the wind drift component to the right of the direction of the wind force, and the amount of this deflection depends on the relative magnitude of drag and Coriolis forces, i.e. on the magnitude of C_A and C_W. Lacking any other influence on direction, our "optimization" in certain cases has selected unreasonable coefficients in order to influence the direction of the modelled track through the Coriolis term in the model, but this was not our original intention in adjusting the drag coefficients. In these cases we have found that rotating the wind force by an angle of up to 30° relative to the wind (selected for best fit) allows the model to reproduce the track with smaller errors and with more reasonable values of the drag coefficients. A deflection of the wind force appears plausible in view of the shapes of the above-water portions of the icebergs, but like the drag coefficients we can estimate the values only indirectly through the dynamic model, not directly from our field measurements.

1. Iceberg 83-1

The track of this small pinnacled berg in the Strait of Belle Isle (Fig. A4.1) was modelled from 0600 to 1700 UT on June 24, 1983. After this period it drifted into shallower water and, based on its measured draft, was believed to have slowed and then stopped due to contact with the seabed. The currents during this period are strong and towards the east, rotating anticlock-wise and reducing slightly with depth. The current shear in the upper layers may well have continued above our shallowest (9m) data, but in modelling iceberg drift we will assume that currents above our shallowest measurement remain uniform with depth.

The dynamic model with drag coefficients $C_A = C_W = 1.0$ reproduces the observed track with 0.52 km rms error in the hourly positions over a distance of $L_s = 14$ km (Fig. 1a, Table 4). By iteration of the drag coefficients, a minimum rms error in position of only 0.24 km was achieved with $C_A = 0.6$ and $C_W = 2.6$ (Fig. 1b).

An examination of the accelerations due to the various modelled forces acting on the iceberg showed water drag, air drag and water acceleration (presumably due to horizontal pressure gradients) to be the major terms, while the Coriolis term was generally an order of magnitude smaller. Deleting the water acceleration term had a remarkably small influence on the modelled track, since the resultant small differences in velocity quickly produced compensating changes in water drag.

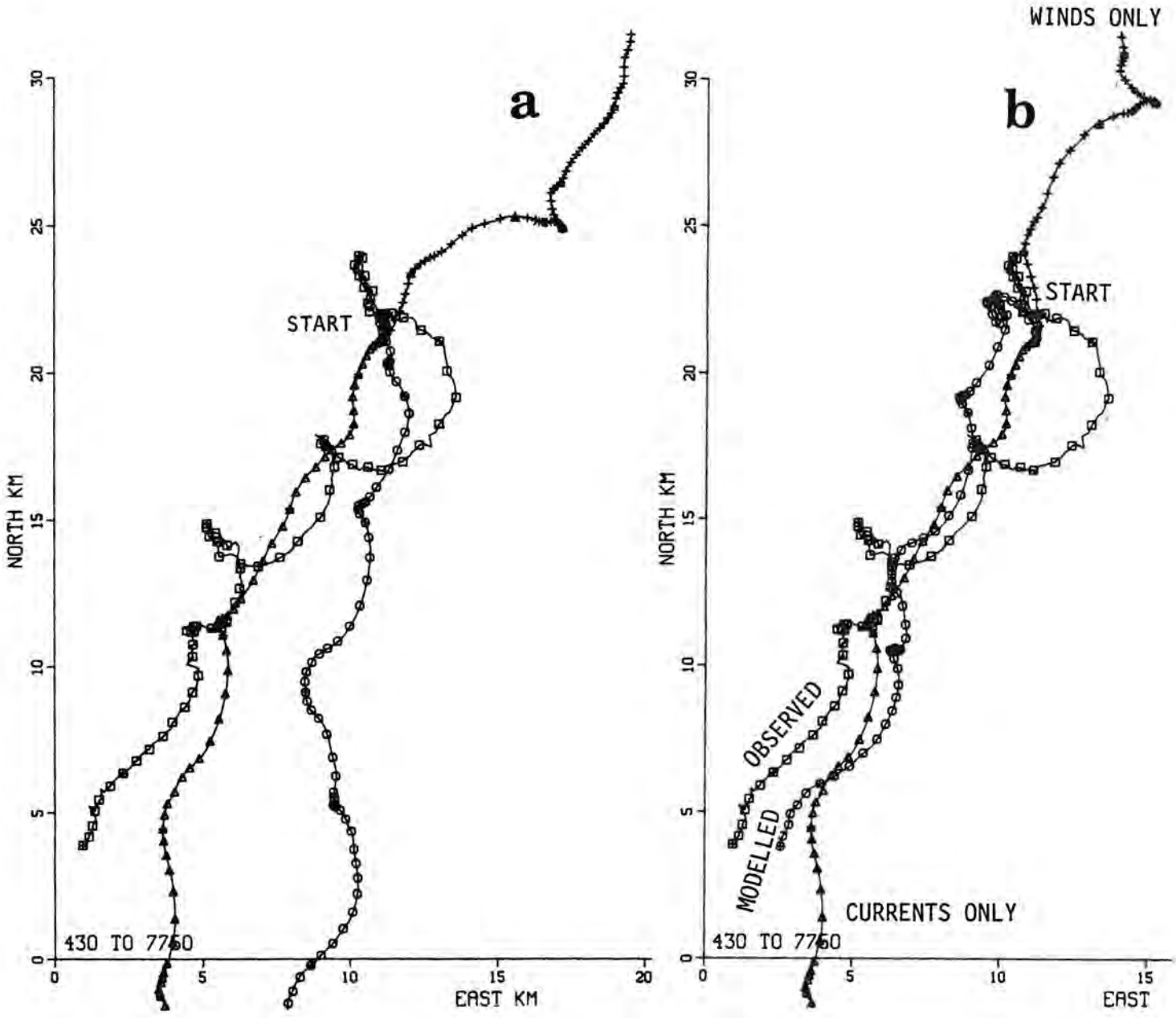

Fig. 2 Modelled (O) and observed (□) tracks of Iceberg 83-2: (a) with $C_A = C_W = 1.0$, (b) with wind forces rotated 30° anticlockwise and optimized coefficients $C_A = 1.6$, $C_W = 1.0$; winds only (+) and currents only (Δ).

By setting the currents to zero, the wind-drift component is seen to be 1.3 km toward the northeast. With the winds set to zero the drift due to current differs from the full model by only 0.3 km, and the net influence of deleting wind drift is only 21% of the wind drift modelled in the absence of currents (Fig. 1b), due to the influence of the quadratic water drag formula in the presence of current shear. A further illustration of the importance of measuring the current profile is that no individual layer (Fig. A6.1) reproduces the iceberg track nearly as well as the modelled drift due to all the currents. In a later chapter we will examine the relative merits of a simple kinematic model which attempts to model the drift as a linear combination of the wind and the current in one selected layer.

2. *Iceberg 83-2*

Iceberg 83-2 (Fig. A4.2), on the southern Labrador Shelf just outside of the Strait of Belle Isle, followed a generally southwesterly course with three tight loops and a cusp from 0430 June 25 to 0550 UT on June 28, 1983. The currents during this period (Appendix 6) again rotated anticlockwise and decreased with depth. There was a strong shear in the top three 10 m layers, and much less variation below 30 m. The currents were more southerly than southwesterly, and the winds were generally from the southwest, opposing the drift.

The modelled track with $C_A = C_W = 1.0$ (Fig. 2a) carries this iceberg farther to the south and not as far to the west as the observed track, and the loops in the observed track are replaced by cusps. While the general features of the observed track are reproduced, an rms model error of 5.6 km in a net drift of 20 km is much less satisfactory than our initial model of Iceberg 1. Optimizing the air and water drag coefficients did not in itself produce a substantial improvement in model performance. Current shear in the missing part (0 to 9 m) of the top layer should not account for much of this error since this layer contained only 13% of the total underwater cross-section.

Noting that the above-water portion consisted of several tall, narrow fins, we experimented with several amounts of constant rotation of the wind force relative to the wind direction. With 30° anticlockwise rotation, the optimum drag coefficients are $C_A = 1.6$ and $C_W = 1.0$, and the drift track is reproduced with a smaller rms error of 1.9 km (Fig. 2b). The higher air drag coefficient appears consistent with the finned and jagged above-water shape. The details of the track are still not reproduced as well as the track of Iceberg 1, and in particular the clockwise circle from 2000 on June 25 to 1200 on June 26 is poorly reproduced. Although we did not keep a record of iceberg orientation to the wind, the iceberg was qualitatively observed from time to time to rotate. The constant wind force deflection which we have applied may be an oversimplification, but our data do not justify a more complex adjustment.

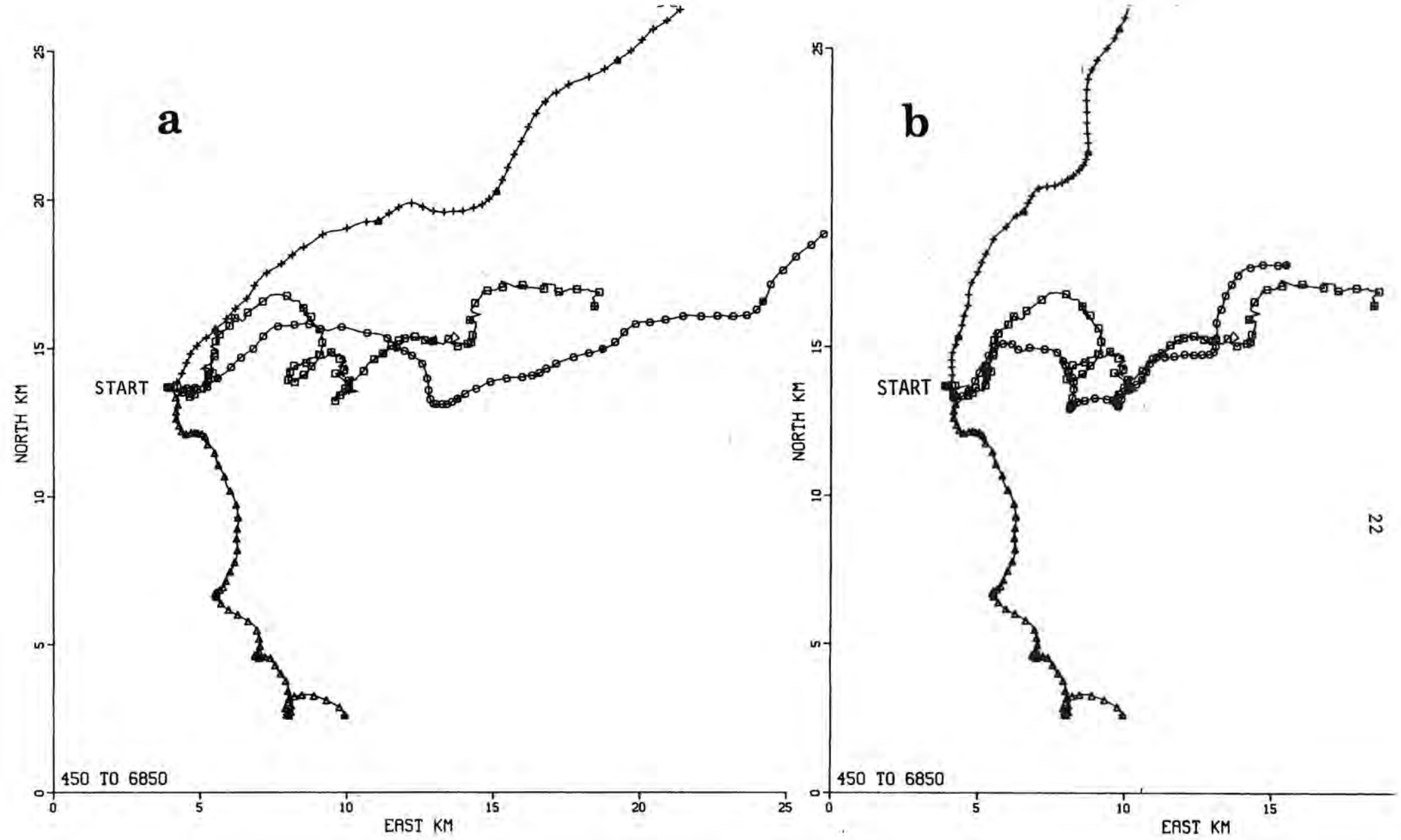

Fig. 3 Modelled (O) and observed (□) tracks of Iceberg 83-3: (a) with $C_A = C_W = 1.0$, (b) with wind forces rotated 30° anticlockwise and optimized coefficients $C_A = 0.6$, $C_W = 1.1$; winds only (+) and currents only (Δ).

To investigate the relative influence of the terms in the model, the track of Iceberg 83-2 was modelled without the pressure term (i.e. the water column acceleration term). This had negligible effect, changing the end point by only 0.11 km after 46 km of travel. The pressure and water drag terms are complementary in that with the pressure term removed, only small changes in velocity are needed to produce water drag forces which quickly eliminate the perturbation in velocity. Removal of the Coriolis force rotates the net wind influence anticlockwise and in this particular case rotates the track clockwise, since the net drift is against the wind. The end point is altered by only 1.1 km. The above tests were carried out with $C_A = C_W = 1.0$; if we used variable coefficients the optimization process would reduce the influence of the changes.

3. Icebergs 83-3 and 83-5

These icebergs, further offshore than Iceberg 83-2, were tracked simultaneously from 0450 UT on June 29 until 1130 on July 1. Iceberg 83-3, the larger one of the pair, travelled 11 km to the west while Iceberg 83-5 drifted 22 km in a southwesterly direction (Fig. A4.5). With increasing separation, only Iceberg 83-3 continued to be tracked until 2050 on July 1. Currents in the upper layer again sheared strongly with depth, flowing in a south-easterly direction in a series of semidiurnal loops, while deeper currents were weaker and generally southerly. The clockwise rotation with depth is opposite to the previous two cases.

With $C_A = C_W = 1$ our model indicates a net drift of 23 km for Iceberg 83-3, overshooting the observed easterly drift of 15 km (Fig. 3a). With coefficients $C_A = 2.7$ and $C_W = 5.0$ (the upper limit in our iteration), the overshoot is reduced but we are still unable to represent the observed track closely (not shown). The effect of the large drag coefficients is to minimize the clockwise influence of the Coriolis term, relative to air and water drag forces. By rotating the wind force 30° anticlockwise we fit the observed track much better (1.20 km rms error) with physically reasonable drag coefficients, $C_A = 0.6$ and $C_W = 1.1$ (Fig. 3b). A reduced wind force rotation of 20° anticlockwise (not shown) gives nearly as good a fit (1.27 km rms error) but requires unreasonably large drag coefficients $C_A = 2.8$, $C_W = 4.9$. As in the previous case (Iceberg 83-2), we have had to introduce a wind force deflection to satisfactorily model the observed track. The more rounded shape of Iceberg 83-3, as compared to Iceberg 83-2, is not as suggestive of aerodynamic lifting forces, but does appear compatible with a relatively low air drag coefficient of 0.6. The clockwise loops in the track have not been well reproduced by the model. The range from the ship to the iceberg was up to 15 km around 1600 UT on June 30, and it is during this period that the errors in the modelled velocity are worst.

We modelled only the first 19 hours of the track of Iceberg 83-5, since after this time the range from the ship to the berg was too long for the measured currents to be consider-

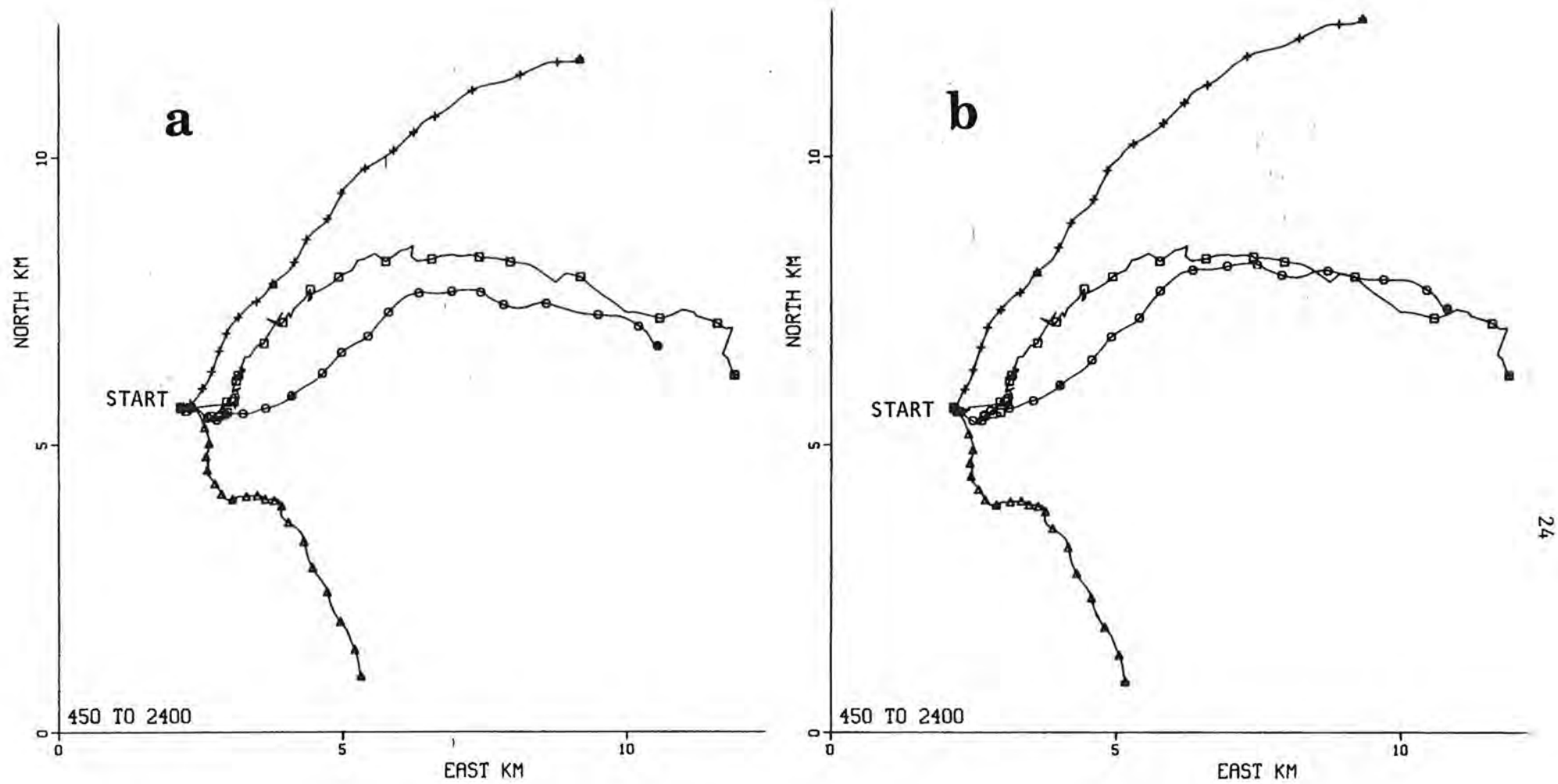

Fig. 4 Modelled (O) and observed (□) tracks of Iceberg 83-5 (a) with $C_A = C_W = 1.0$, (b) with $C_A = 2.0$, $C_W = 1.7$; winds only (+) and currents only (Δ).

ed representative. With $C_A = C_W = 1$ the track was reproduced with an rms error of 0.87 km (Fig. 4a). A marginal improvement to 0.76 km rms error was obtained with $C_A = 2.0$ and $C_W = 1.7$ (Fig. 4b).

The simultaneous but diverging tracks of Icebergs 83-3 and 83-5 test the model's ability to reproduce diverging tracks using identical wind and current data. The smaller and shallower Iceberg 83-5 drifted nearly twice as fast as Iceberg 83-3. With $C_A = C_W = 1$ the modelled tracks of the two icebergs are qualitatively similar and only part of the divergence of the two tracks was reproduced by differences in draft and underwater cross-section in the presence of current shear. Differences in the relative air and water drag coefficients (Iceberg 83-3 had about half as large a ratio of C_A/C_W as did Iceberg 83-5) account for more of the divergence, but the track of Iceberg 83-3 is well reproduced only with a 30° deflection of the wind force.

4. *Iceberg tracks 84-5D and 84-7D*

In response to winds from the west and currents toward the west, Iceberg 84-5 drifted about 2 km to the northeast and then returned to its position 15 minutes from the start. With $C_A = C_W = 1.0$ the dynamic model is dominated by the current and moves the iceberg 2.5 km to the west during this period, while optimized coefficients $C_A = 2.4$, $C_W = 0.5$ give an rms error of 0.61 km (Fig. 5). This is not impressive when compared to near-zero net drift, but it represents a good balance between about 5 km drift due to currents alone and a similar amount due to opposing winds. The relatively high air drag and low water drag coefficients were not valid during subsequent segments of the drift of Iceberg 84-5.

During the same period Iceberg 84-7 travelled in a clockwise semicircle of about 2.5 km diameter. The dimensions of this iceberg were similar to those of Iceberg 84-5. With identical wind and current data and with $C_A = C_W = 1.0$ the modelled track again runs 2.5 km in the wrong direction, while with $C_A = 2.0$ and $C_W = 0.3$ the observed track is reproduced with 0.70 km rms position error (Fig. 6). In this case the model performance is not significantly worse at a range of 7 to 10 km than for a nearby iceberg. Both Icebergs 84-5 and 84-7 required relatively high air drag and low water drag coefficients to fit their tracks during Period D.

5. *Iceberg track 84-5E*

This 64 hour drift segment was modelled well (2.3 km rms error in 51 km of drift) using the dynamic model with $C_A = C_W = 1$ (Fig. 7a). The optimum coefficients, $C_A = 1.9$ and $C_W = 1.3$, slightly improved the fit to achieve an rms error of 1.95 km (Fig. 7b). The net influence of wind amounts to 15 km, or half of the net distance travelled. Compared with the

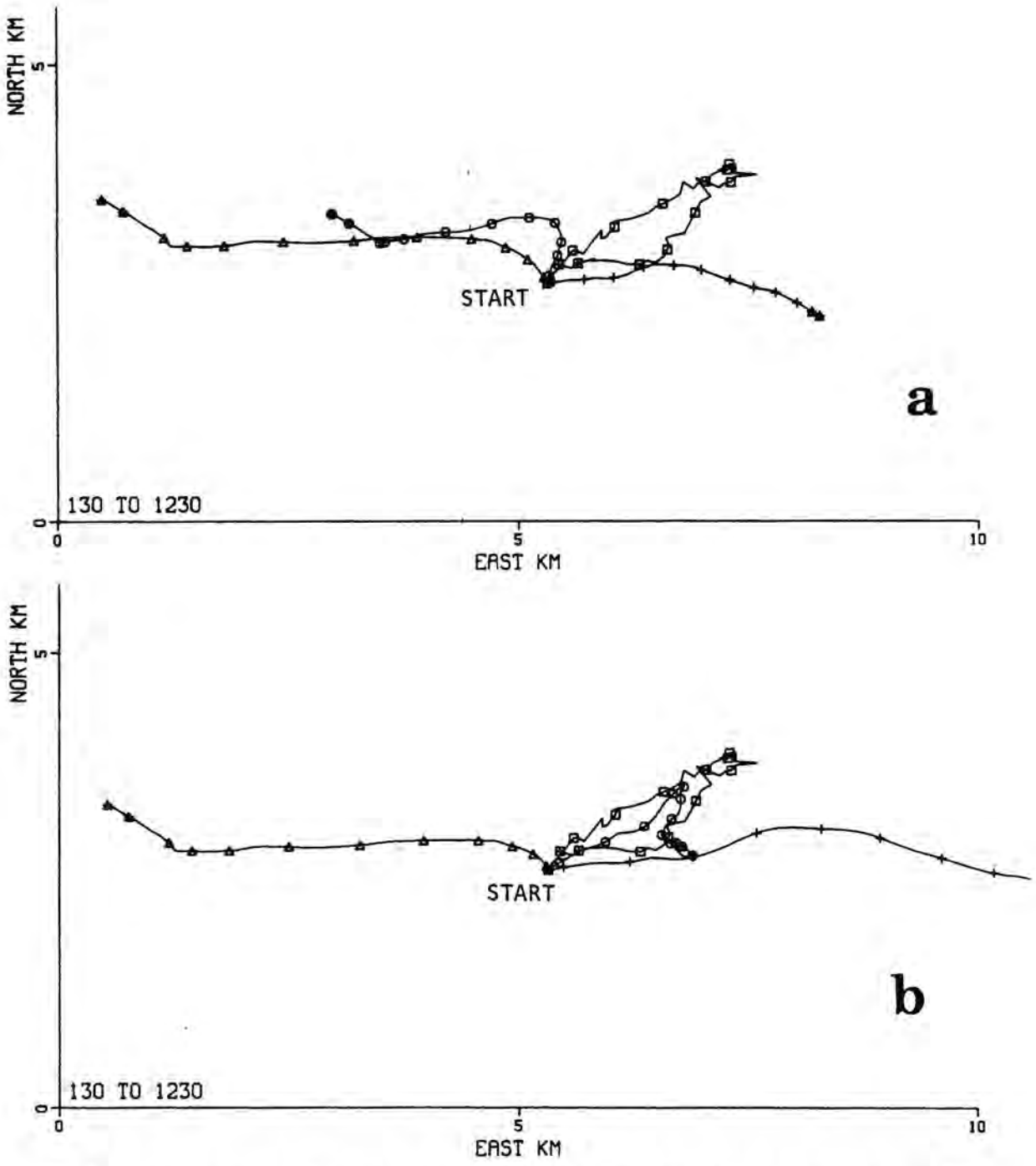

Fig. 5 Modelled (O) and observed (□) tracks of Iceberg 84-5 during Period D: (a) with $C_A = C_W = 1.0$, (b) with $C_A = 2.4$, $C_W = 0.5$; winds only (+) and currents only (Δ).

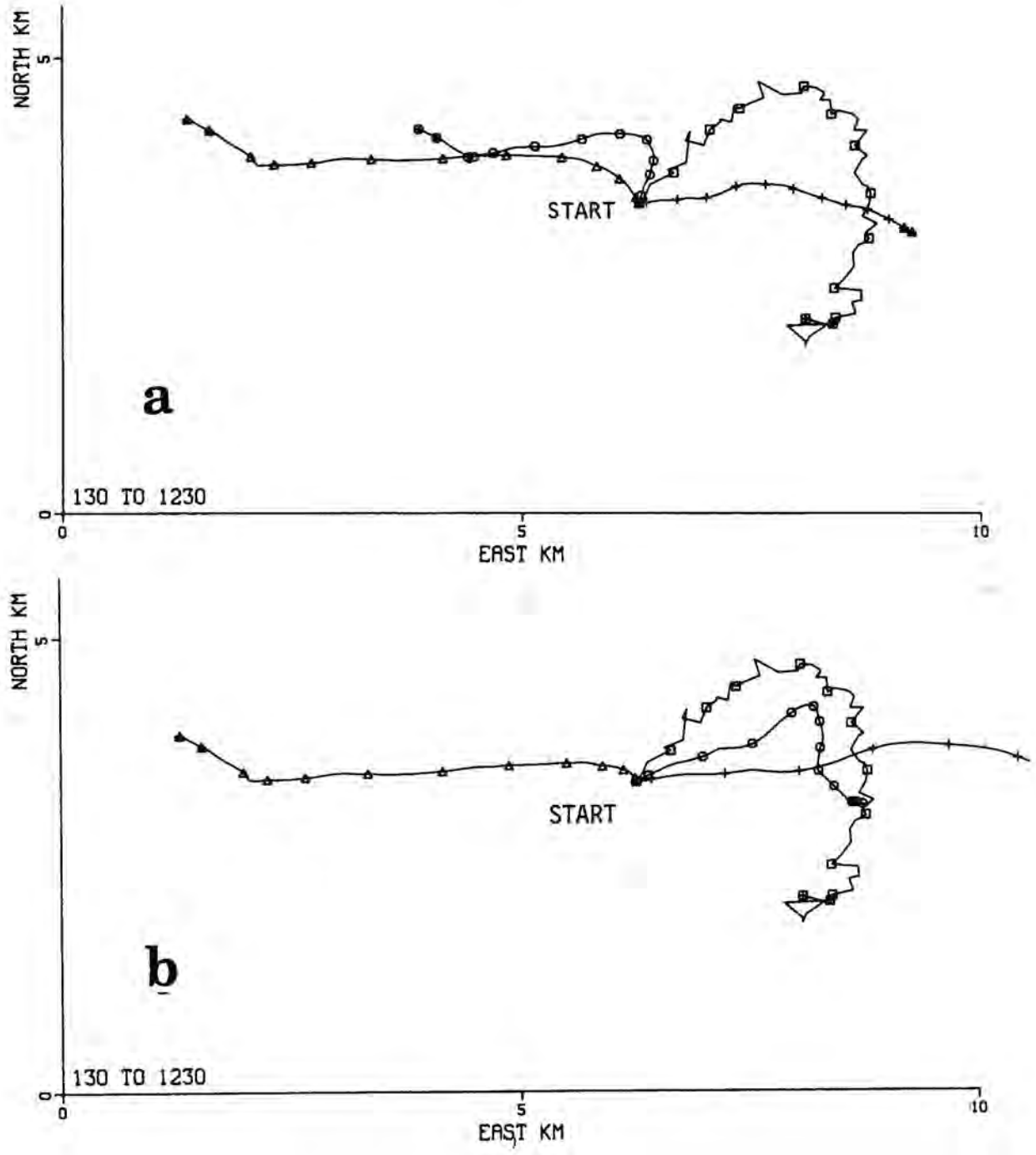

Fig. 6 Modelled (O) and observed (□) tracks of Iceberg 84-7 during Period D: (a) with $C_A = C_W = 1.0$, (b) with $C_A = 2.0$, $C_W = 0.3$; winds only (+) and currents only (Δ)

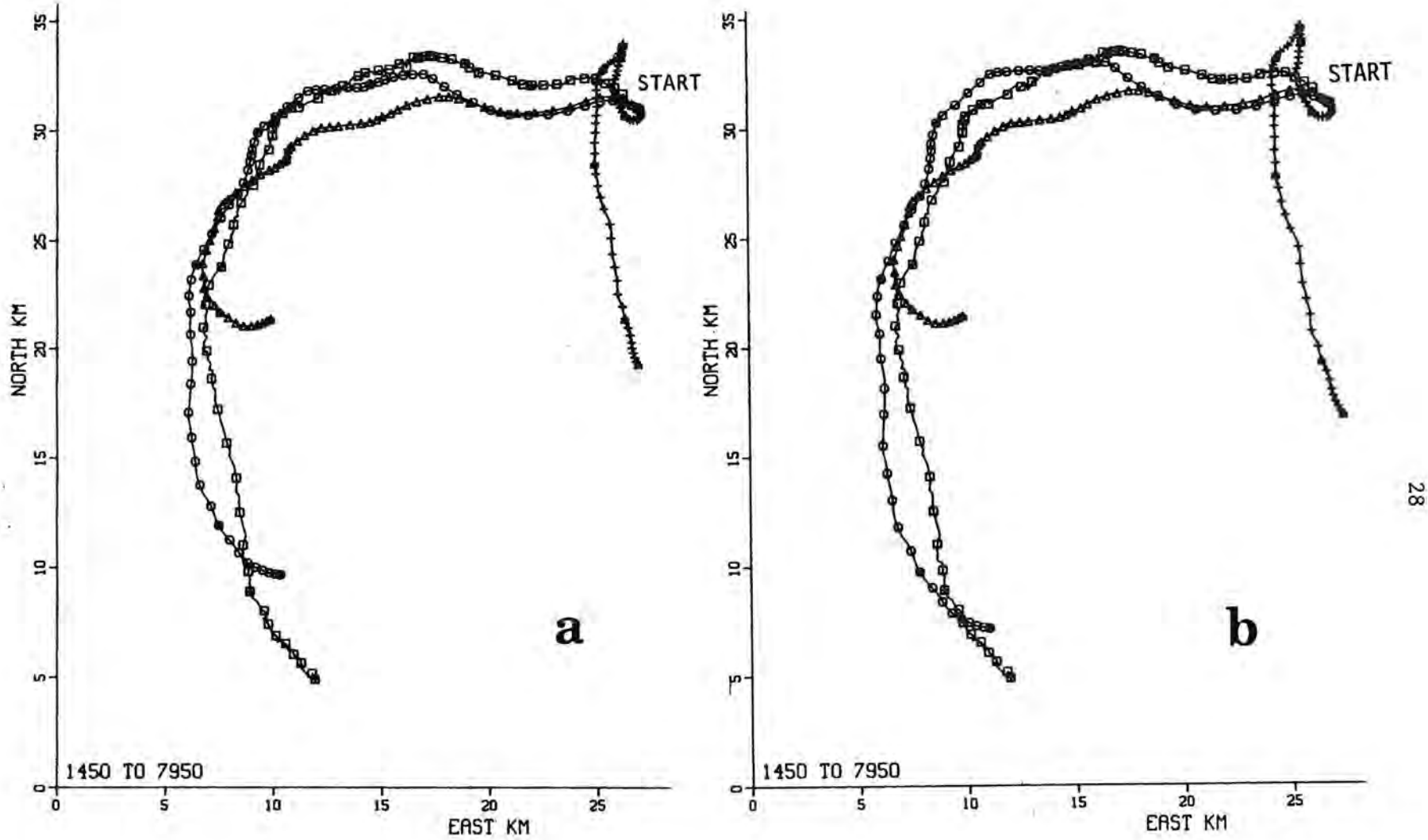

Fig. 7 Modelled (O) and observed (□) tracks of Iceberg 84-5 during Period E: (a) with $C_A = C_W = 1.0$, (b) with $C_A = 1.9$, $C_W = 1.3$; winds only (+) and currents only (Δ).

earlier segment 84-5D of the track of this iceberg, with optimum coefficients of $C_A = 2.4$ and $C_W = 0.5$, it appears that the high air drag in relation to water drag coefficient may have been selected for the earlier segment to overcome some deficiency in the data rather than to represent the actual dynamics of this iceberg.

6. Iceberg track 84-6E

The data for this iceberg run from 1450 UT on June 14 to 1500 on June 16. With $C_A = C_W = 1$ the dynamic model produces a track generally similar to the corresponding portion of the track of Iceberg 84-5E, but ending about 4 km further west because its cross-sectional area weights the model more strongly to shallower layers where currents toward the west are stronger. The observed track, on the other hand, travels only about half as far to the west (Fig. 8) and the rms model error is 10.9 km. Optimized coefficients $C_A = 0.1$ and $C_W = 4.8$ are not physically realistic and negligibly improve the fit to 10.2 km rms error (not shown). Clearly the currents with which we modelled the track of Iceberg 84-5E are not representative of those driving Iceberg 84-6E, at a range of 7 to 12 km from the ship. The results are particularly poor for the second half of the period.

7. Iceberg track 84-7E

The data for this iceberg start 3-1/2 hours later than for Iceberg 84-5E. With identical winds and current profiles and with a similar distribution of cross-sectional area, the model-led track is nearly identical to that for Iceberg 84-5E with $C_A = C_W = 1$, and does not closely resemble the observed drift of Iceberg 84-7E (Fig. 9). The rms error is 13.4 km. Again the opti mum coefficients, $C_A = 2.6$ and $C_W = 4.9$ give only a marginal improvement to 13.2 km rms error (not shown) and at a range of 7 to 18 km we again conclude that the measured currents are not representative of those driving Iceberg 84-7.

8. Iceberg track 84-6F

During the final 41 hour tracking period of Cruise 84-023 the ship followed Iceberg 84-6. This track was reasonably well modelled by the dynamical model with $C_A = C_W = 1$, the rms position error being 2.62 km over a 25 km drift track (Fig. 10a). The optimized coefficients, $C_A = 0.3$ and $C_W = 0.2$ reduced the rms position error to only 1.42 km; the larger ratio of C_A/C_W increased the amount of wind drift and the small values of both coefficients allowed the Coriolis term to rotate the wind drift in a clockwise direction. A 10° clockwise rotation of the wind forces results in optimized coefficients $C_A = 0.6$ and $C_W = 0.5$ which are more realistic, and a slightly smaller fitting error of 1.32 km (Fig. 10b). The wind drift to the northeast accounts for most of the the motion with currents transporting the iceberg 7.5 km to the

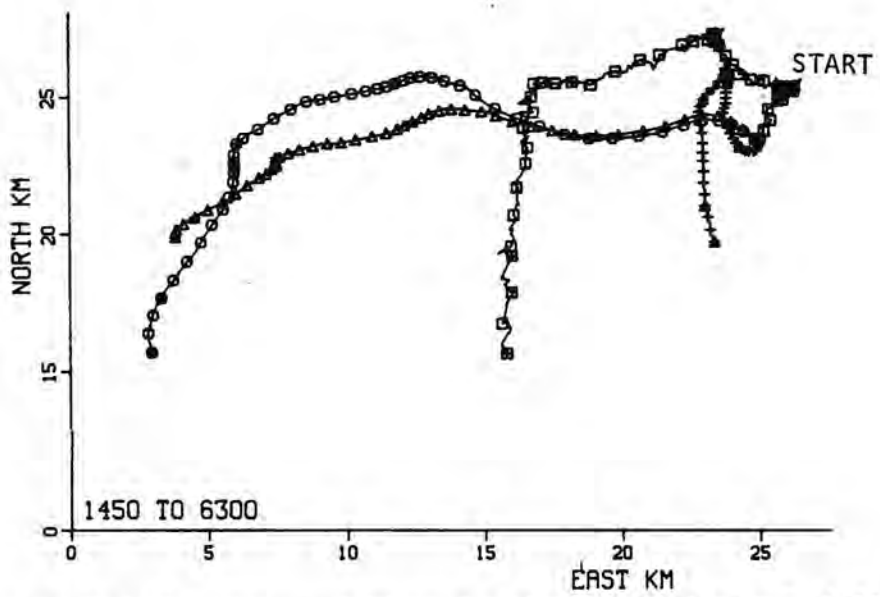

Fig. 8 Modelled (O) and observed (□) tracks of Iceberg 84-6 during Period E with $C_A = C_W = 1.0$; winds only (+) and currents only (Δ).

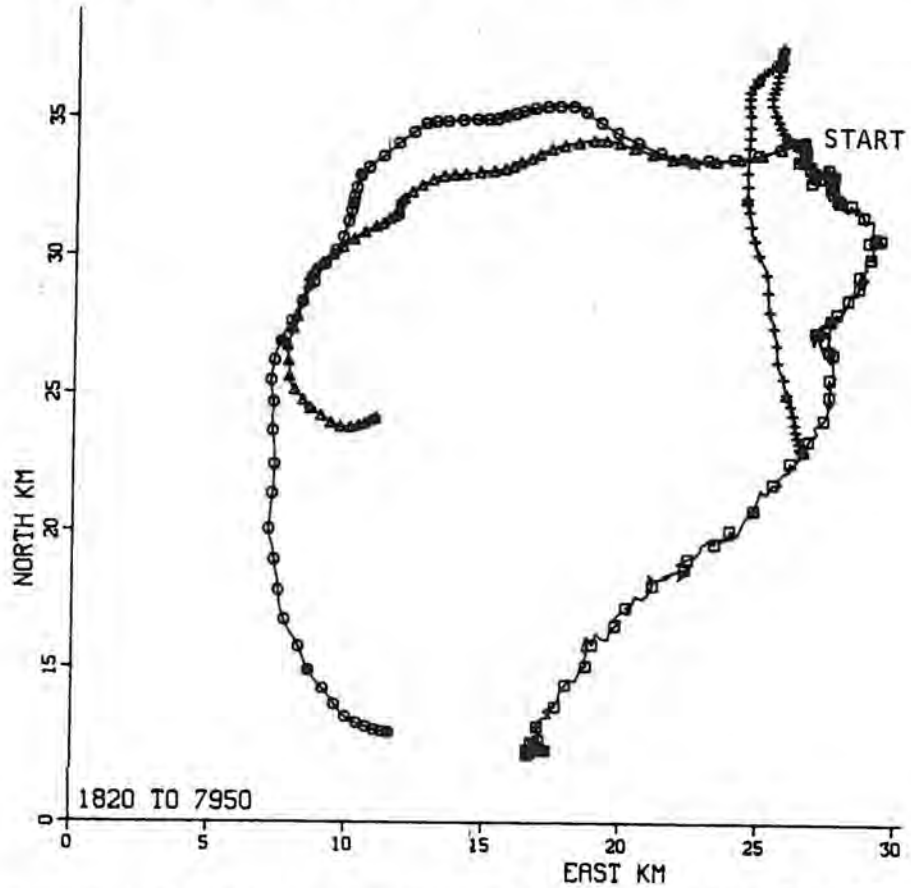

Fig. 9 Modelled (O) and observed (□) tracks of Iceberg 84-7 during Period E with $C_A = C_W = 1.0$; winds only (+) and currents only (Δ).

southeast. The previous drift segment 84-6E of this iceberg was not well modelled, while our success in modelling track 84-6F is attributed to the currents being measured at a closer mean range of 1 km as compared to 10 km (Table 5).

9. Iceberg track 84-5F

Due to a 4 hour interruption in logging ranges and bearings to this iceberg, this data file starts at 2300 on June 17, 1984 and runs for 22 hours. With the dynamic model ($C_A = C_W = 1$) the direction of the modelled track is correct but it falls short of the observed drift and the rms error is 3.79 km in 29 km of travel (Fig. 11a). With $C_A = 1.3$ and $C_W = 0.7$, this error is reduced to 1.1 km (Fig. 11b) and so in this instance we have no evidence that at a range of 8 to 10 km the measured currents are not representative. During this period the range and bearing remained relatively constant; in other words the tracks of Icebergs 84-5 and 84-6 were similar in spite of their separation of about 9 km.

This would appear to contradict our conclusion that a 10 km mean range the currents were not the same at the ship as at Iceberg 84-6 during period E. In fact, the quantity of data reported here is not nearly sufficient to establish the statistics of spatial variability of currents and we can only conclude that at intermediate ranges we have partial success.

10. Iceberg track 84-7F

The final segment of the track of Iceberg 84-7 was observed at a longer range (17 to 24 km), at which our experience would not lead us to expect the measured currents to be representative. With $C_A = C_W = 1$ the observed track is reproduced with 7.3 km rms error in 14 km of drift (Fig. 12), while selection of $C_A = 2.2$ and $C_W = 5.0$ slightly reduces the error to 5.4 km, mainly by choosing large drag coefficients which tend to rotate the wind drift component anticlockwise by overwhelming the effect of the Coriolis term. Even though the currents may have been similar over a 9 km range between Icebergs 5 and 6 during this period, they did not remain similar when the range was doubled.

11. Discussion

A multi-layer dynamic iceberg drift model is able to reproduce the observed tracks of a variety of icebergs on the Grand Banks, the Labrador Shelf and in the Strait of Belle Isle, given detailed environmental data. The data consist of winds and current profiles averaged over 10 minute intervals, and with the currents averaged in 10 m depth layers. Currents measured at a range of 10 km or more do not give consistently good model results. Sonar

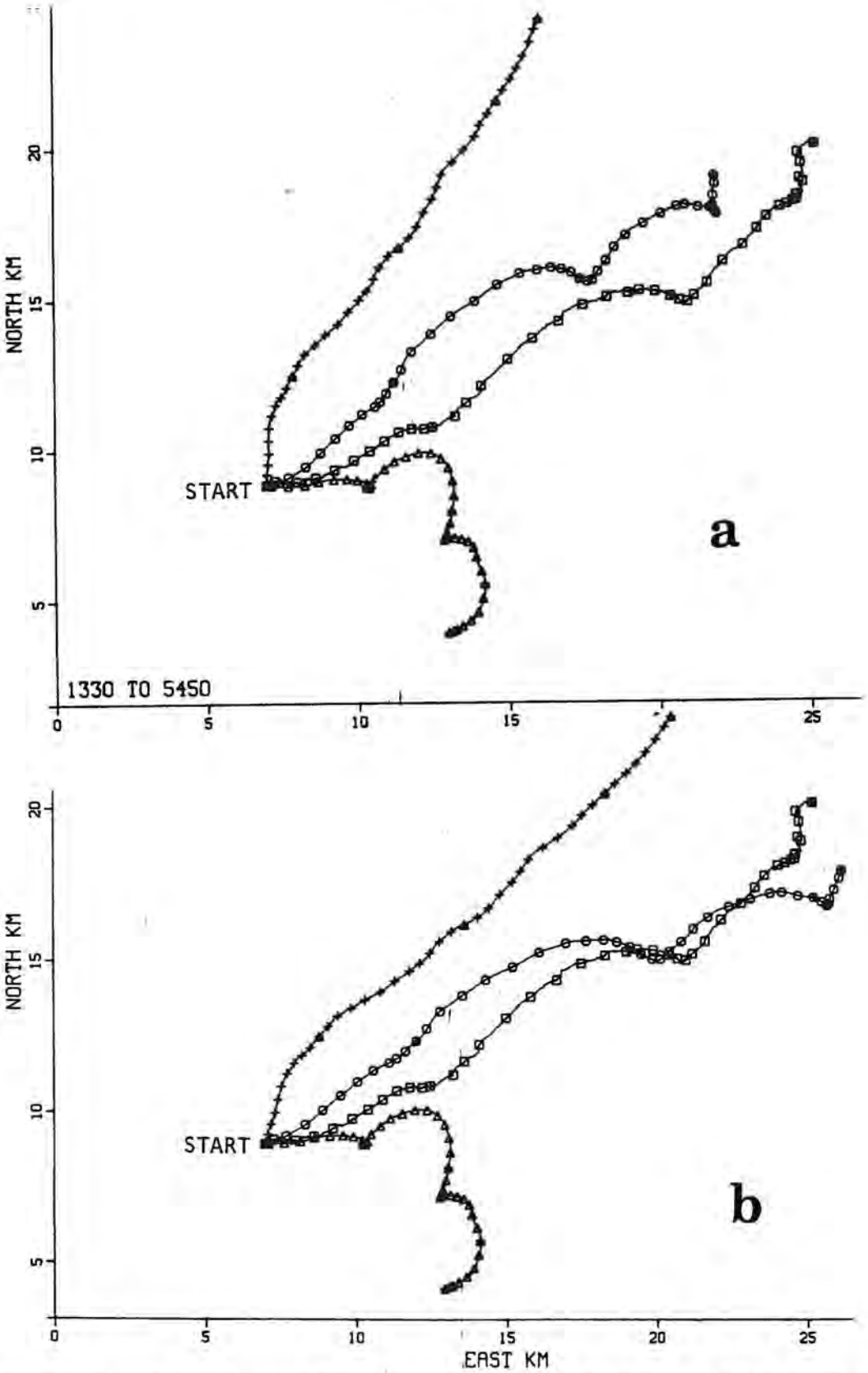

Fig. 10 Modelled (O) and observed (□) tracks of Iceberg 84-6 during Period F: (a) with $C_A = C_W = 1.0$, (b) with wind forces rotated 10° clockwise and optimized coefficients $C_A = 0.6$, $C_W = 0.5$; winds only (+) and currents only (Δ).

surveys and photographs were used to estimate the cross-sectional areas of each iceberg in air and in 10 m depth layers.

Air and water drag coefficients were adjusted within limits to optimize the fit of the modelled track to the observed track, and in three cases the wind force was rotated by a fixed amount, relative to the wind direction. Table 6 summarizes the rms error before and after optimizing the coefficients. Deleting tracks 6E, 7E and 7F which were at relatively long mean range of 10 to 21 km, the mean ratio of rms model error to distance travelled is 0.05. We were consistently unable to model the clockwise loops which are a common characteristic of iceberg drift tracks; this deficiency must be inherent either in our model or in our data.

We have not yet investigated the consequences of simplifying the data to reflect the amount of detail which might be available in an operational situation.

F. KINEMATIC MODEL

1. Model formulation

In operational situations it will not usually be possible to monitor the currents at all depths. To find out which current layers made the best predictors of iceberg motion we used a simple linear regression

$$V = aU + bW_i \tag{15}$$

to represent the iceberg velocity as a linear sum of constant multiples of the wind velocity and of the current velocity in a single layer i, where layer 1 is from 0 to 10 m, layer 2 from 10 to 20 m, etc. As before we allow the model to select two coefficients to minimize the mean square error in modelled position, d, as compared to the observed position D

$$\varepsilon^2 = \frac{1}{n}\sum_{t=1}^{n}\left(D-d\right)^2 = \frac{1}{n}\sum_{t=1}^{n}\left[D-D_o-\sum_{k=1}^{t} V\Delta t\right]^2 \tag{16}$$

The layer i which resulted in the least mean squared error (with appropriately chosen values of a and b) was selected. As in the dynamic model of the previous chapter, we have not directly allowed the iceberg to move in directions other than those of the wind and currents. No constraints have been placed on the values of the coefficients a and b, and we shall see that the selection of the "best" current layer i is strongly influenced by the current direction, since in this model variation of the b coefficient can amplify or reduce the rate of travel of the iceberg relative to the current.

To test the importance of including wind drift, we have also fitted an even simpler model,

$$V = cW_j \tag{17}$$

in which the iceberg velocity is a multiple of the current in one selected layer. The modelled

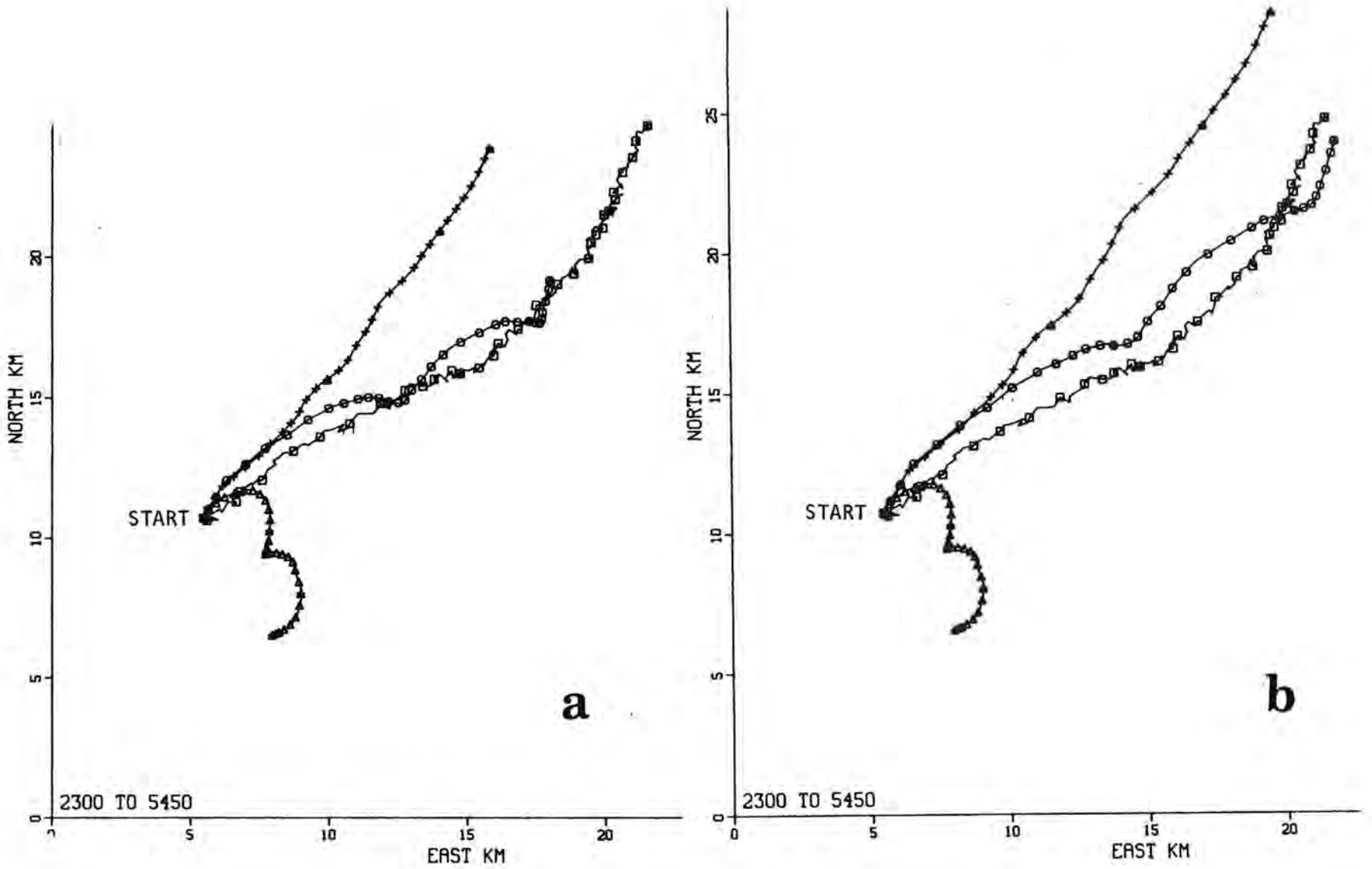

Fig. 11 Modelled (O) and observed (□) tracks of Iceberg 84-5 during Period F: (a) with $C_A = C_W = 1.0$, (b) with $C_A = 1.3$, $C_W = 0.7$; winds only (+) and currents only (Δ).

track is in this case the same as the progressive current vector (Appendix 6) for the appropriate layer, enlarged or shrunk by the coefficient c.

2. Results and discussion

The coefficients of the kinematic models and the "best" current layer are listed in Table 7, and the correlation coefficients of the east and north iceberg velocity components with the corresponding wind and current components in the upper six layers (0 to 50, 10 - 20, . . . , 50 - 60 m) are listed in Table 8.

The average value of the wind drift coefficient a (Table 7) was 0.017 ± 0.008, in good agreement with the wind drift factor of 0.018 ± 0.007 obtained by correlating winds with a large number of trajectories of icebergs off the Labrador coast (Garrett *et al.*, 1985b). The current drift coefficients have a mean value of 0.64 ± 0.45, and so in general we have obtained a best fit by choosing a current layer which moves faster than the iceberg and then attenuating the drift rate. Because we have allowed freedom to fit the rate of drift but no other means of influencing the direction, the selection of the "best" layer was strongly influenced by the direction of the current. All four of the 1983 tracks were best fitted by one of the upper two layers, which were missing from the 1984 data, but in 1984 the shallowest available layer (layer 3) was selected only once.

Errors in fitting the observed tracks by the kinematic model, with two fitted coefficients and selected layer depth, are very similar to errors of the dynamic model with two selected coefficients and occasional rotation of wind forces (Fig. 13). For icebergs at a mean range of less than 5 km from the ship the rms fitting error was $\leq 5\%$ of the track length L_s, except for track 84-5D where opposing winds and currents resulted in a very small amount of movement. A negative current coefficient was fitted to track 84-7D during this same period, and the negative coefficient was not included in calculating the mean value of b above.

Tracks at longer mean ranges of 8 to 21 km were fitted with generally larger rms errors of up to 16% of L_s. In these cases, where we do not necessarily expect the measured currents to be the same as those driving the iceberg, the kinematic model did not perform as poorly as the dynamic model discussed in the previous chapter. In the absence of wind drift the dynamic model is constrained to follow a depth-weighted mean current, regardless of the choice of coefficients, and this physically realistic constraint is a handicap if the correct currents are not supplied. The kinematic model, on the other hand, is free to choose a layer in which the currents follow the right direction, and then amplify or attenuate the current drift as needed. No rotation of winds has been used.

Table 6. Summary of dynamic modelling results.

Iceberg Track	C_A	C_W	θ deg.	E km	E_1 km	E/L_s %	E_1/L_s %
83-1	0.6	2.6	0	0.2	0.5	2	4
83-2	1.6	1.0	-30	1.9	5.5	4	12
83-3	0.6	1.1	-30	1.2	6.3	3	17
83-5	0.9	0.8	0	1.1	1.1	5	5
84-5D	2.4	0.5	0	0.6	3.9	10	70
84-5E	1.9	1.3	0	2.0	2.3	4	5
84-5F	1.3	0.7	0	1.1	3.8	4	13
84-6E	(0.1)	(4.8)	0	(10.2)	(10.9)	(28)	(30)
84-6F	0.6	0.5	10	1.3	2.6	5	10
84-7D	2.0	0.3	0	0.7	3.2	9	43
84-7E	(2.6)	(4.9)	0	(13.2)	(13.4)	(25)	(26)
84-7F	(2.2)	(5.0)	0	(5.4)	(7.3)	(11)	(16)
Mean (9 runs)	1.3	1.0		1.1	3.2	5	20
± Std. Dev.	0.7	0.7		0.6	1.9	3	22

C_A and C_W are optimized air and water drag coefficients.
θ is clockwise rotation angle of wind force relative to wind direction.
E is rms error in fitting observed track.
E_1 is rms error with $C_A = C_W = 1$, $\theta = 0$.
L_s is smoothed track length from Table 4.
Bracketed values for icebergs at mean range ≥ 10 km.

Table 7.Summary of kinematic modelling results.

Iceberg Track	Wind and current (Eq. 15)					Current only (Eq. 17)		
	a	b	i	ε km	e/L_s %	c	j	ε_c km
83-1	0.024	0.796	2	0.37	3	1.077	3	1.23
83-2	0.013	0.797	2	1.75	4	0.445	2	2.30
83-3	0.006	0.226	1	0.94	3	0.188	1	6.43
83-5	0.007	0.761	1	2.35	11	0.707	1	6.97
84-5D	0.029	0.713	5	0.63	11	-.328	6	1.35
84-5E	0.022	0.796	5	1.60	3	0.992	6	6.38
84-5F	0.021	1.268	5	1.30	4	1.259	3	12.64
84-6E	0.019	0.151	4	2.84	8	0.290	4	3.53
84-6F	0.014	1.365	5	1.35	5	1.516	3	9.66
84-7D	(0.013)	(-.074)	3	(1.10)	(15)	(-.509)	5	(1.31)
84-7E	0.025	0.141	5	8.38	16	0.387	5	11.13
84-7F	0.011	0.056	5	1.43	3	0.250	3	7.66
Mean (11 runs)	0.017	0.642		2.09	6	0.617		6.30
Std. Dev.	0.008	0.449		2.20	4	0.546		3.89

Table 8. Percent correlation of iceberg velocity components with corresponding components of wind and currents.

Iceberg Track	Wind		Current											
			0-10 m		10-20 m		20-30 m		30-40 m		40-50 m		50-60 m	
	E	N	E	N	E	N	E	N	E	N	E	N	E	N
83-1	67	46	75	81	82*	82	59	71	40	72	70	35	72	-39
83-2	53	16	47	76	31*	62	24	50	-1	56	-8	54	-5	40
83-3	22	18	41*	50	20	34	-27	1	-21	-12	-6	14	1	5
83-5	28	28	49*	36	39	33	-18	7	-37	-2	-18	6	-6	9
84-5D	53	28	-	-	-	-	44	65	42	74	43*	44	22	22
84-5E	60	81	-	-	-	-	71	83	77	83	75*	70	74	51
84-5F	14	8	-	-	-	-	51	33	54	36	48*	38	40	43
84-6E	19	67	-	-	-	-	-7	66	-10*	62	-12	38	-21	14
84-6F	2	22	-	-	-	-	63	60	63	64	60*	64	58	67
84-7D	36	42	-	-	-	-	18*	62	13	82	18	64	2	44
84-7E	-30	50	-	-	-	-	-7	42	-12	47	-12*	43	-14	29
84-7F	15	-6	-	-	-	-	21	1	18	3	18*	6	15	7

* Asterisk indicates layer selected in kinematic model.

Attempting to model the iceberg tracks only from the current in one layer resulted in much (3 times) larger errors (Table 7). As in dynamic modelling, we find that wind drift must be included in order to hindcast iceberg tracks. Different layers i and j were selected in fitting Equations 14 and 16 in the majority of cases. The mean value of the c coefficients, 0.62 ± 0.55, was nearly the same as the mean of the b coefficients. We again excluded a negative value for track 84-7D but we did not delete a negative value of c for track 84-5D in calculating the mean.

3. Autocorrelation of velocity

Statistical iceberg drift models (Garrett, 1985a; Gaskill and Rochester, 1984) rely on a site-specific knowledge of the mean iceberg drift rate and the mean autocorrelation time of the iceberg velocity. The icebergs which we located during our cruises were dispersed over a wide area and the quantity of data which we obtained is not sufficient to establish reliable mean autocorrelations. Nevertheless, it is useful to compare the autocorrelations of currents and winds with those of observed iceberg velocities because of the clues which they offer to understanding the physics of iceberg drift. They may also be of value if the present data are to be included in data for statistical modelling.

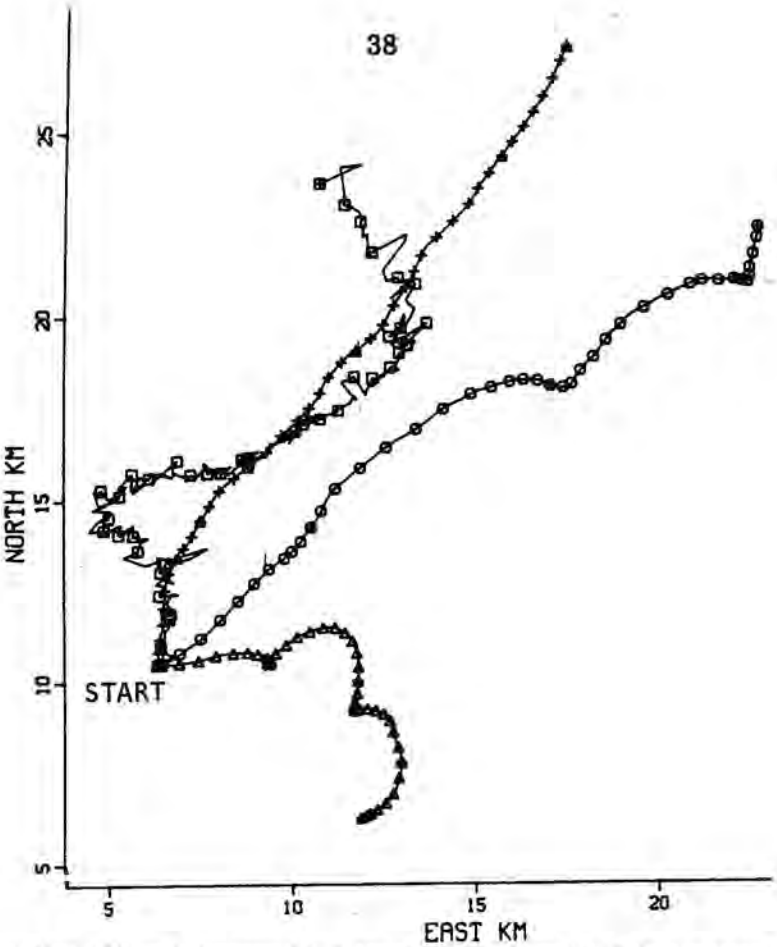

Fig. 12. Modelled (O) and observed (□) tracks of Iceberg 84-7 during period F with $C_A = C_W = 1.0$; winds only (+) and currents only (Δ).

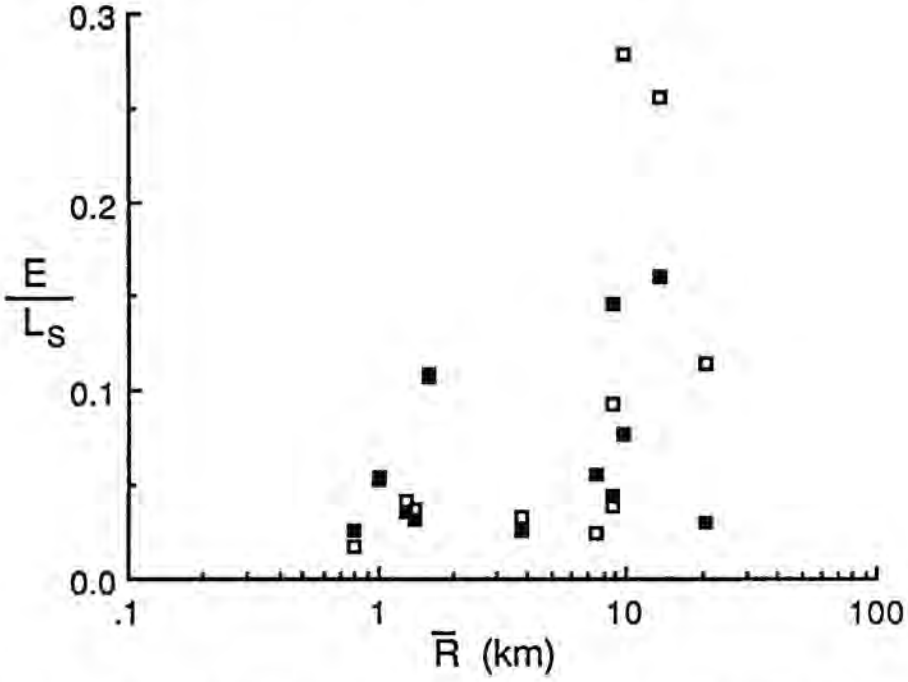

Fig. 13. Comparison of errors in dynamic model (■) and kinematic model (□), as a fraction of distance travelled, plotted, against average range from ship to iceberg.

For each iceberg track the velocity autocorrelation is shown in Appendix 7 in two different forms. The first plot shows the autocorrelation of the east and north components of velocity, calculated independently:

$$C_i(\tau) = \overline{V_i(t)V_i(t+\tau)} / \overline{V_i^2}, \; i = 1, 2 \tag{18}$$

By definition $C_i(0) = 1$. Typically the autocorrelation falls to zero at a lag of from 3 to 6 hours and then oscillates about zero for longer lags. This is generally characteristic of either semi-diurnal tidal motion or of motion at inertial periods; our records are not long enough to distinguish unambiguously between the two. An exception is period E of 1984 (tracks 6E, 7E and 8E), during which the autocorrelations fall off more or less linearly to zero at a lag of 6 to 18 hours.

In the second type of plot we express the velocity vector as a complex number

$$V(t) = V_1(t) + iV_2(t) \tag{19}$$

where V_1 and V_2 are the east and northward components, respectively. The correlation coefficient

$$C(\tau) = \overline{V(t)^* V(T+\tau)} / \overline{|V^2|} \tag{20}$$

is also a complex number which can be expressed as

$$C(\tau) = R(\tau)e^{i\theta(\tau)} \tag{21}$$

where $R(\tau)$ is the magnitude of the correlation and $\theta(\tau)$ is the rotation of the velocity vector during the lag time τ. At zero lag, by definition, $R(0) = 1$ and $\theta(0) = 0$. Predominantly clockwise motion results in anticlockwise rotation of C with increasing τ, and vice versa. For example, purely inertial motion of an iceberg in a circular or elliptical track is characterized by $R(\tau) = 1$ and $\theta(\tau)$ sweeping through a full circle in one inertial period. The track of Iceberg 83-2 (Appendix 7) resembles this case except that R decreases with increasing τ due to other components of the motion.

Complex autocorrelation of the current in the 20-30 m layer is shown in Appendix 7, except for track 83-5, 84-7D, 84-7E and 84-7F in which the measured currents were identical to those for other tracks and in these cases the complex autocorrelation of the wind is shown instead. The current tends to be more rotational than the iceberg velocity. The autocorrelations for iceberg velocity and currents show generally cyclonic motion (turning to the right) with periods of approximately 12 to 16 hours, indicating tidal or inertial influences. Period E of 1984 is the only one with anticyclonic rotation. The motions in 1983, in the Strait of Belle Isle and on the southern Labrador shelf, are more periodic than those in 1984 on the Grand Banks. The wind has a much longer period of autocorrelation, of the order of 24 to 48 hours, and is less influenced by regular oscillation.

G. CONCLUSIONS

1. A data set has been collected in the Strait of Belle Isle, on the Labrador shelf and on the Grand Banks with iceberg drift tracks, current profiles, winds, and estimates of iceberg mass and cross-sections. The use of an acoustic Doppler current profiler has resulted in unprecedented detail of the current profile.

2. A dynamic model with fixed air and water drag coefficients was able to reasonably represent the majority of the observed tracks with currents measured within 9 km average range from the iceberg. The mean rms error in position was 3.2 km. Clockwise loops in several of the tracks were not very well reproduced by the model.

3. A multi-layer dynamic model with optimized air and water drag coefficients was able to hindcast the measured iceberg tracks with a mean rms error of 1.2 km, if currents were measured within 9 km average range of an iceberg.

4. In three cases it was necessary in the dynamic model to rotate the wind force by up to 30° from the measured wind direction. Failure to rotate wind forces in these cases resulted in the selection of extremely high or low drag coefficients in an attempt to influence the direction of modelled wind drift through the Coriolis deflection.

5. The principal force balance in the model was between wind and water drag. For a given set of coefficients the presence of current shear greatly reduced the rate of wind drift due to the nonlinear (quadratic) water drag formulation.

6. In cases where the currents were measured at a longer average range of 10 to 21 km from an iceberg, the dynamic model fitted the observed tracks with relatively larger rms errors of 11 to 28% of the length of the track.

7. A simple kinematic model, using wind velocity and current velocity in one selected layer, was able to represent the iceberg tracks with about the same accuracy as the dynamic model. Where the currents were measured at longer ranges from the iceberg the kinematic model performed somewhat better than the dynamic model, primarily due to relaxing a constraint of the dynamic model to follow a depth-weighted current plus wind-induced drift.

8. The wind drift component of the kinematic model averaged 1.7% of the wind speed. Deletion of the wind drift term resulted in greatly increased the errors.

9. Sample data are listed in Appendix 8. The dynamic model and the data files are available on computer diskette by writing to the authors.

10. In an operational situation, forecasts of tidal and wind-driven components of current may be developed, based on accumulated data at the site, and may be used together with forecast winds to drive a dynamic or kinematic forecast model. Statistics of forecast verification errors at a given site can then be accumulated and used to estimate probability

distributions surrounding the forecst drift track, following the methods of Garrett (1984, 1985).

REFERENCES

Banke, E.G. and S.D. Smith. 1984. A Hindcast Study of Iceberg Drift on the Labrador Coast. Can. Tech. Rep. Hydrogr. Ocean Sci. 49, vi + 161 p.

Bowen, A.J. and H.W. Teunissen. 1986. Correction factors for the directional response of Gill propeller anemoneters. Boundary-layer Meteorol. 37, 407-413.

Cochrane, N.A. 1985. An operational evaluation of an Ametek Straza DCP-4400 300 kHz Doppler current profiler aboard CSS Dawson. Can. Tech. Rep. Hydrogr. Ocean Sci. 68, iii + 52 p.

Elliott, J.A. 1981. Anemometer blockage on CSS Dawson. AOL Research Note No. 1, 14 pp. (Available from the author).

Garrett, C.J.R. 1984. Statistical prediction of iceberg trajectories. Iceberg Research, 1, 7, 3-7.

Garrett, C.J.R. 1985. Statistical prediction of iceberg trajectories. Cold Regions Sci Technol., 11, 255-266.

Garrett, C.J.R., J. Middleton, M. Hazen and F. Majaess. 1985a. Tidal currents and eddy statistics from iceberg trajectories off Labrador. Science, 227, 1333-1335.

Garrett, C.J.R., J.F. Middleton, F. Majaess and M. Hazen. 1985b. Analysis and prediction of iceberg trajectories. Internal Report, Dept. of Oceanography, Dalhousie University, 86 pp. (Available from the Authors).

Gaskill, H.S. and J. Rochester. 1984. A new technique for iceberg drift prediction. Cold Regions Sci. Technol. 8, 223-234.

Ice Engineering Ltd. 1983. Iceberg Survey, The Strait of Belle Isle, Newfoundland (Revised April, 1985). PERD Contract Report. (Available at BIO Library, C-CORE Library).

Ice Engineering Ltd. 1984. Iceberg Survey, Grand-Banks-Hibernia, Newfoundland. PERD Contract Report. (Available at BIO Library, C-CORE Library).

Ice Engineering Ltd. 1985. Iceberg Survey, Grand-Banks-Hibernia, Newfoundland. PERD Contract Report, 91 pp. (Available at BIO Library, C-CORE Library).

Mountain, D.C. 1980. On predicting iceberg drift. Cold Regions Sci. Tech., 1, 273-282.

Smith, S.D. 1983. Cruise Report 83-018, CSS Dawson, June 21 - July 4, 1983. Bedford Institute of Oceanography, 42 pp.

Smith, S.D and E.G. Banke. 1983. The influence of winds, currents and towing force on the drift of icebergs. Cold Regions Sci. Technol. 6, 241-245.

Smith, S.D. 1983. Cruise Report 83-018, CSS Dawson, June 21-July 4, 1983. Bedford Institute of Oceanography, 42 pp.

Smith, S.D. 1984. Cruise Report 84-023, CSS Dawson, Iceberg Tracking, Newfoundland Shelf, June 5 - 20, 1984. Bedford Institute of Oceanography, 26 pp.

Smith, S.D. 1985. Cruise Report 85-008, CSS Dawson, Iceberg Dynamics, Grand Banks, April 22 - May 6, 1985. Bedford Institute of Oceanography, 25 pp.

Smith, S.D. and N.R. Donaldson. 1987. Innovations in dynamic modelling of iceberg drift. Prlc. IEEE Oceans 87, Halifax, Sept. 28 - Oct. 1, 1987, 6 pp.

Sodhi, D.S. and M. El-Tahan. 1980. Prediction of an iceberg drift trajectory during a storm. Ann. Glaciol., 1, 77-82.

APPENDIX 1 PHOTOGRAPHS OF ICEBERGS

Fig. A1.1. Iceberg 83-1 (Photo by D. Hendsbee)

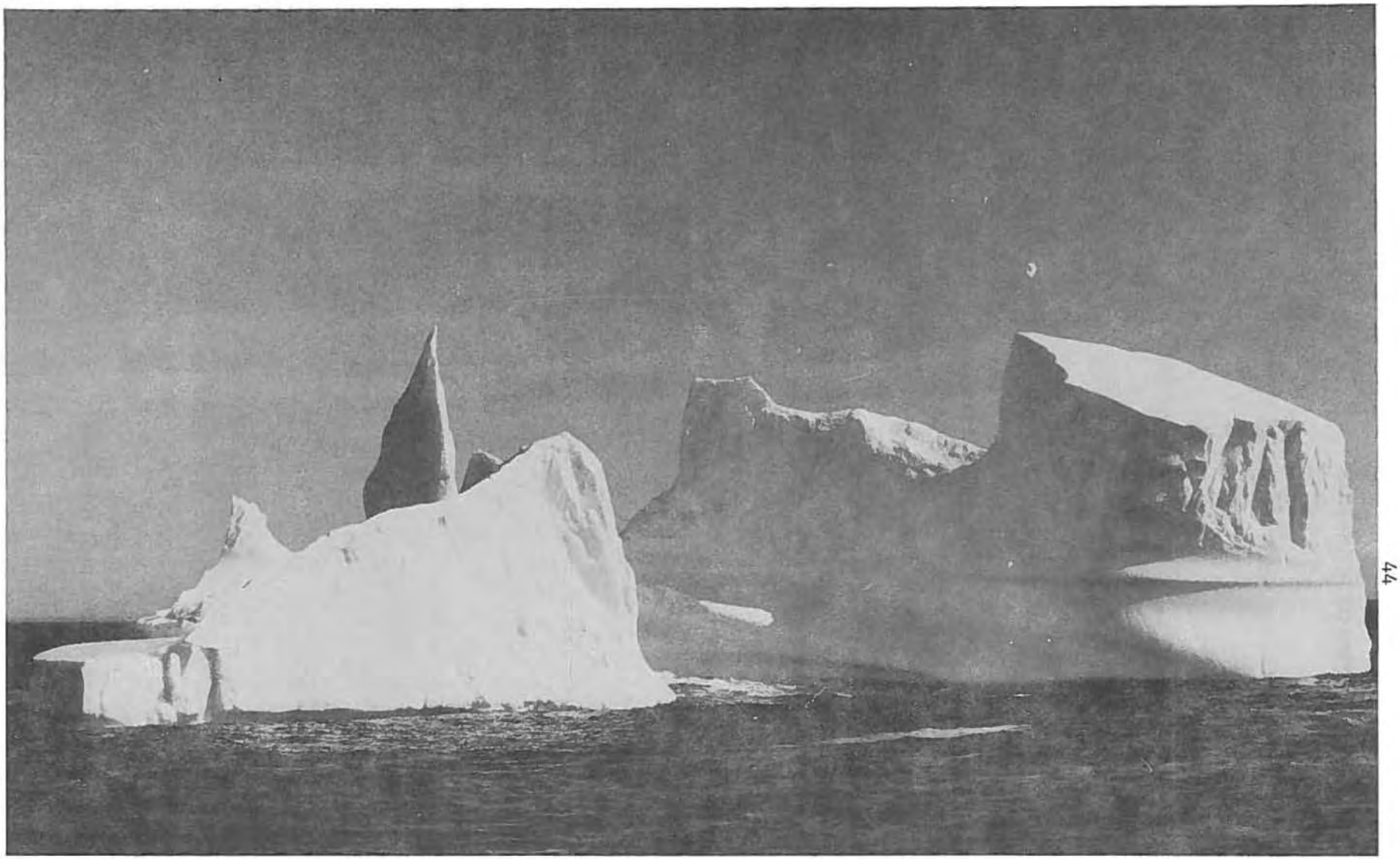

Fig. A1.2. Iceberg 83-2

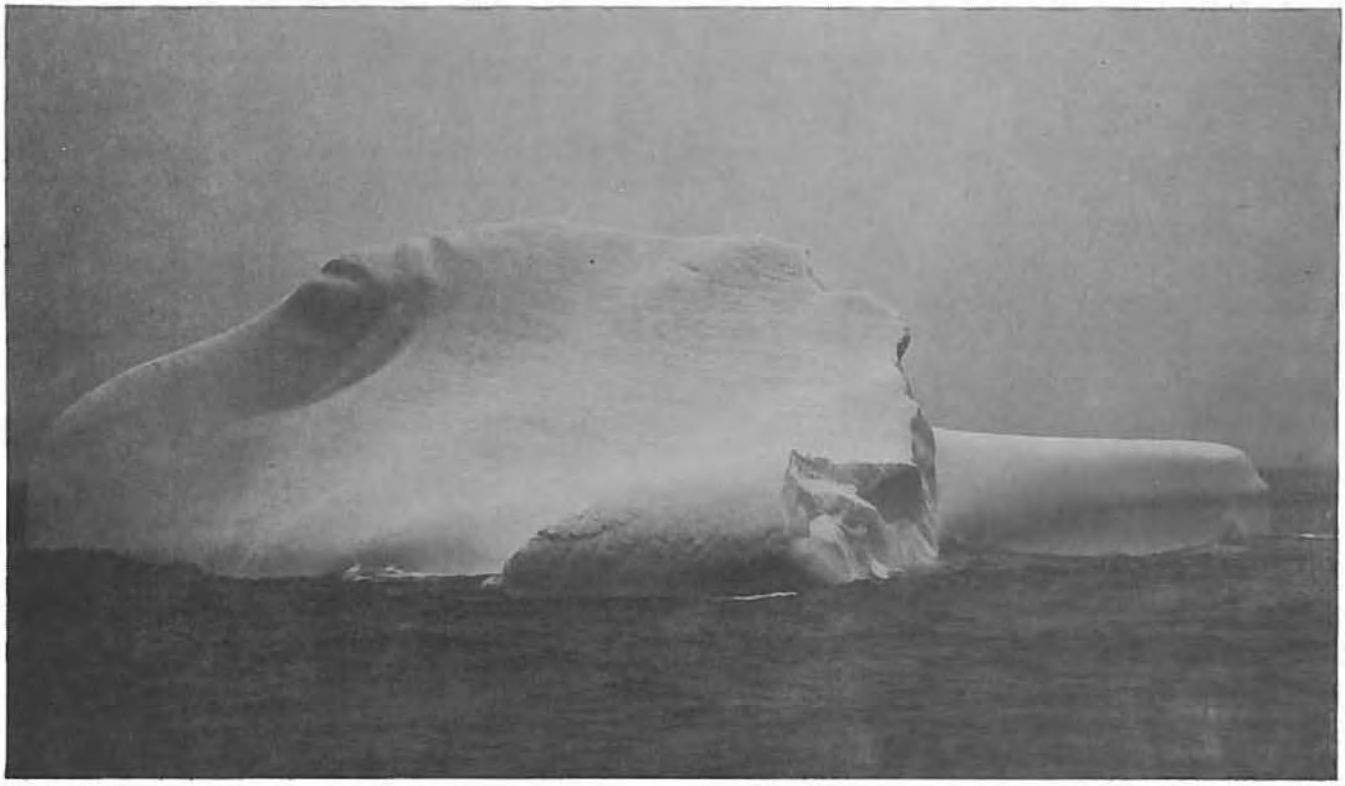

Fig. A1.3. Iceberg 83-3

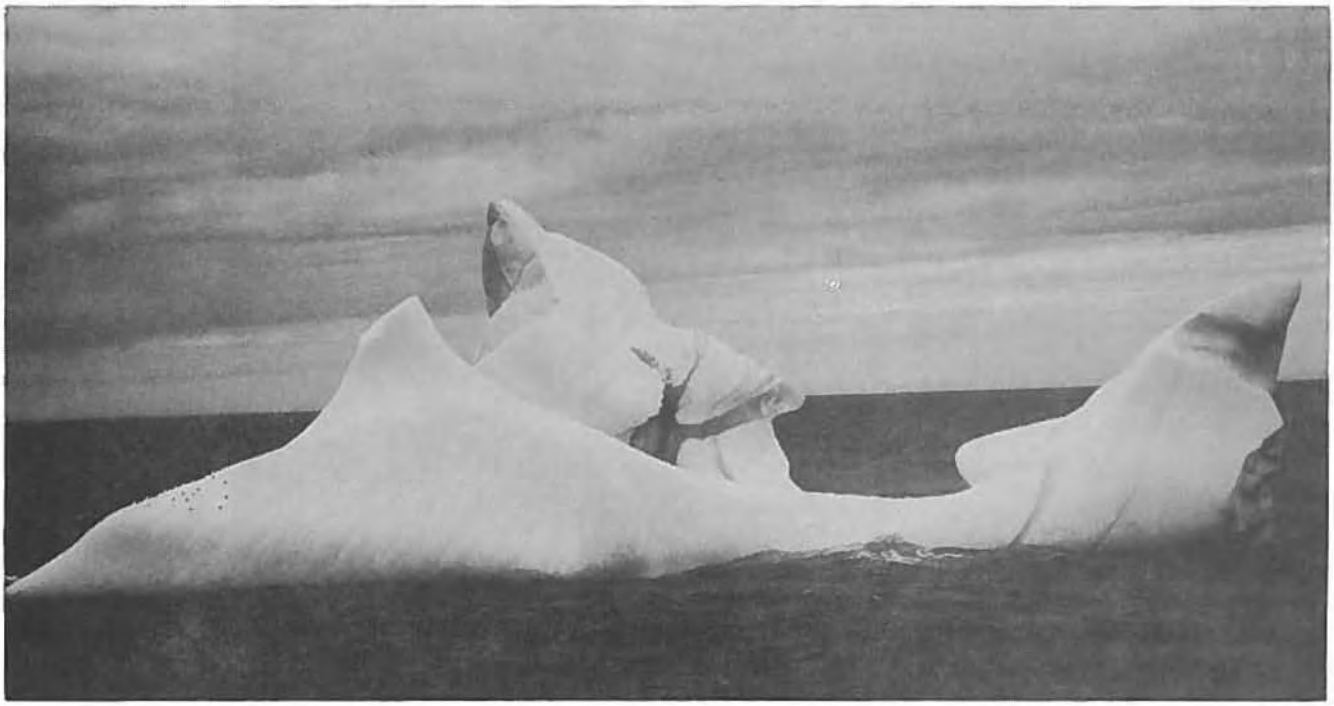

Fig. A1.4. Iceberg 83-5

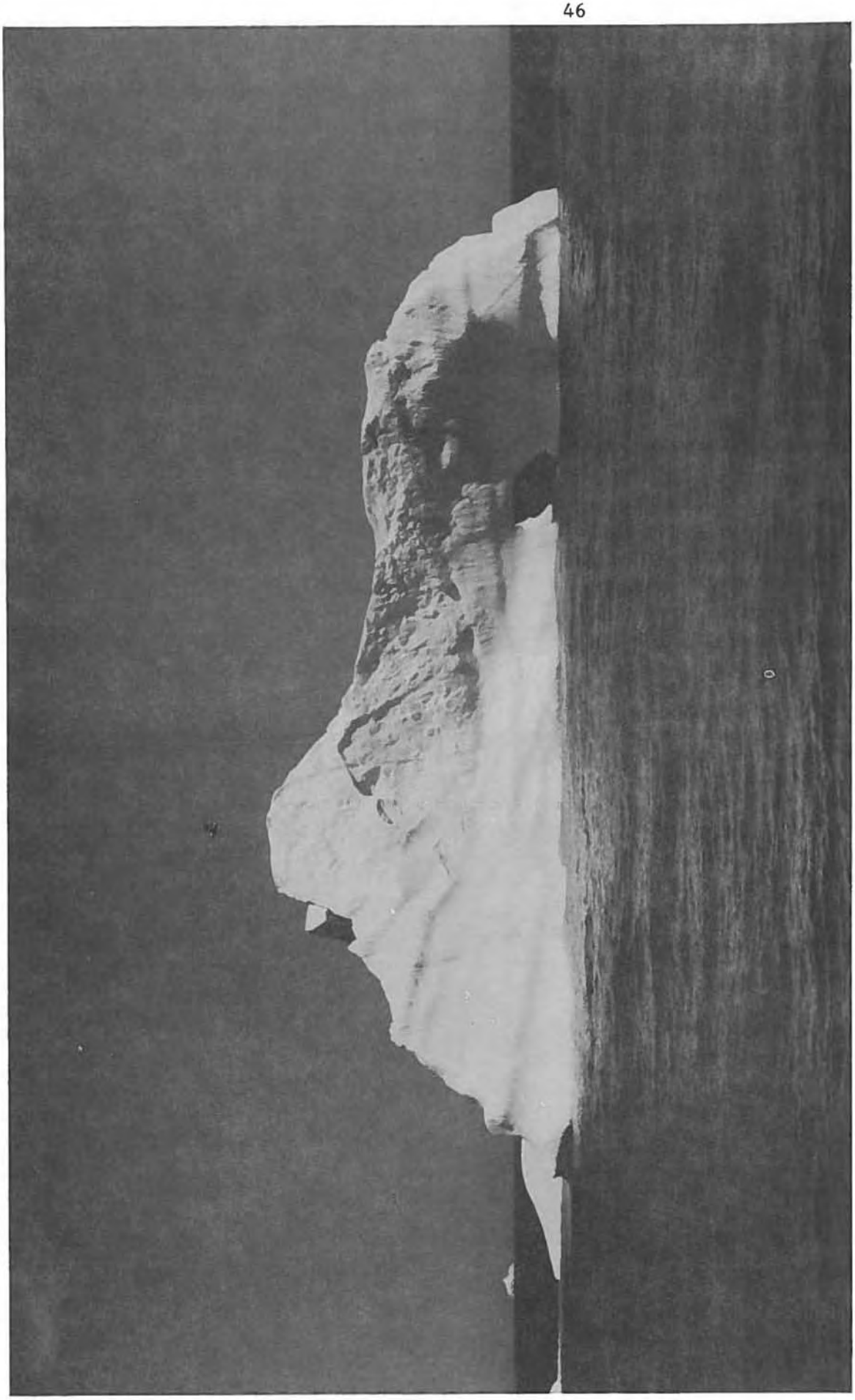

Fig. A1.5. Iceberg 84-5

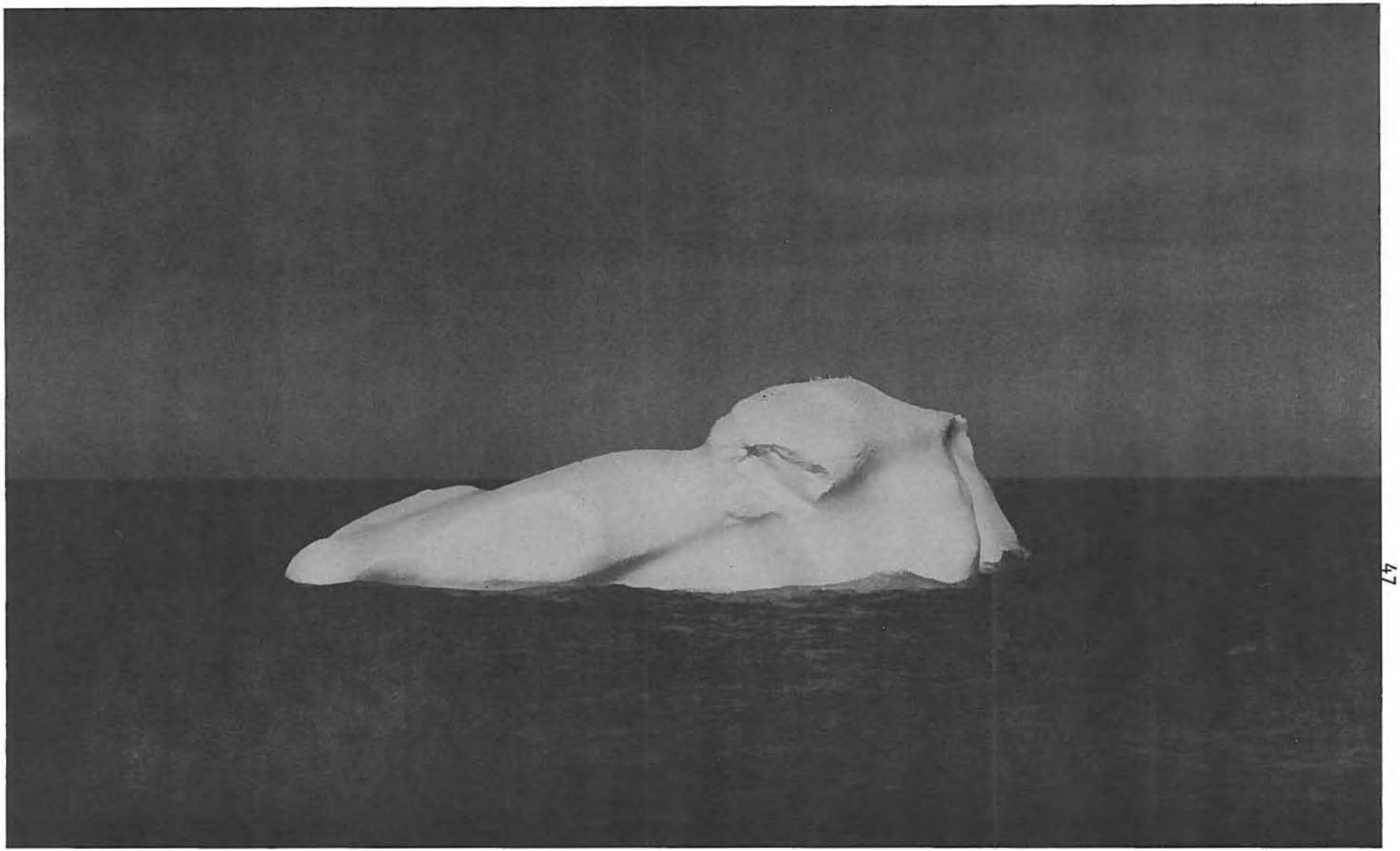

Fig. A1.6. Iceberg 84-6

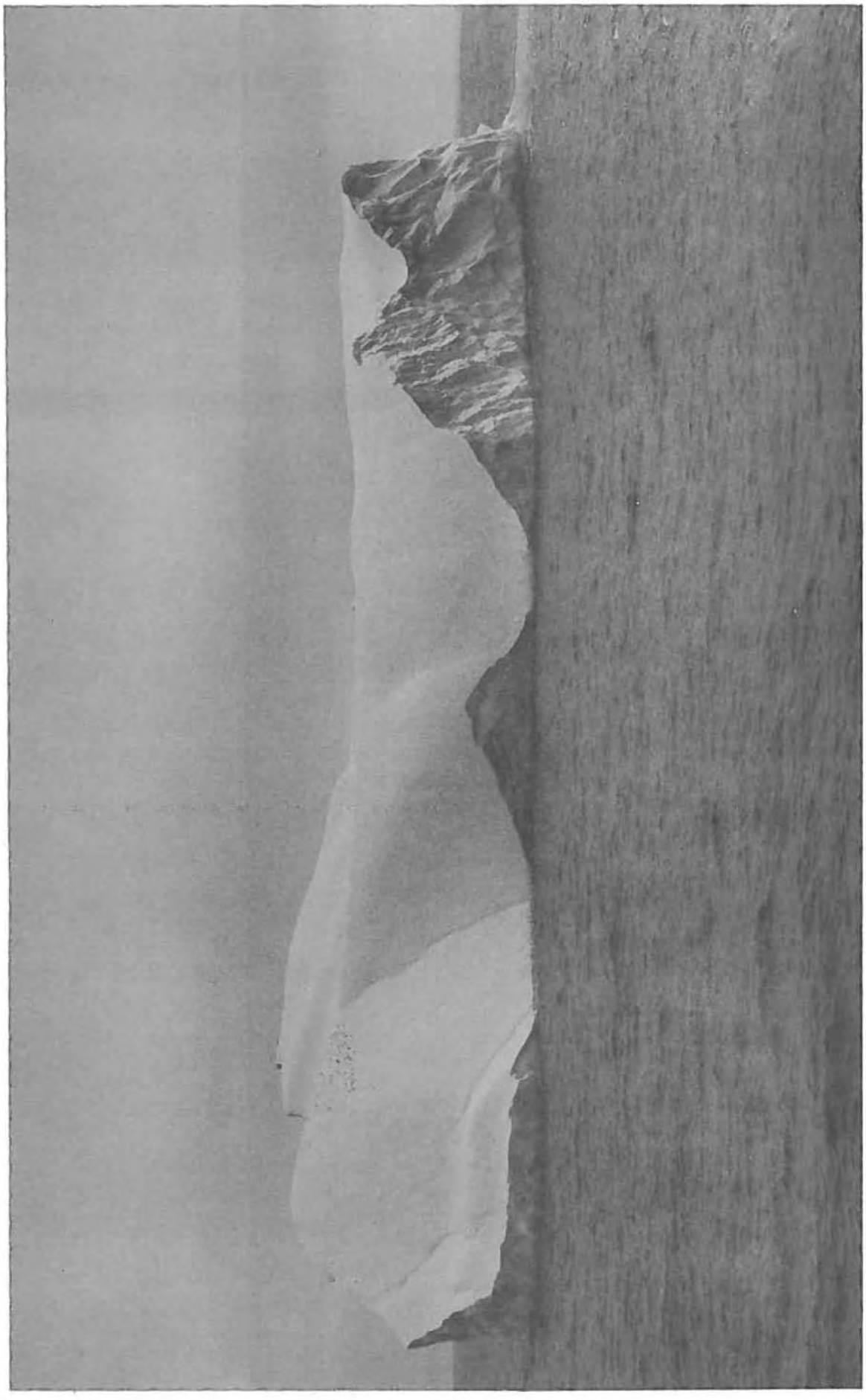

Fig. A1.7. Iceberg 84-7

Fig. A1.8. Iceberg 85-1

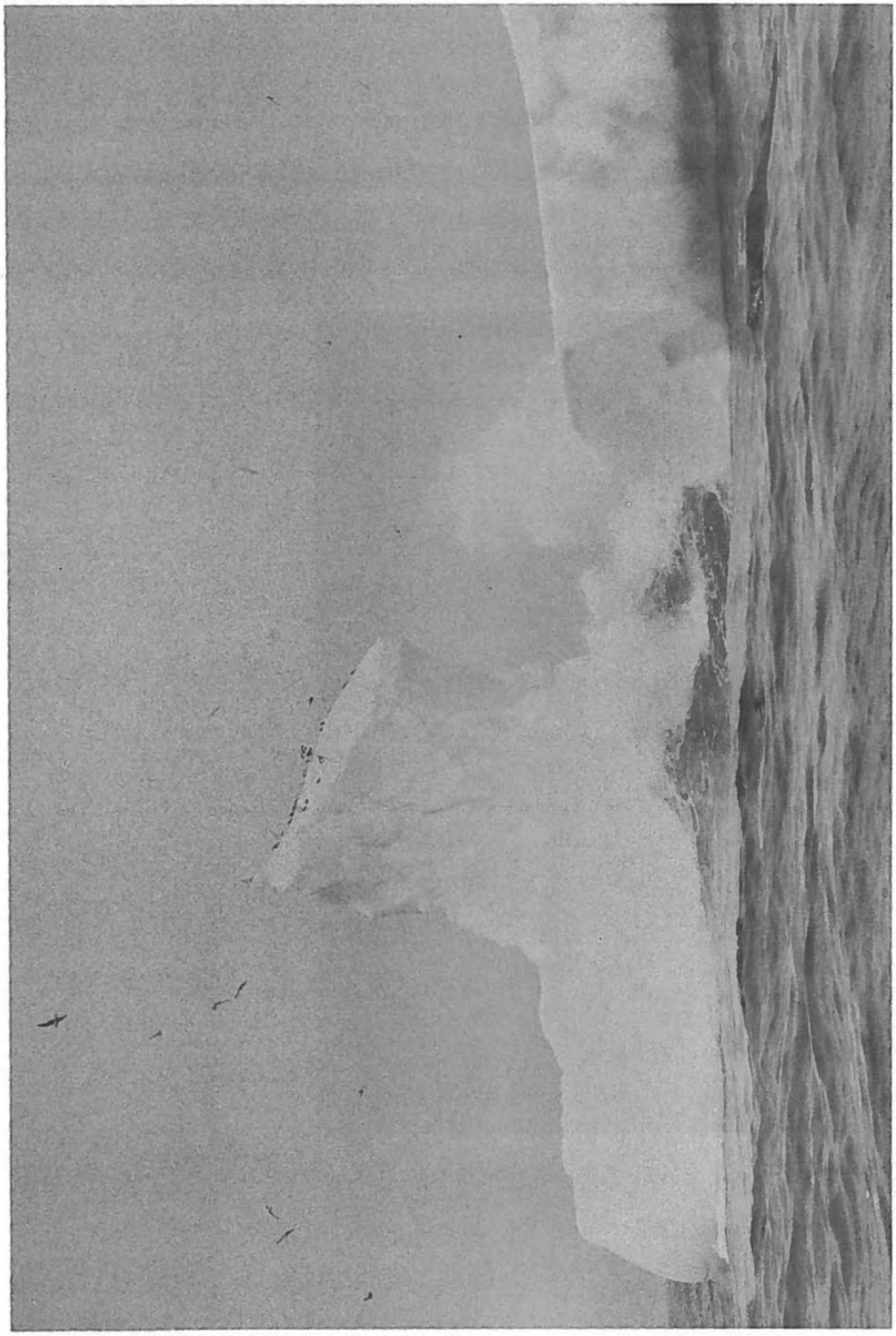

Fig. A1.9. Iceberg 85-4

APPENDIX 2 CROSS-SECTIONS OF ICEBERGS

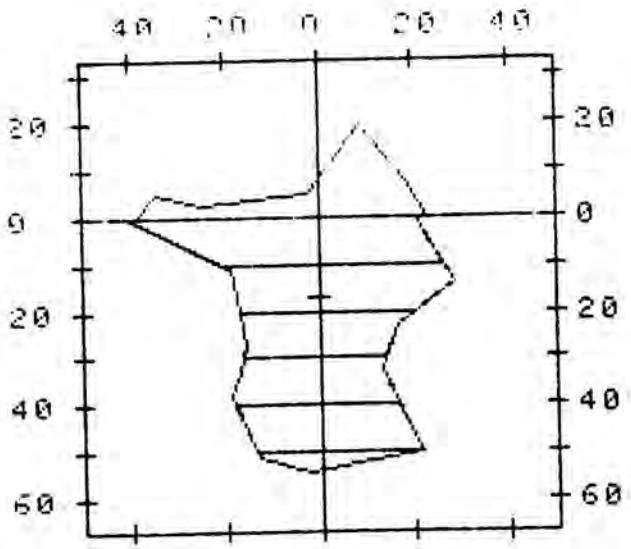

BIO 1 36 deg. S of W

THE TOTAL CROSSSECTION IS
2,444.4 m sq.

THE ABOVE-WATER CROSSSECTION IS
403.3 m sq.

THE BELOW-WATER CROSSSECTION IS
2,041.1 m sq.

SLICE AREA:

Upper m	Lower m	AREA m sq
0.0	10.0	541.6
10.0	20.0	434.8
20.0	30.0	319.6
30.0	40.0	322.3
40.0	50.0	348.6
50.0	54.0	74.7

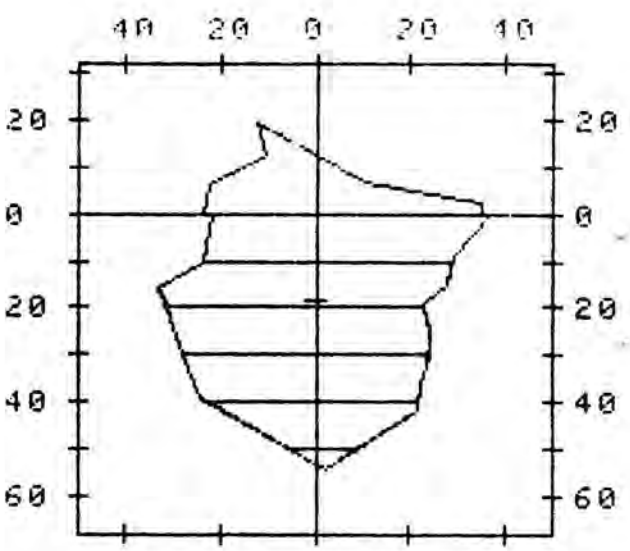

BIO 1 23 Deg EAST of SOUTH

THE TOTAL CROSSSECTION IS
2,947.5 m sq.

THE ABOVE-WATER CROSSSECTION IS
486.3 m sq.

THE BELOW-WATER CROSSSECTION IS
2,461.3 m sq.

SLICE AREA:

Upper m	Lower m	AREA m sq
0.0	10.0	549.9
10.0	20.0	566.2
20.0	30.0	533.6
30.0	40.0	484.5
40.0	50.0	300.1
50.0	54.0	26.9

Fig. A2.1. Cross-sections of Iceberg 83-1

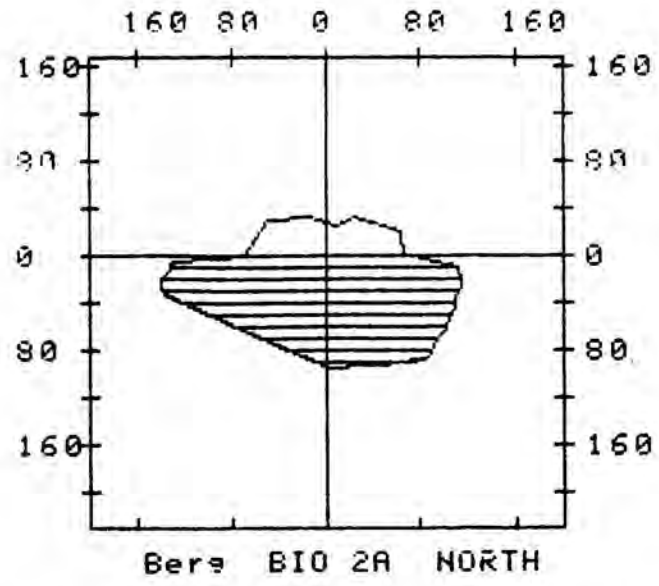

THE TOTAL CROSSSECTION IS
21,424.8 m sq.

THE ABOVE-WATER CROSSSECTION IS
3,534.9 m sq.

THE BELOW-WATER CROSSSECTION IS
17,889.9 m sq.

SLICE AREA:

Upper m	Lower m	AREA m sq
0.0	10.0	2,049.7
10.0	20.0	2,469.5
20.0	30.0	2,533.8
30.0	40.0	2,425.6
40.0	50.0	2,191.7
50.0	60.0	1,916.9
60.0	70.0	1,646.0
70.0	80.0	1,345.1
80.0	90.0	1,065.8
90.0	96.0	245.8

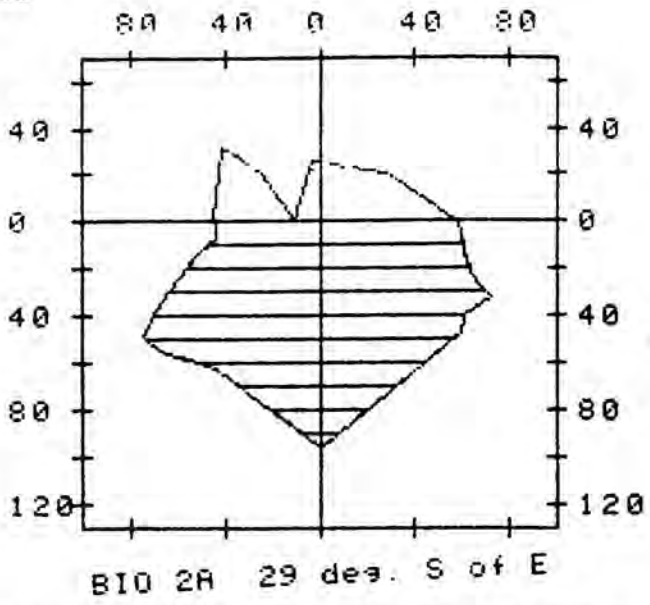

THE TOTAL CROSSSECTION IS
10,652.4 m sq.

THE ABOVE-WATER CROSSSECTION IS
1,757.7 m sq.

THE BELOW-WATER CROSSSECTION IS
8,894.7 m sq.

SLICE AREA:

Upper m	Lower m	AREA m sq
0.0	10.0	1,034.7
10.0	20.0	1,140.3
20.0	30.0	1,257.1
30.0	40.0	1,345.3
40.0	50.0	1,327.4
50.0	60.0	1,148.9
60.0	70.0	784.9
70.0	80.0	531.2
80.0	90.0	278.6
90.0	96.0	45.6

Fig. A2.2. Cross-sections of Iceberg 83-2A

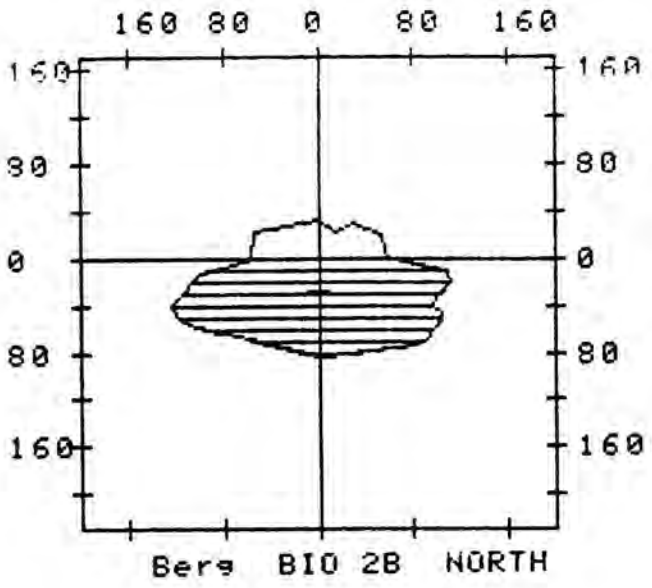

THE TOTAL CROSSSECTION IS
17,997.2 m sq.

THE ABOVE-WATER CROSSSECTION IS
2,969.4 m sq.

THE BELOW-WATER CROSSSECTION IS
15,027.8 m sq.

SLICE AREA:

Upper m	Lower m	AREA m sq
0.0	10.0	1,533.0
10.0	20.0	2,093.4
20.0	30.0	2,179.0
30.0	40.0	2,187.2
40.0	50.0	2,219.2
50.0	60.0	2,078.6
60.0	70.0	1,675.9
70.0	80.0	1,001.8
80.0	83.0	59.7

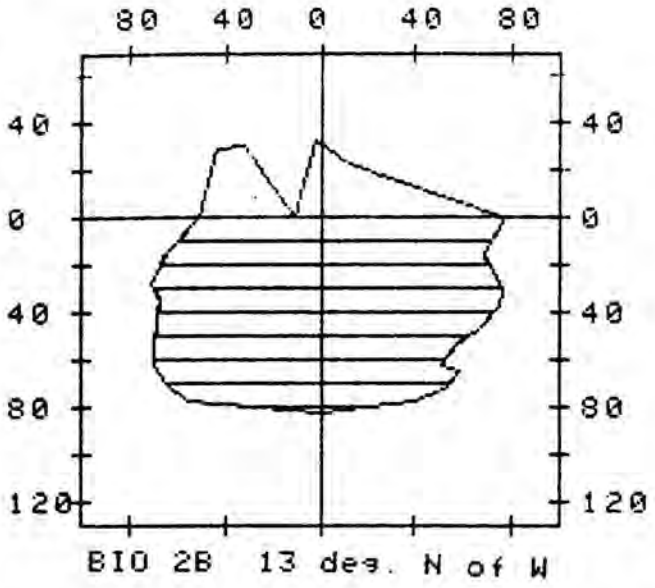

THE TOTAL CROSSSECTION IS
12,425 8 m sq.

THE ABOVE-WATER CROSSSECTION IS
2,050.2 m sq.

THE BELOW-WATER CROSSSECTION IS
10,375.6 m sq.

SLICE AREA:

Upper m	Lower m	AREA m sq
0.0	10.0	1,289.8
10.0	20.0	1,336.1
20.0	30.0	1,420.9
30.0	40.0	1,431.3
40.0	50.0	1,362.3
50.0	60.0	1,265.1
60.0	70.0	1,227.0
70.0	80.0	971.4
80.0	83.0	71.7

Fig. A2.3. Cross-sections of Iceberg 83-2B

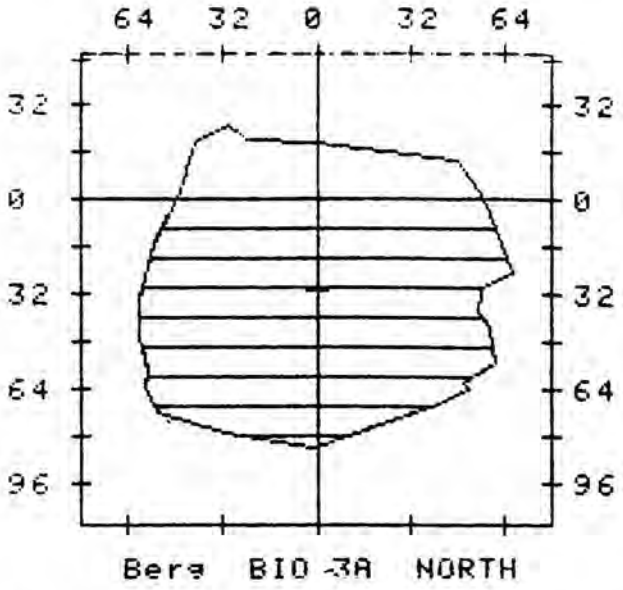

THE TOTAL CROSSSECTION IS
10,477.2 m sq.

THE ABOVE-WATER CROSSSECTION IS
1,728.6 m sq.

THE BELOW-WATER CROSSSECTION IS
8,748.5 m sq.

SLICE AREA:

Upper m	Lower m	AREA m sq
0.0	10.0	1,082.3
10.0	20.0	1,173.1
20.0	30.0	1,209.0
30.0	40.0	1,147.4
40.0	50.0	1,187.6
50.0	60.0	1,163.1
60.0	70.0	1,042.6
70.0	80.0	673.6
80.0	84.0	69.9

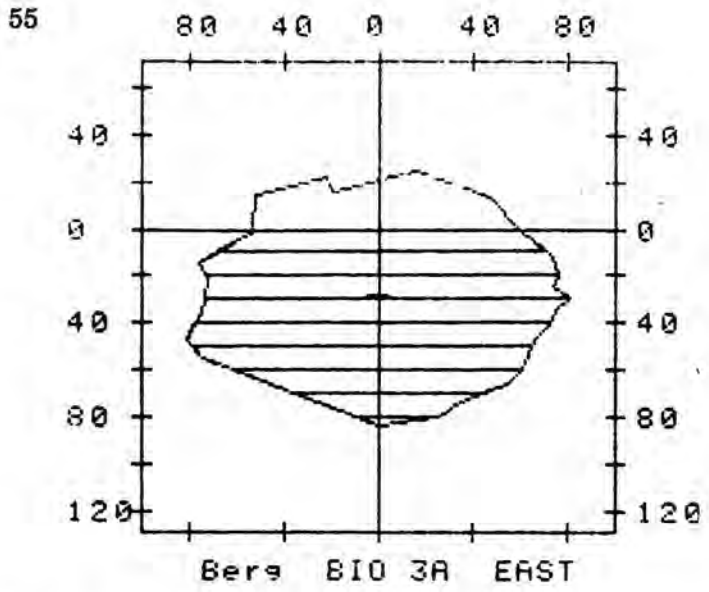

THE TOTAL CROSSSECTION IS
12,203.8 m sq.

THE ABOVE-WATER CROSSSECTION IS
2,013.7 m sq.

THE BELOW-WATER CROSSSECTION IS
10,190.1 m sq.

SLICE AREA:

Upper m	Lower m	AREA m sq
0.0	10.0	1,258.8
10.0	20.0	1,475.7
20.0	30.0	1,486.5
30.0	40.0	1,497.8
40.0	50.0	1,471.6
50.0	60.0	1,346.8
60.0	70.0	1,028.5
70.0	80.0	553.8
80.0	84.0	70.5

Fig. A2.4. Cross-sections of Iceberg 83-3A

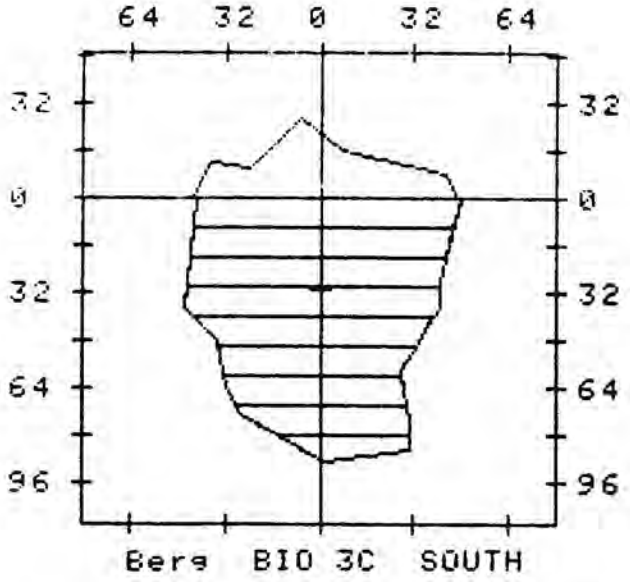

THE TOTAL CROSSSECTION IS
7,484.5 m sq.

THE ABOVE-WATER CROSSSECTION IS
1,234.9 m sq.

THE BELOW-WATER CROSSSECTION IS
6,249.6 m sq.

SLICE AREA:

Upper m	Lower m	AREA m sq
0.0	10.0	888.1
10.0	20.0	873.2
20.0	30.0	858.7
30.0	40.0	852.9
40.0	50.0	733.6
50.0	60.0	633.4
60.0	70.0	596.8
70.0	80.0	534.3
80.0	89.0	278.6

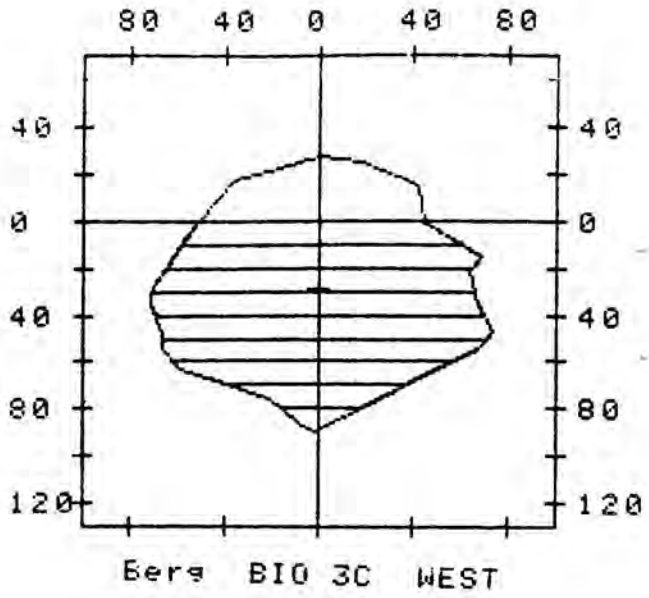

THE TOTAL CROSSSECTION IS
11,275.0 m sq.

THE ABOVE-WATER CROSSSECTION IS
1,860.3 m sq.

THE BELOW-WATER CROSSSECTION IS
9,414.7 m sq.

SLICE AREA:

Upper m	Lower m	AREA m sq
0.0	10.0	1,064.9
10.0	20.0	1,268.8
20.0	30.0	1,324.3
30.0	40.0	1,376.3
40.0	50.0	1,390.3
50.0	60.0	1,305.9
60.0	70.0	993.0
70.0	80.0	527.5
80.0	89.0	163.7

Fig. A2.5. Cross-sections of Iceberg 83-3C

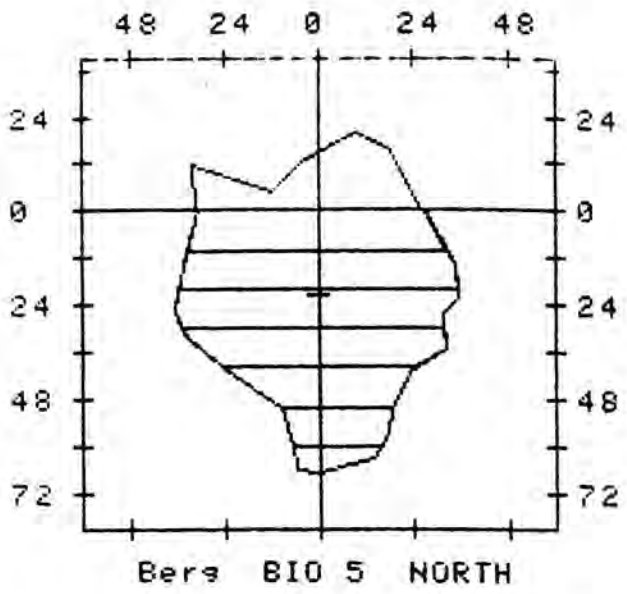

THE TOTAL CROSSSECTION IS
3,978.9 m sq.

THE ABOVE-WATER CROSSSECTION IS
656.5 m sq.

THE BELOW-WATER CROSSSECTION IS
3,322.4 m sq.

SLICE AREA:

Upper m	Lower m	AREA m sq
0.0	10.0	614.8
10.0	20.0	685.1
20.0	30.0	685.7
30.0	40.0	598.6
40.0	50.0	378.1
50.0	60.0	251.0
60.0	67.0	109.0

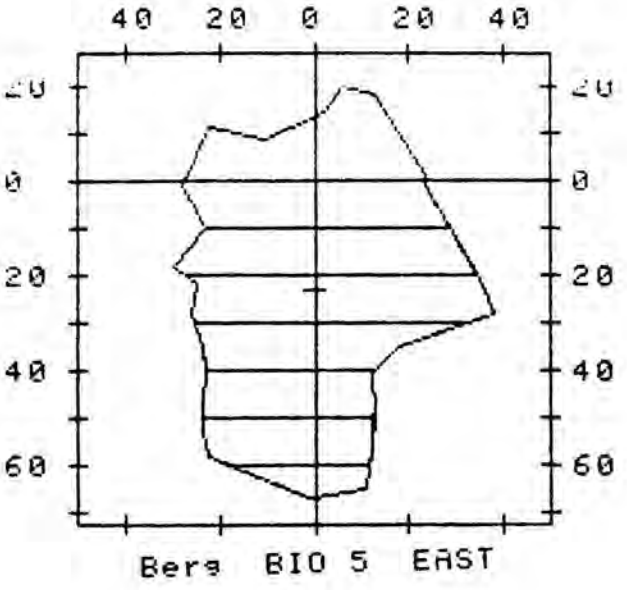

THE TOTAL CROSSSECTION IS
3,584.4 m sq.

THE ABOVE-WATER CROSSSECTION IS
591.4 m sq.

THE BELOW-WATER CROSSSECTION IS
2,993.0 m sq.

SLICE AREA:

Upper m	Lower m	AREA m sq
0.0	10.0	515.0
10.0	20.0	581.0
20.0	30.0	614.4
30.0	40.0	443.6
40.0	50.0	356.8
50.0	60.0	347.7
60.0	67.0	132.6

Fig. A2.6. Cross-sections of Iceberg 83-5

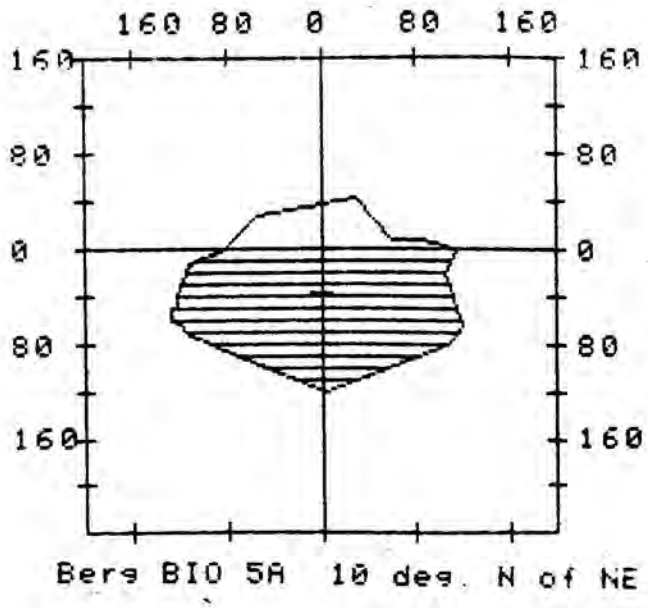

THE TOTAL CROSSSECTION IS
26,445.4 m sq.

THE ABOVE-WATER CROSSSECTION IS
4,363.3 m sq.

THE BELOW-WATER CROSSSECTION IS
22,082.1 m sq.

SLICE AREA:

Upper m	Lower m	AREA m sq
0.0	10.0	2,045.6
10.0	20.0	2,192.4
20.0	30.0	2,221.1
30.0	40.0	2,305.6
40.0	50.0	2,349.6
50.0	60.0	2,425.3
60.0	70.0	2,363.9
70.0	80.0	2,175.2
80.0	90.0	1,750.6
90.0	100.0	1,256.5
100.0	110.0	750.3
110.0	120.0	256.1

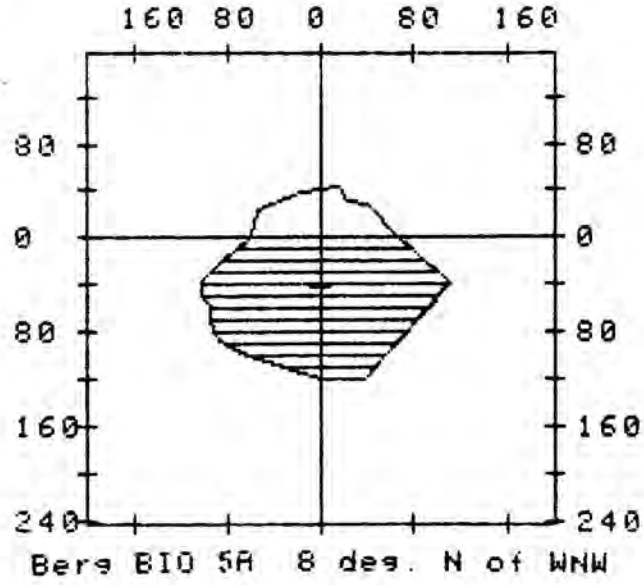

THE TOTAL CROSSSECTION IS
22,514.1 m sq.

THE ABOVE-WATER CROSSSECTION IS
3,714.7 m sq.

THE BELOW-WATER CROSSSECTION IS
18,799.3 m sq.

SLICE AREA:

Upper m	Lower m	AREA m sq
0.0	10.0	1,372.2
10.0	20.0	1,608.3
20.0	30.0	1,845.3
30.0	40.0	2,045.6
40.0	50.0	2,060.6
50.0	60.0	1,922.5
60.0	70.0	1,801.0
70.0	80.0	1,701.6
80.0	90.0	1,566.3
90.0	100.0	1,327.1
100.0	110.0	973.6
110.0	120.0	573.1

Fig. A2.7. Cross-sections of Iceberg 84-5A

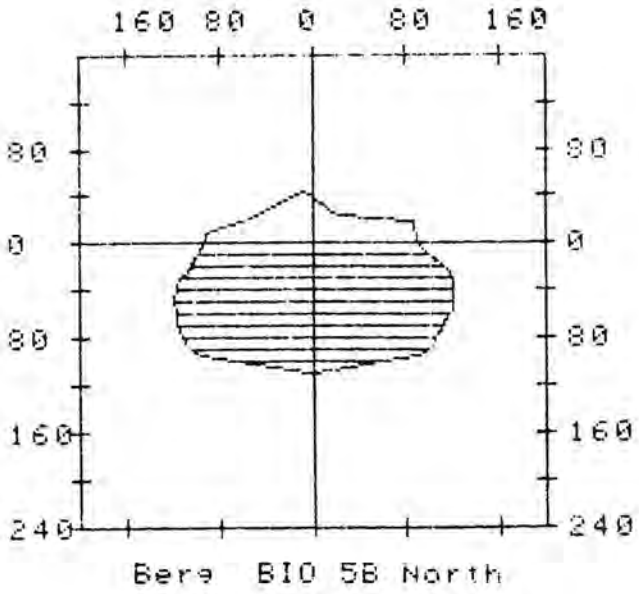

THE TOTAL CROSSSECTION IS
26,712.0 m sq.

THE ABOVE-WATER CROSSSECTION IS
4,407.2 m sq.

THE BELOW-WATER CROSSSECTION IS
22,304.7 m sq.

SLICE AREA:

Upper m	Lower m	AREA m sq
0.0	10.0	1,897.8
10.0	20.0	2,072.7
20.0	30.0	2,243.9
30.0	40.0	2,342.0
40.0	50.0	2,377.6
50.0	60.0	2,371.2
60.0	70.0	2,300.5
70.0	80.0	2,216.3
80.0	90.0	2,097.7
90.0	100.0	758.1
100.0	110	37.0

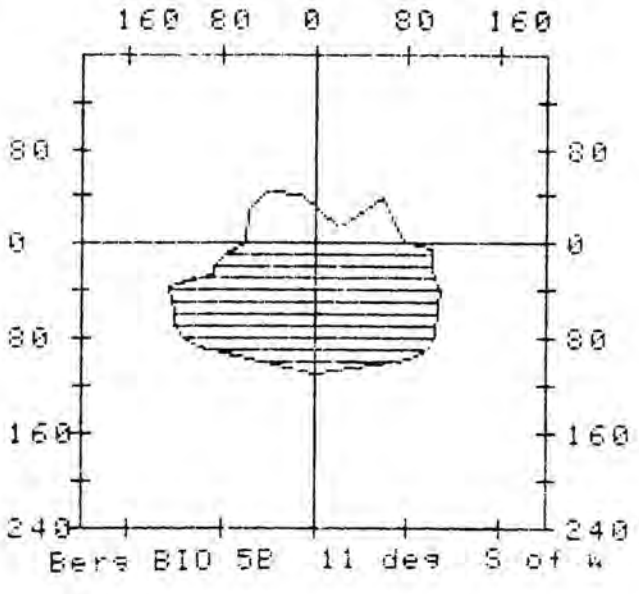

THE TOTAL CROSSSECTION IS
24,854.5 m sq.

THE ABOVE-WATER CROSSSECTION IS
4,101.0 m sq.

THE BELOW-WATER CROSSSECTION IS
20,753.4 m sq

SLICE AREA

Upper m	Lower m	AREA m sq
0.0	10.0	1,625.6
10.0	20.0	1,823.0
20.0	30.0	1,927.3
30.0	40.0	2,243.4
40.0	50.0	2,322.7
50.0	60.0	2,272.3
60.0	70.0	2,244.5
70.0	80.0	2,193.5
80.0	90.0	2,024.3
90.0	100.0	1,523.6
100.0	110.0	546.6

Fig. A2.8. Cross-sections of Iceberg 84-5B

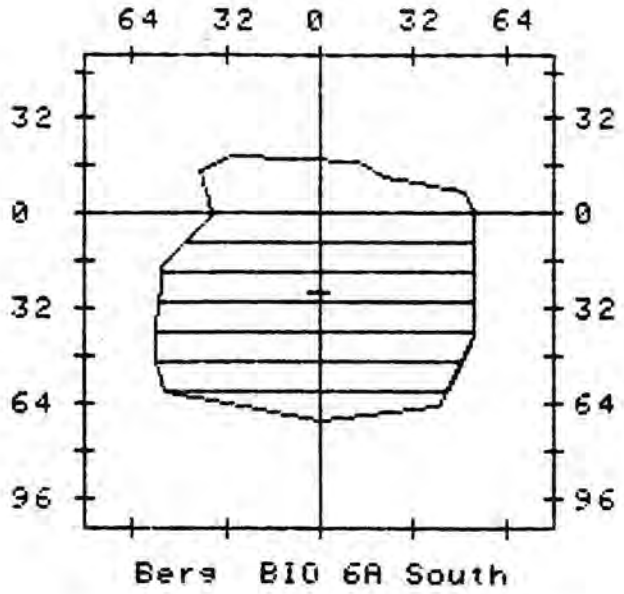

THE TOTAL CROSSSECTION IS
8,079.6 m sq.

THE ABOVE-WATER CROSSSECTION IS
1,333.1 m sq.

THE BELOW-WATER CROSSSECTION IS
6,746.5 m sq.

SLICE AREA:

Upper m	Lower m	AREA m sq
0.0	10.0	935.8
10.0	20.0	1,034.3
20.0	30.0	1,068.0
30.0	40.0	1,077.7
40.0	50.0	1,060.7
50.0	60.0	996.7
60.0	70.0	573.2

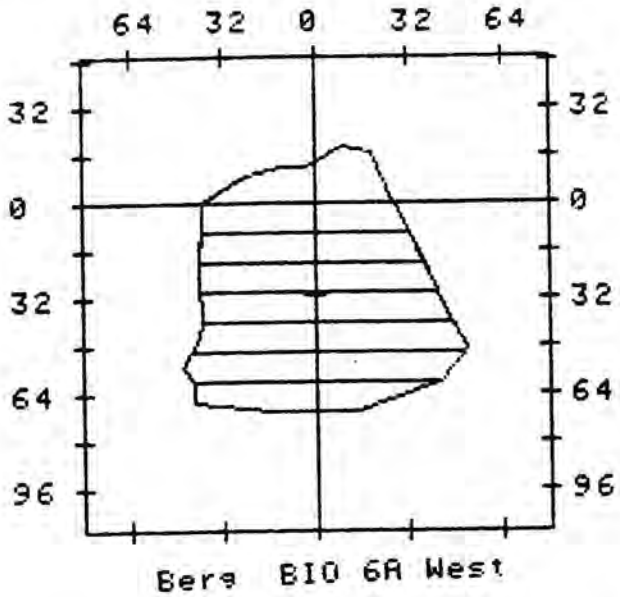

THE TOTAL CROSSSECTION IS
6,233.4 m sq.

THE ABOVE-WATER CROSSSECTION IS
733.5 m sq.

THE BELOW-WATER CROSSSECTION IS
5,499.9 m sq.

SLICE AREA:

Upper m	Lower m	AREA m sq
0.0	10.0	690.8
10.0	20.0	736.2
20.0	30.0	785.8
30.0	40.0	823.5
40.0	50.0	894.5
50.0	60.0	903.9
60.0	70.0	656.2

Fig. A2.9. Cross-sections of Iceberg 84-6A

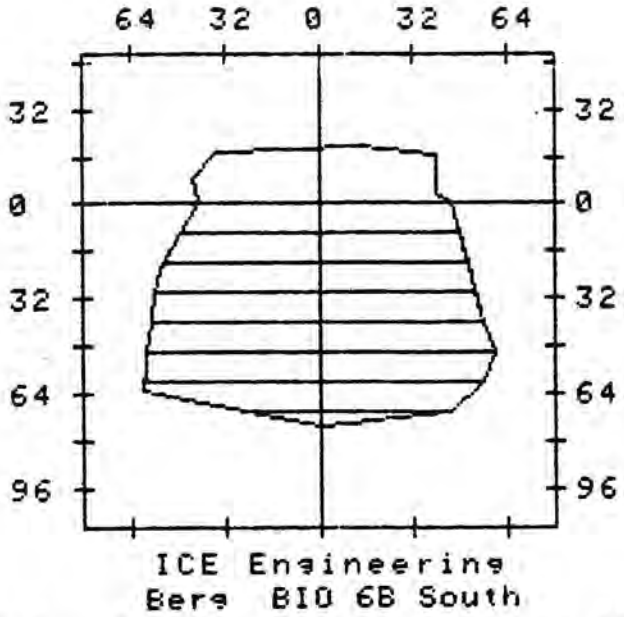

THE TOTAL CROSSSECTION IS

9,014.4 m sq.

THE ABOVE-WATER CROSSSECTION IS

1,487.4 m sq.

THE BELOW-WATER CROSSSECTION IS

7,527.0 m sq.

SLICE AREA:

Upper m	Lower m	AREA m sq
0.0	10.0	897.7
10.0	20.0	985.4
20.0	30.0	1,056.1
30.0	40.0	1,108.2
40.0	50.0	1,159.0
50.0	60.0	1,166.6
60.0	70.0	978.5
70.0	75.0	173.5

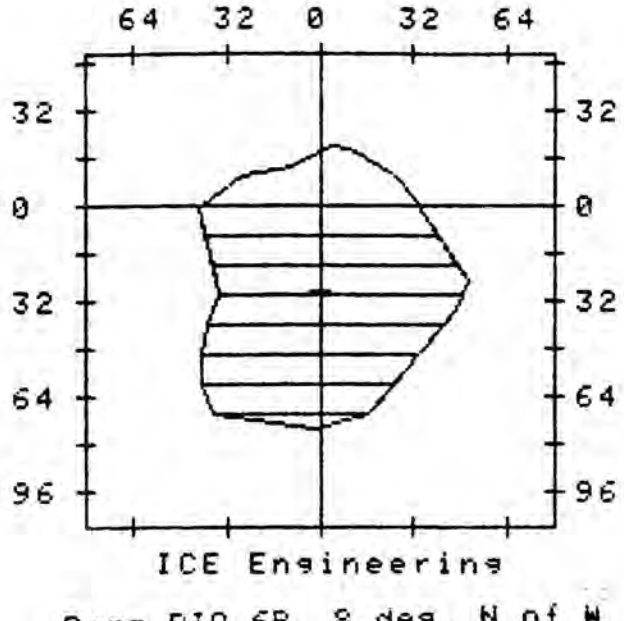

THE TOTAL CROSSSECTION IS

6,389.6 m sq.

THE ABOVE-WATER CROSSSECTION IS

894.5 m sq.

THE BELOW-WATER CROSSSECTION IS

5,495.2 m sq.

SLICE AREA:

Upper m	Lower m	AREA m sq
0.0	10.0	777.3
10.0	20.0	820.9
20.0	30.0	851.4
30.0	40.0	829.4
40.0	50.0	779.8
50.0	60.0	704.1
60.0	70.0	598.4
70.0	75.0	133.9

Fig. A2.10. Cross-sections of Iceberg 84-6B

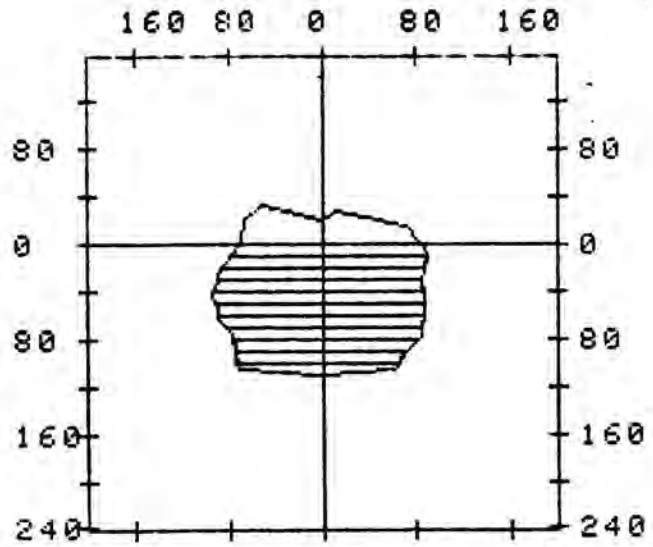

THE TOTAL CROSSSECTION IS

21,120.0 m sq.

THE ABOVE-WATER CROSSSECTION IS

3,484.8 m sq.

THE BELOW-WATER CROSSSECTION IS

17,635.3 m sq.

SLICE AREA:

Upper m	Lower m	AREA m sq
0.0	10.0	1,602.0
10.0	20.0	1,685.2
20.0	30.0	1,727.2
30.0	40.0	1,766.0
40.0	50.0	1,807.0
50.0	60.0	1,767.8
60.0	70.0	1,708.8
70.0	80.0	1,612.1
80.0	90.0	1,519.6
90.0	100.0	1,424.4
100.0	110.0	1,015.2

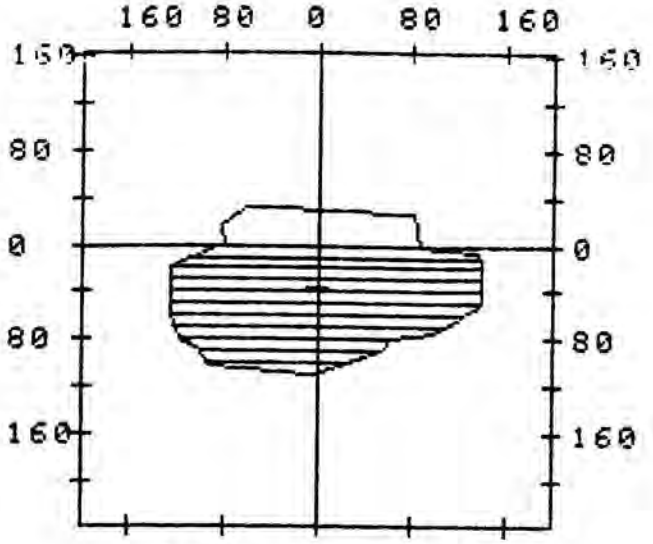

THE TOTAL CROSSSECTION IS

28,035.8 m sq.

THE ABOVE-WATER CROSSSECTION IS

4,625.8 m sq.

THE BELOW-WATER CROSSSECTION IS

23,410.0 m sq.

SLICE AREA:

Upper m	Lower m	AREA m sq
0.0	10.0	2,183.6
10.0	20.0	2,548.7
20.0	30.0	2,641.7
30.0	40.0	2,640.2
40.0	50.0	2,642.5
50.0	60.0	2,551.0
60.0	70.0	2,417.8
70.0	80.0	2,106.8
80.0	90.0	1,633.3
90.0	100.0	1,370.4
100.0	110.0	673.9

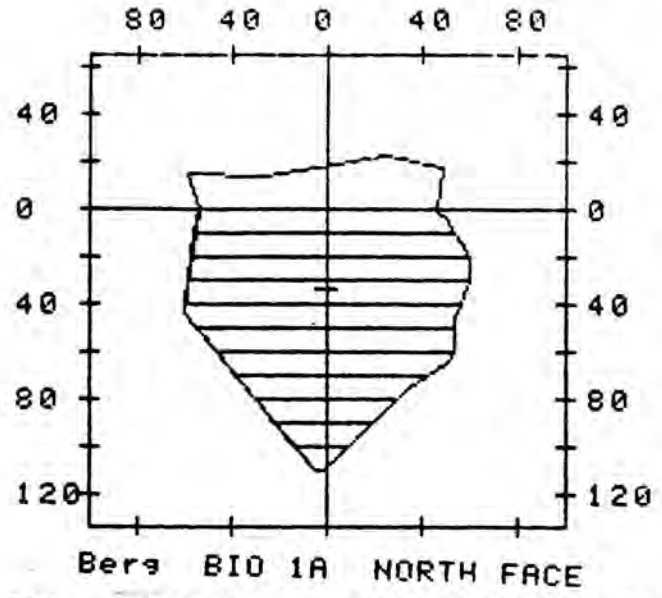

THE TOTAL CROSSSECTION IS

11,042.4 m sq.

THE ABOVE-WATER CROSSSECTION IS

1,822.0 m sq.

THE BELOW-WATER CROSSSECTION IS

9,220.4 m sq.

SLICE AREA:

Upper m	Lower m	AREA m sq
0.0	10.0	1,044.4
10.0	20.0	1,128.1
20.0	30.0	1,168.2
30.0	40.0	1,161.4
40 0	50.0	1,125.4
50.0	60.0	1,041.4
60.0	70.0	905.5
70.0	80.0	695.8
80.0	90.0	503 4
90.0	100.0	316.8
100.0	110.0	130.2

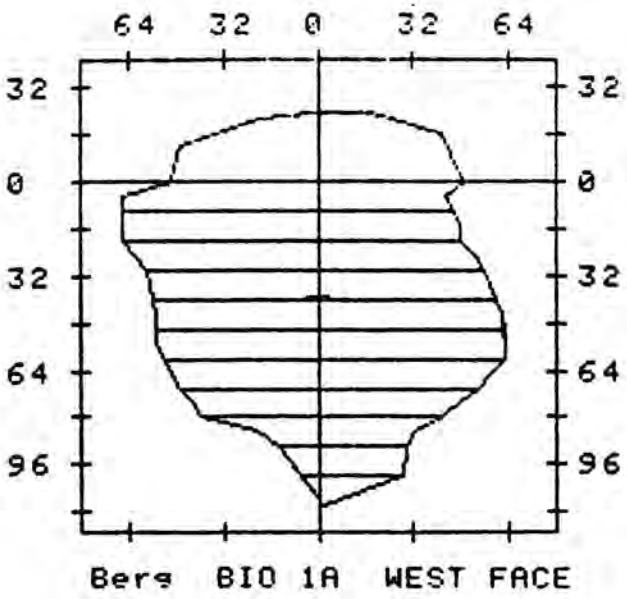

THE TOTAL CROSSSECTION IS

11,733.6 m sq.

THE ABOVE-WATER CROSSSECTION IS

1,818.6 m sq.

THE BELOW-WATER CROSSSECTION IS

9,915.0 m sq.

SLICE AREA:

Upper m	Lower m	AREA m sq
0.0	10.0	1,065.1
10.0	20.0	1,124.0
20.0	30.0	1,138.0
30.0	40.0	1,143.3
40.0	50.0	1,163.7
50.0	60.0	1,163.3
60.0	70.0	1,075.3
70.0	80.0	904.3
80.0	90.0	577.5
90.0	100.0	388.2
100.0	110.0	172.4

Fig. A2.12. Cross-sections of Iceberg 1985-1A

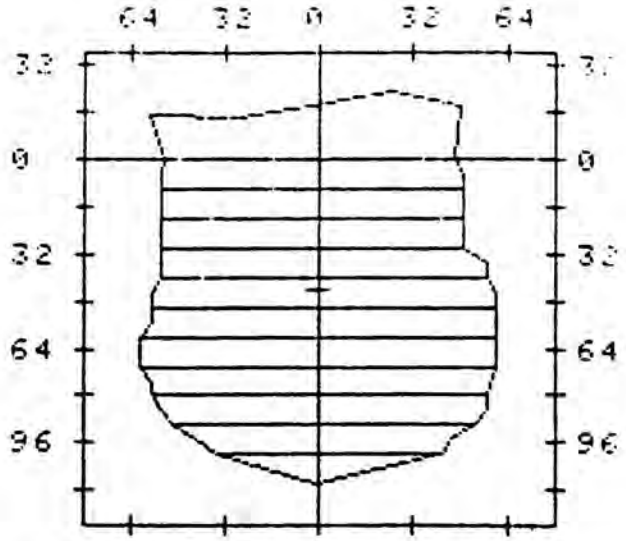

Berg BIO 1B NORTH FACE

THE TOTAL CROSSSECTION IS
12,993.8 m sq.

THE ABOVE-WATER CROSSSECTION IS
1,822.0 m sq.

THE BELOW-WATER CROSSSECTION IS
11,171.8 m sq.

SLICE AREA:

Upper m	Lower m	AREA m sq
0.0	10.0	1,011.2
10.0	20.0	1,020.2
20.0	30.0	1,020.2
30.0	40.0	1,076.5
40.0	50.0	1,151.5
50.0	60.0	1,179.6
60.0	70.0	1,207.7
70.0	80.0	1,160.8
80.0	90.0	1,085.8
90.0	100.0	879.6
100.0	110.0	378.9

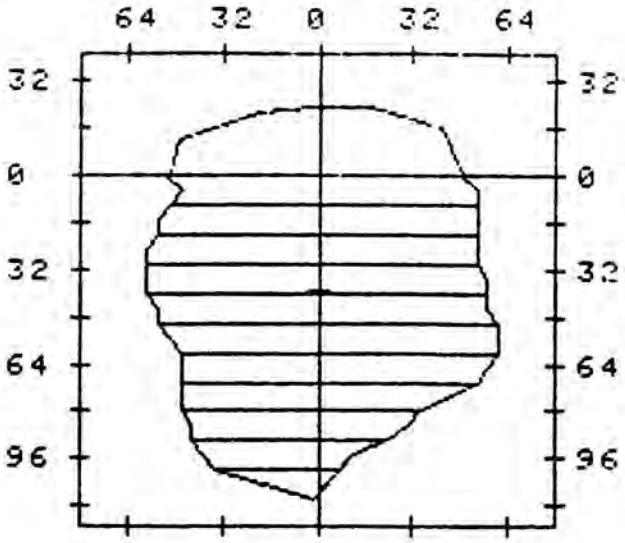

Berg BIO 1B WEST FACE

THE TOTAL CROSSSECTION IS
11,732.7 m sq.

THE ABOVE-WATER CROSSSECTION IS
1,818.6 m sq.

THE BELOW-WATER CROSSSECTION IS
9,914.1 m sq.

SLICE AREA:

Upper m	Lower m	AREA m sq
0.0	10.0	1,000.5
10.0	20.0	1,057.5
20.0	30.0	1,095.2
30.0	40.0	1,133.2
40.0	50.0	1,123.5
50.0	60.0	1,104.5
60.0	70.0	1,029.5
70.0	80.0	907.5
80.0	90.0	729.7
90.0	100.0	521.8
100.0	110.0	211.5

Fig. A2.13. Cross-sections of Iceberg 85-1B

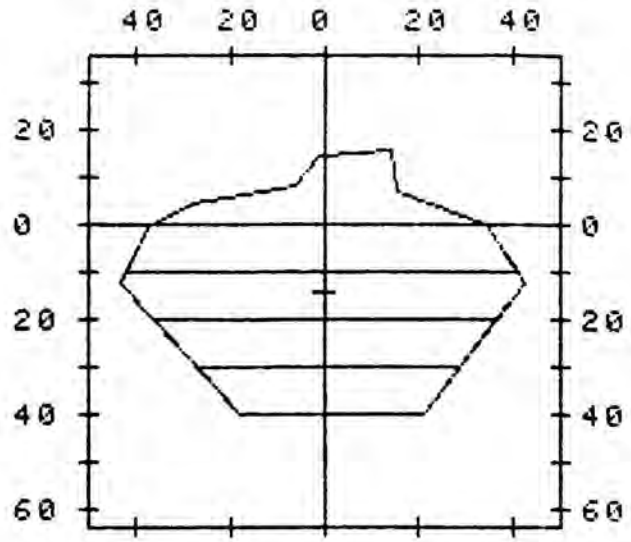

Berg BIO 4 SOUTH FACE

THE TOTAL CROSSSECTION IS
3,210.9 m sq.

THE ABOVE-WATER CROSSSECTION IS
529.8 m sq.

THE BELOW-WATER CROSSSECTION IS
2,681.1 m sq.

SLICE AREA:

Upper m	Lower m	AREA m sq
0.0	10.0	770.6
10.0	20.0	801.1
20.0	30.0	639.3
30.0	40.0	470.2

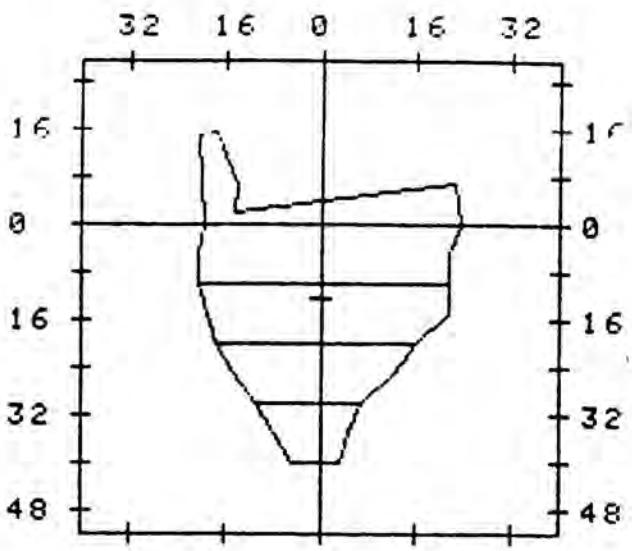

BIO 4 EAST FACE

THE TOTAL CROSSSECTION IS
1,434.7 m sq.

THE ABOVE-WATER CROSSSECTION IS
243.9 m sq.

THE BELOW-WATER CROSSSECTION IS
1,190.8 m sq.

SLICE AREA:

Upper m	Lower m	AREA m sq
0.0	10.0	419.0
10.0	20.0	387.1
20.0	30.0	258.1
30.0	40.0	126.6

Fig. A2.14. Cross-sections of Iceberg 85-4

APPENDIX 3 TIME SERIES OF VELOCITIES OF ICEBERGS, CURRENTS AND WINDS

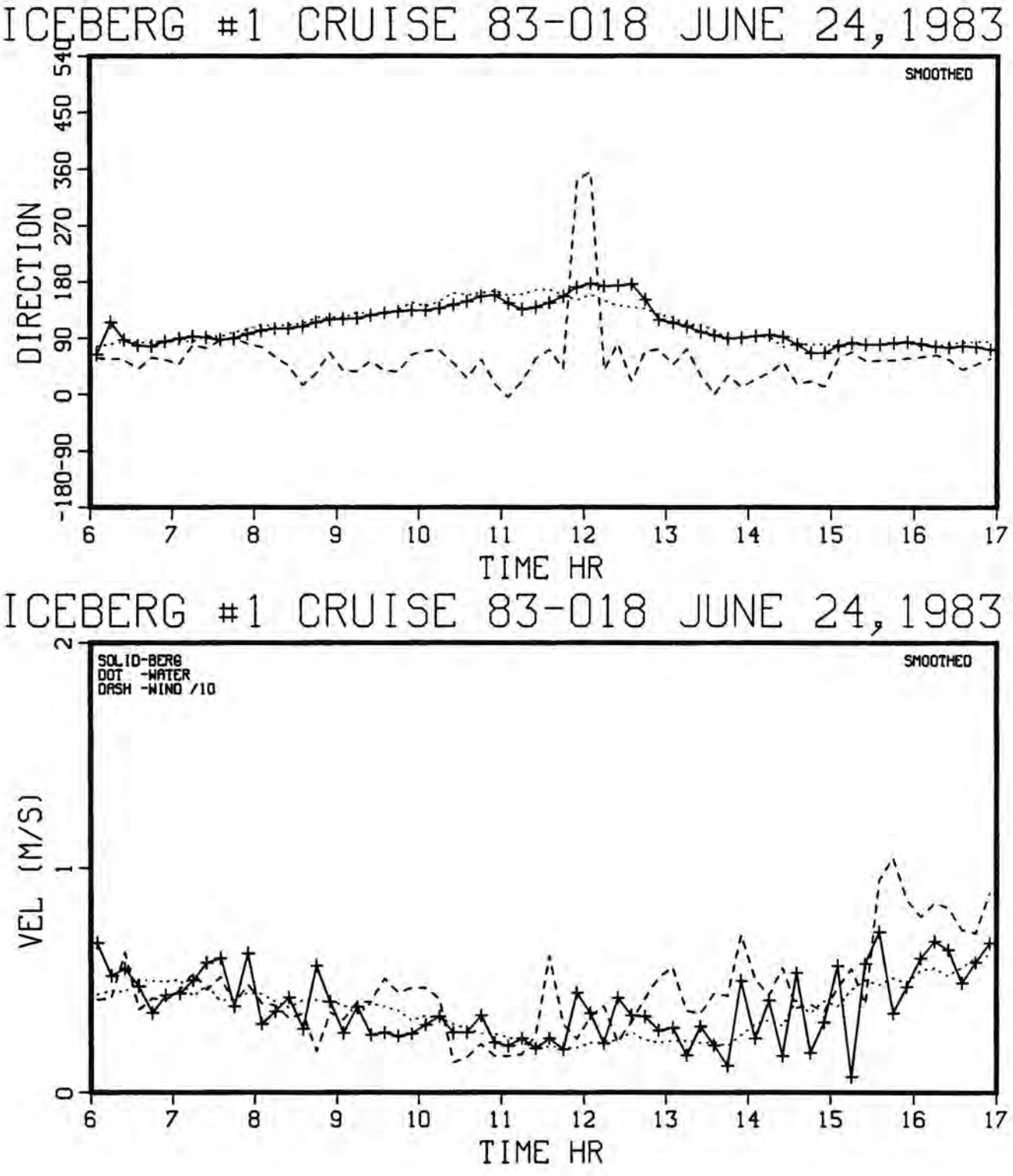

Fig. A3.1. Iceberg 83-1

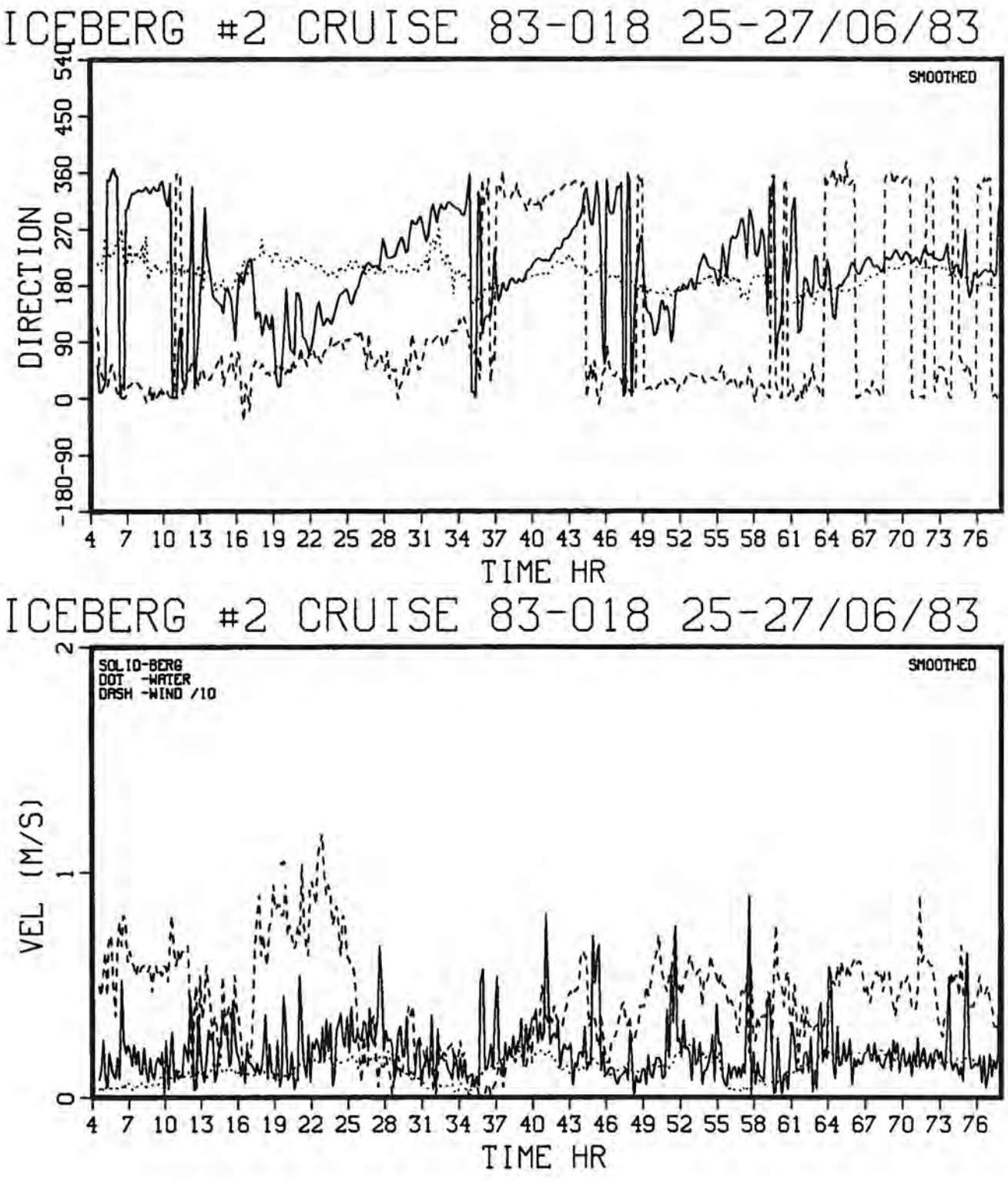

Fig. A3.2. Iceberg 83-2

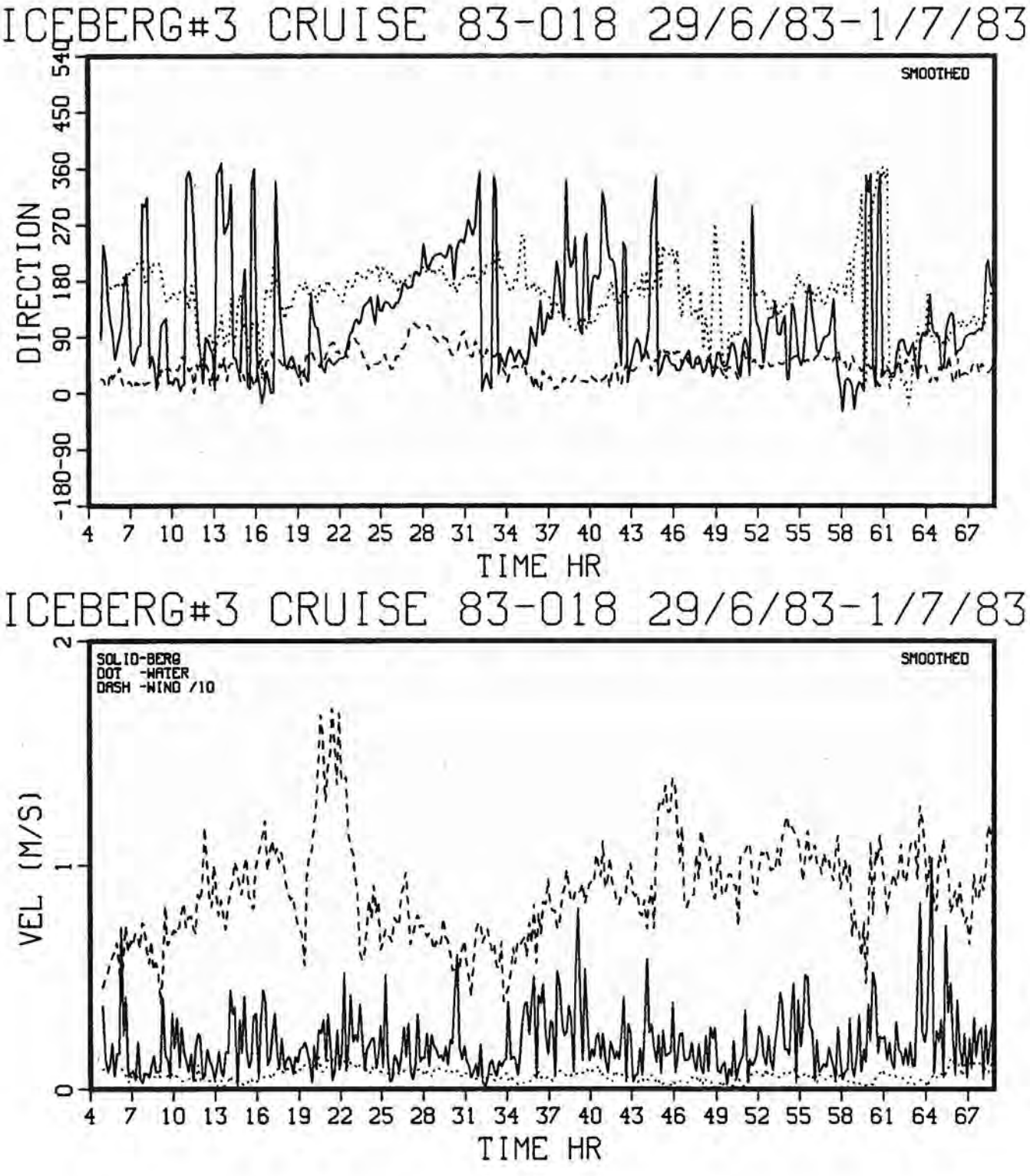

Fig. A3.3. Iceberg 83-3

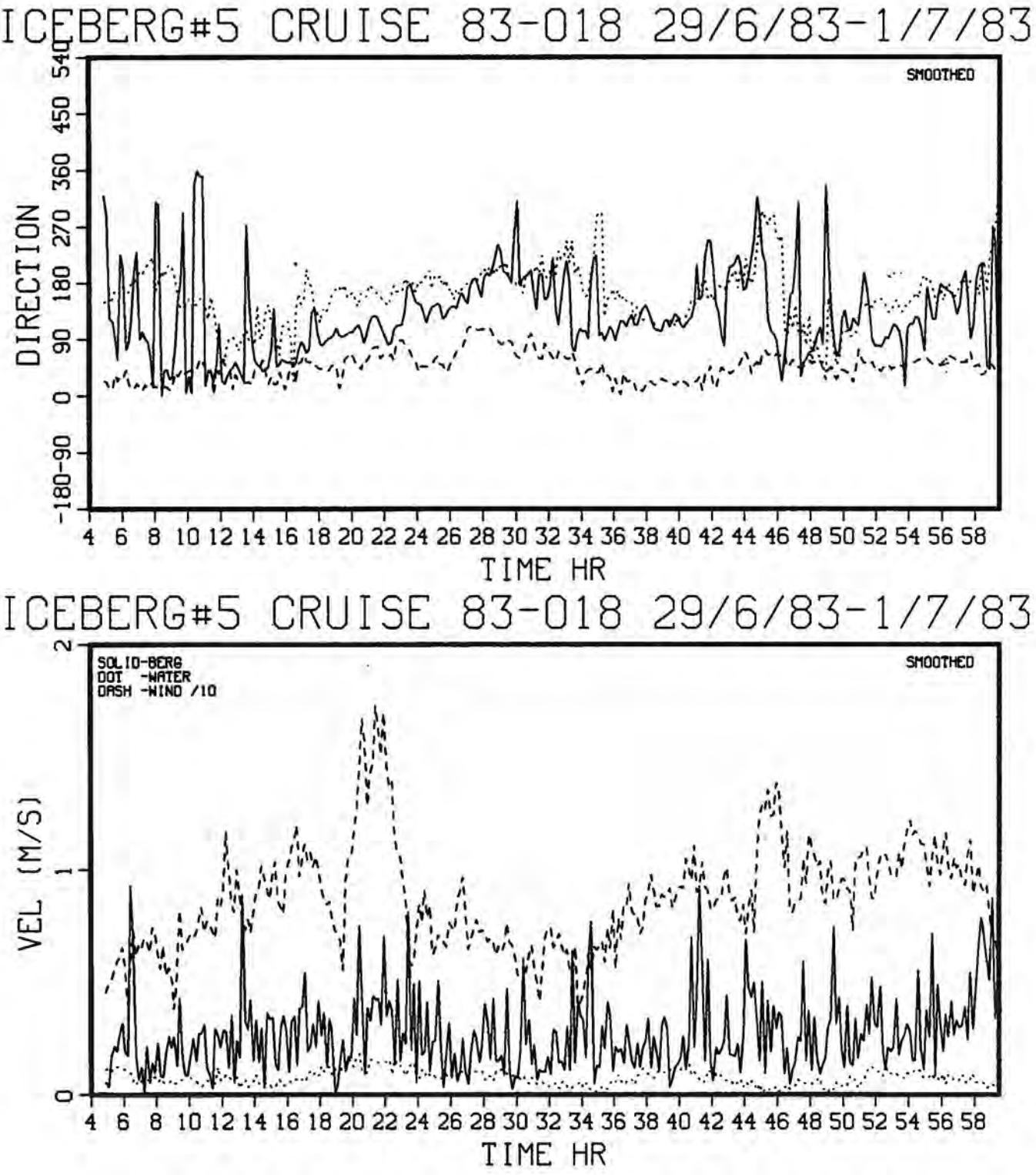

Fig. A3.4. Iceberg 83-5

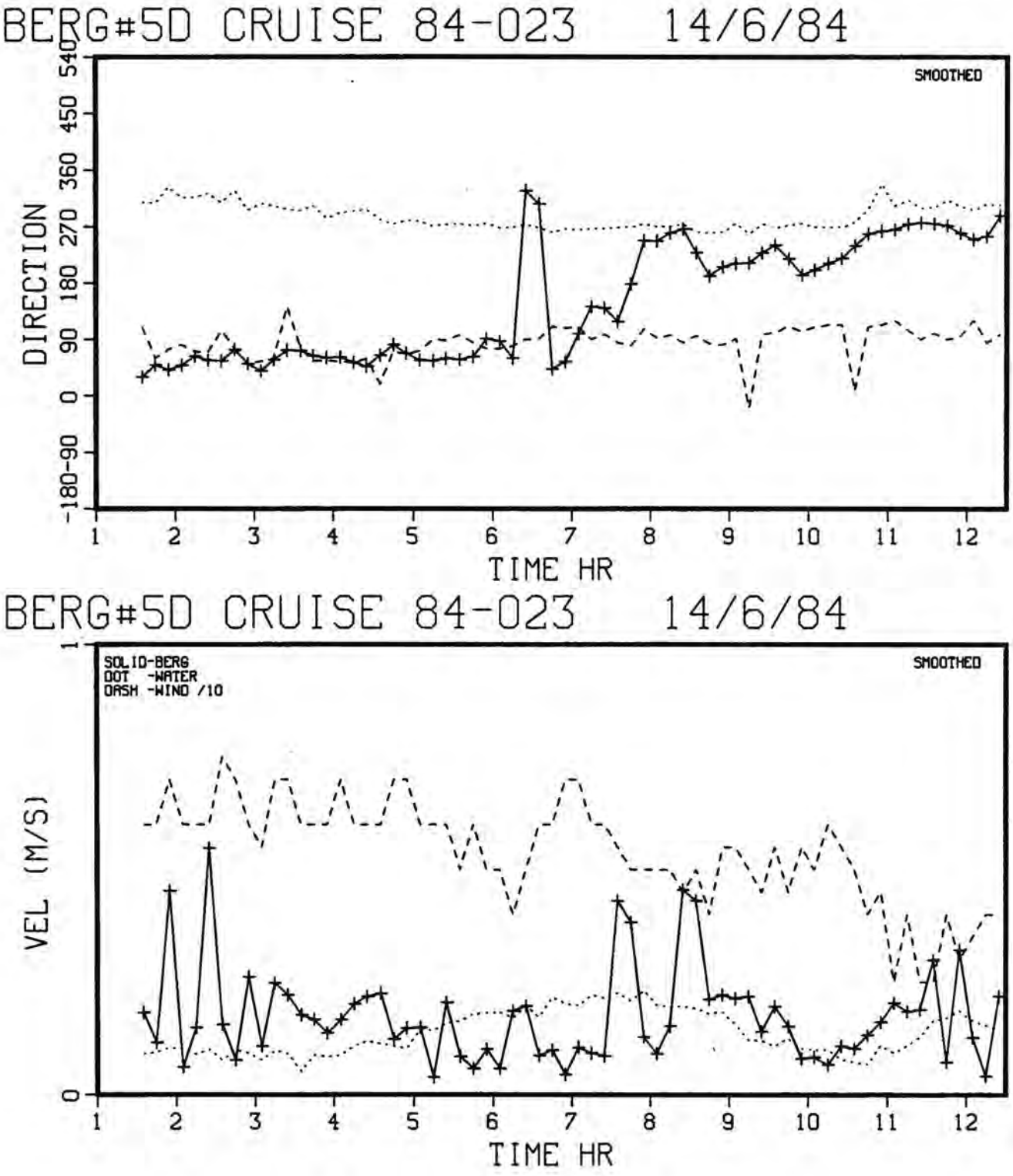

Fig. A3.5. Iceberg track 84-5D

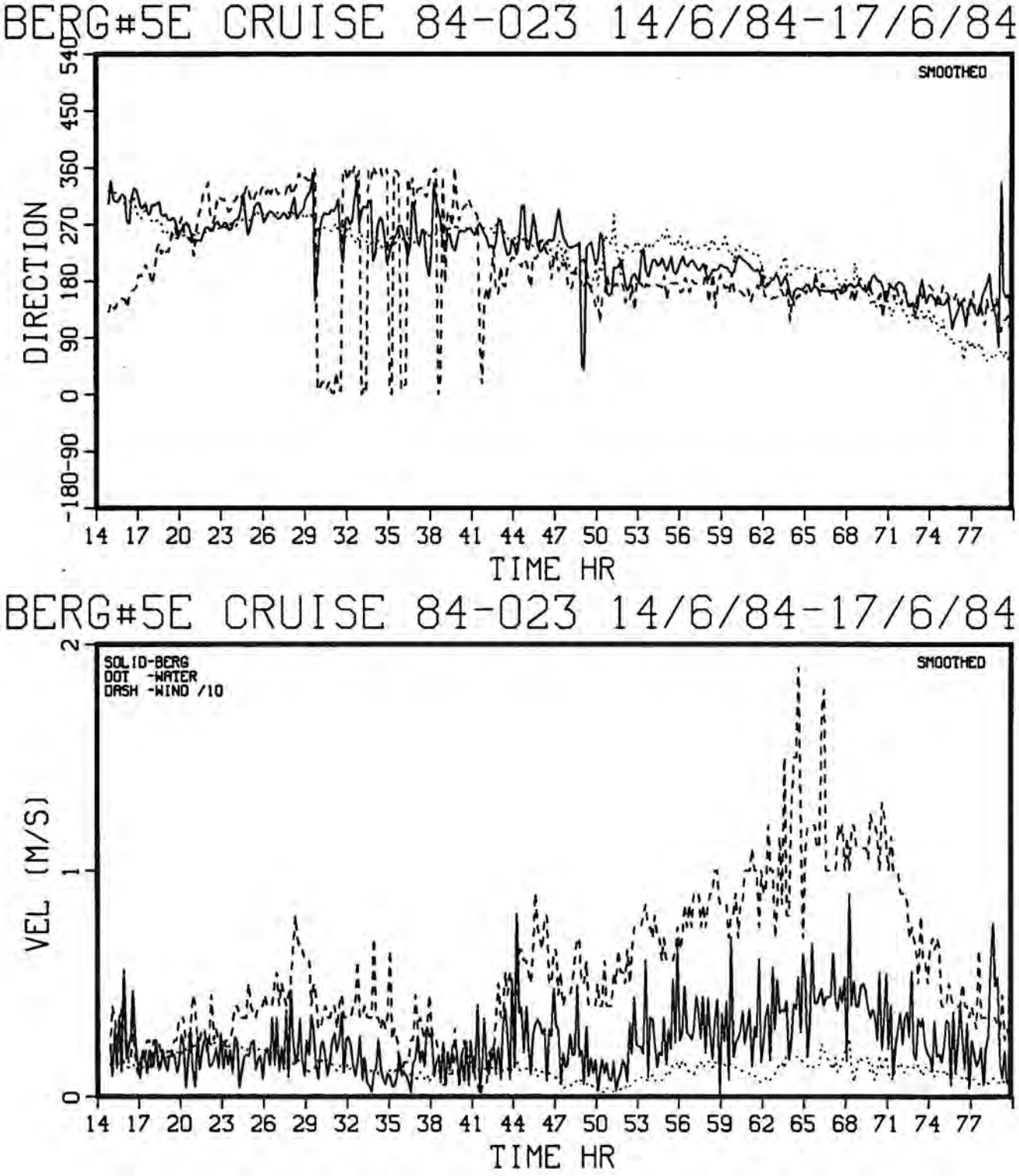

Fig. A3.6. Iceberg track 84-5E

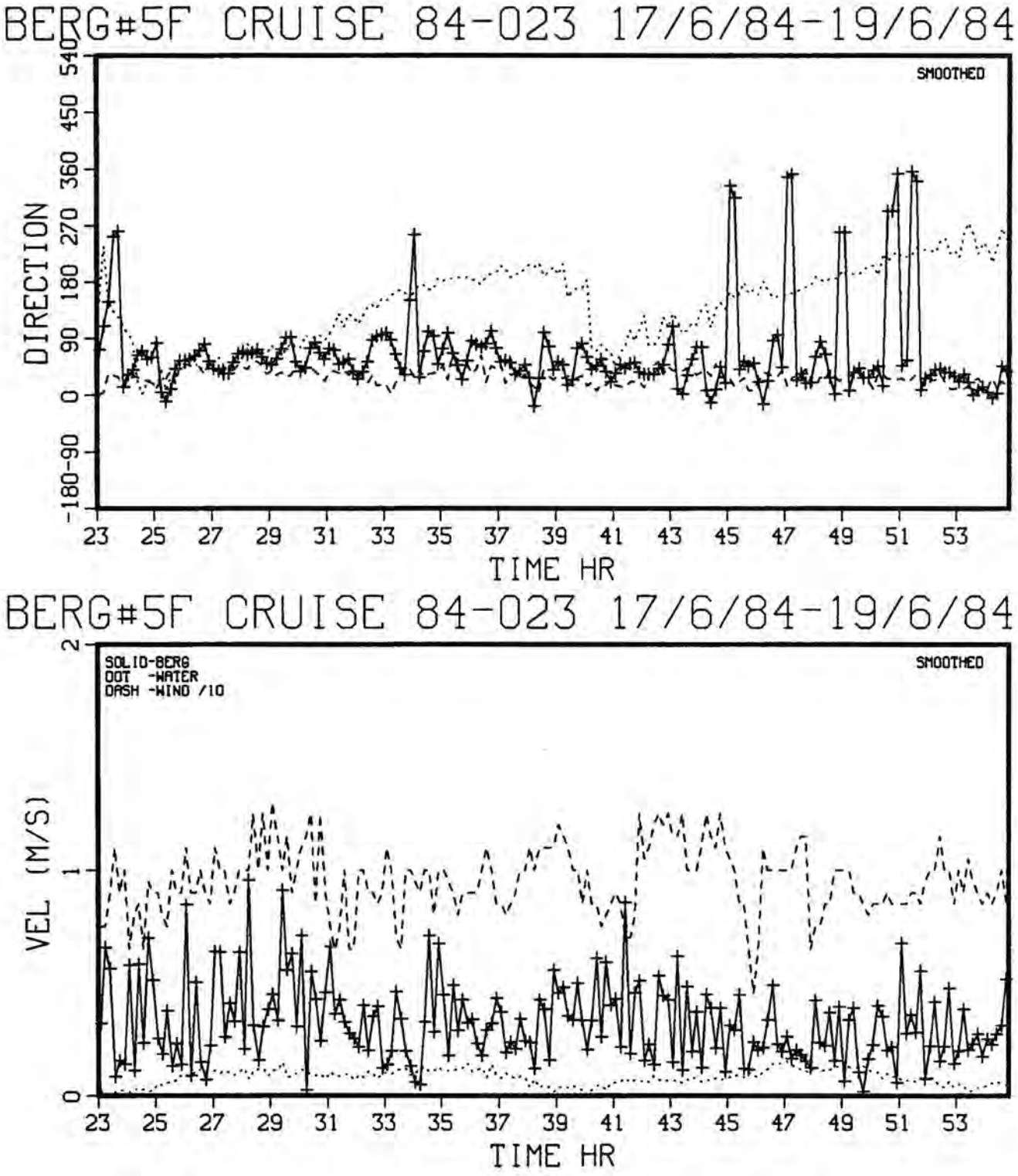

Fig. A3.7. Iceberg track 84-5F

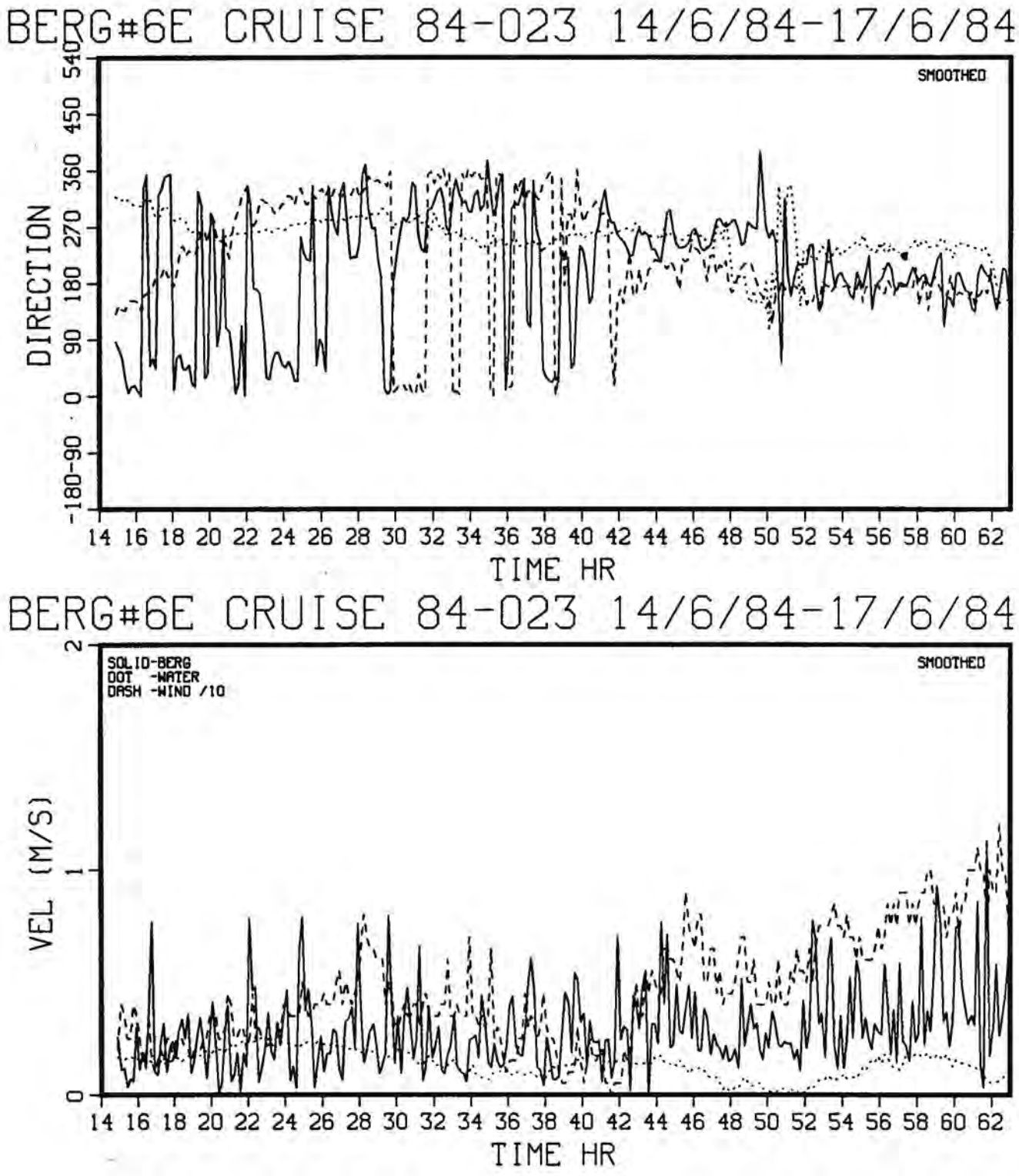

Fig. A3.8. Iceberg track 84-6E

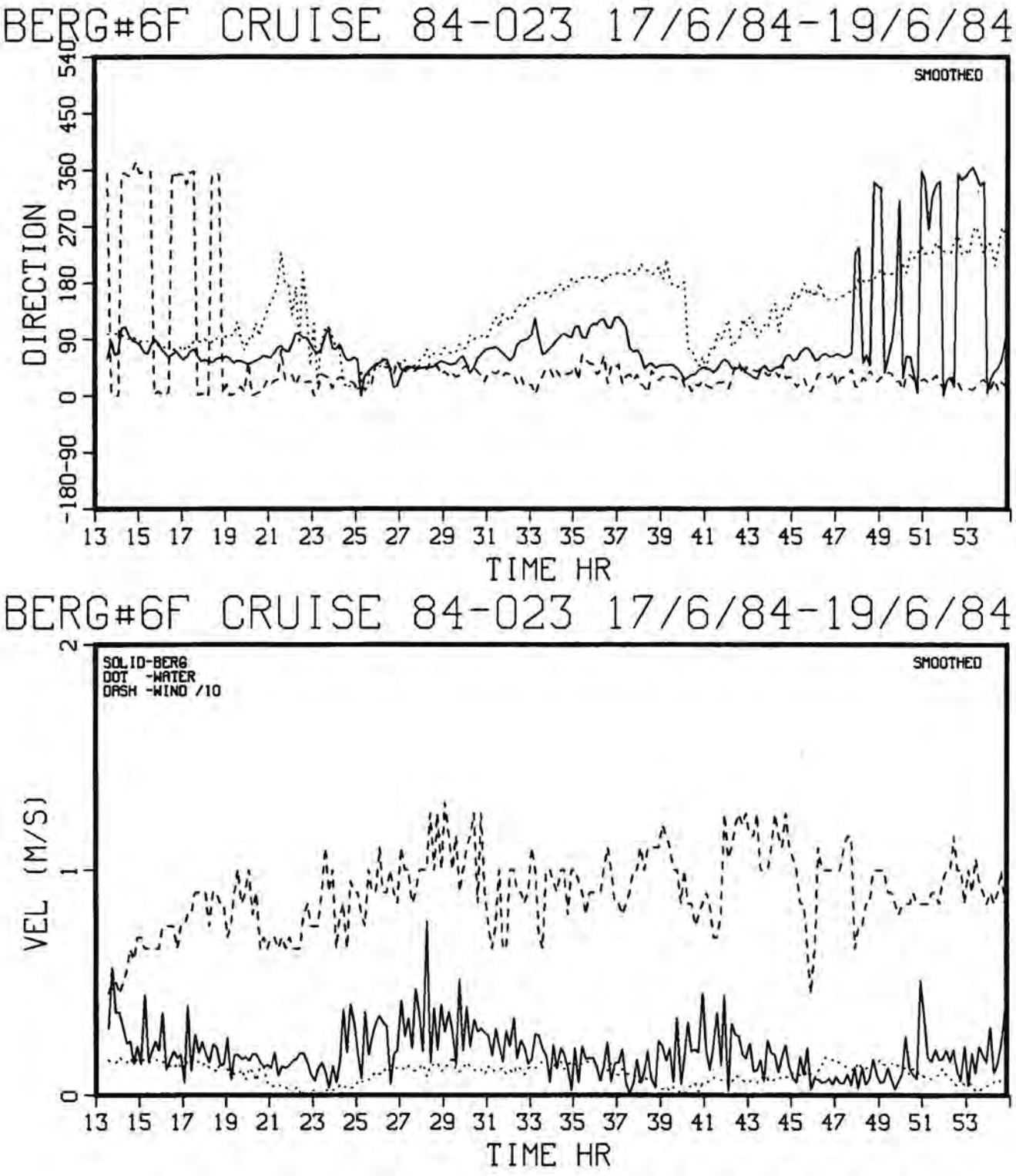

Fig. A3.9. Iceberg track 84-6F

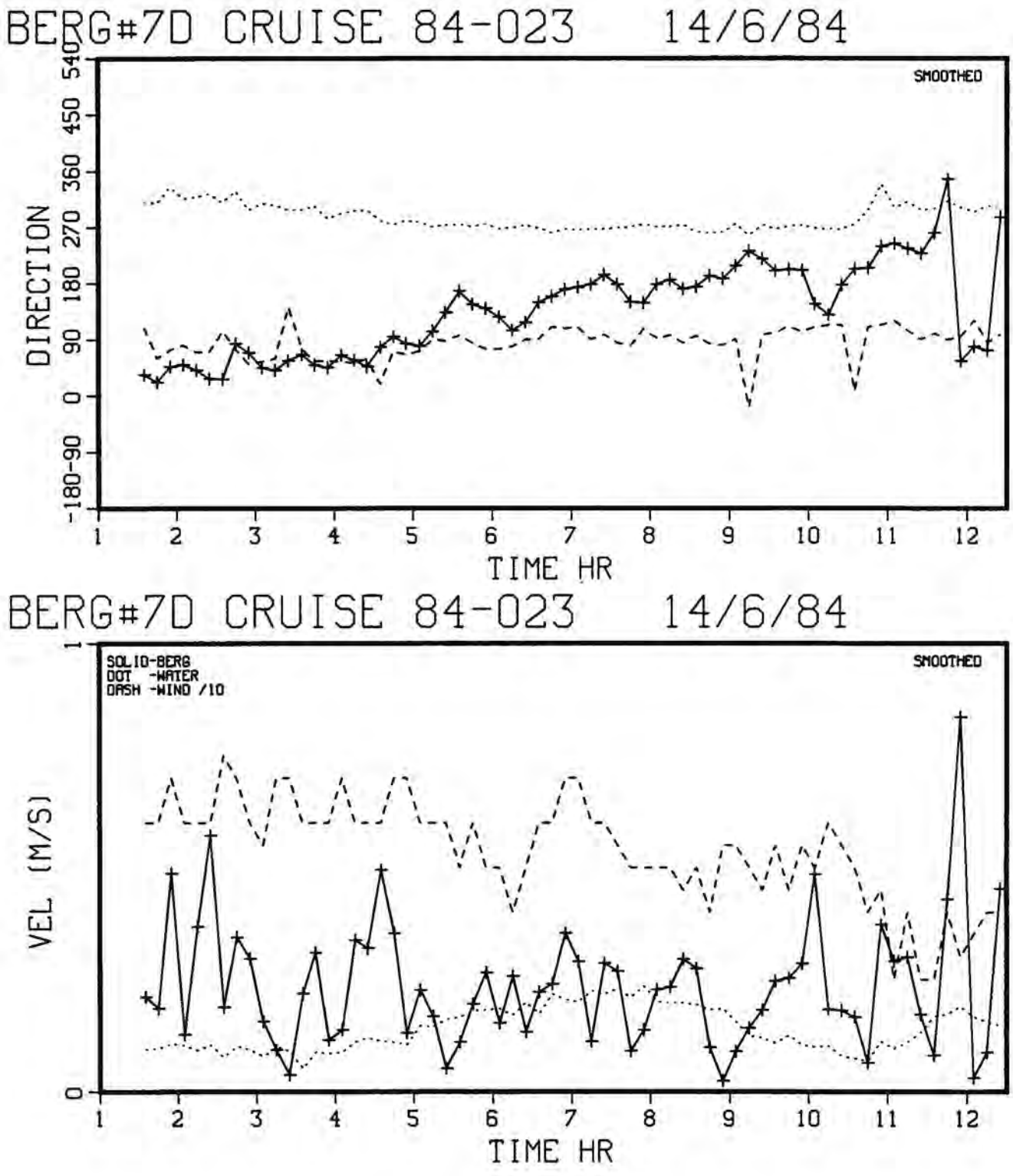

Fig. A3.10. Iceberg track 84-7D

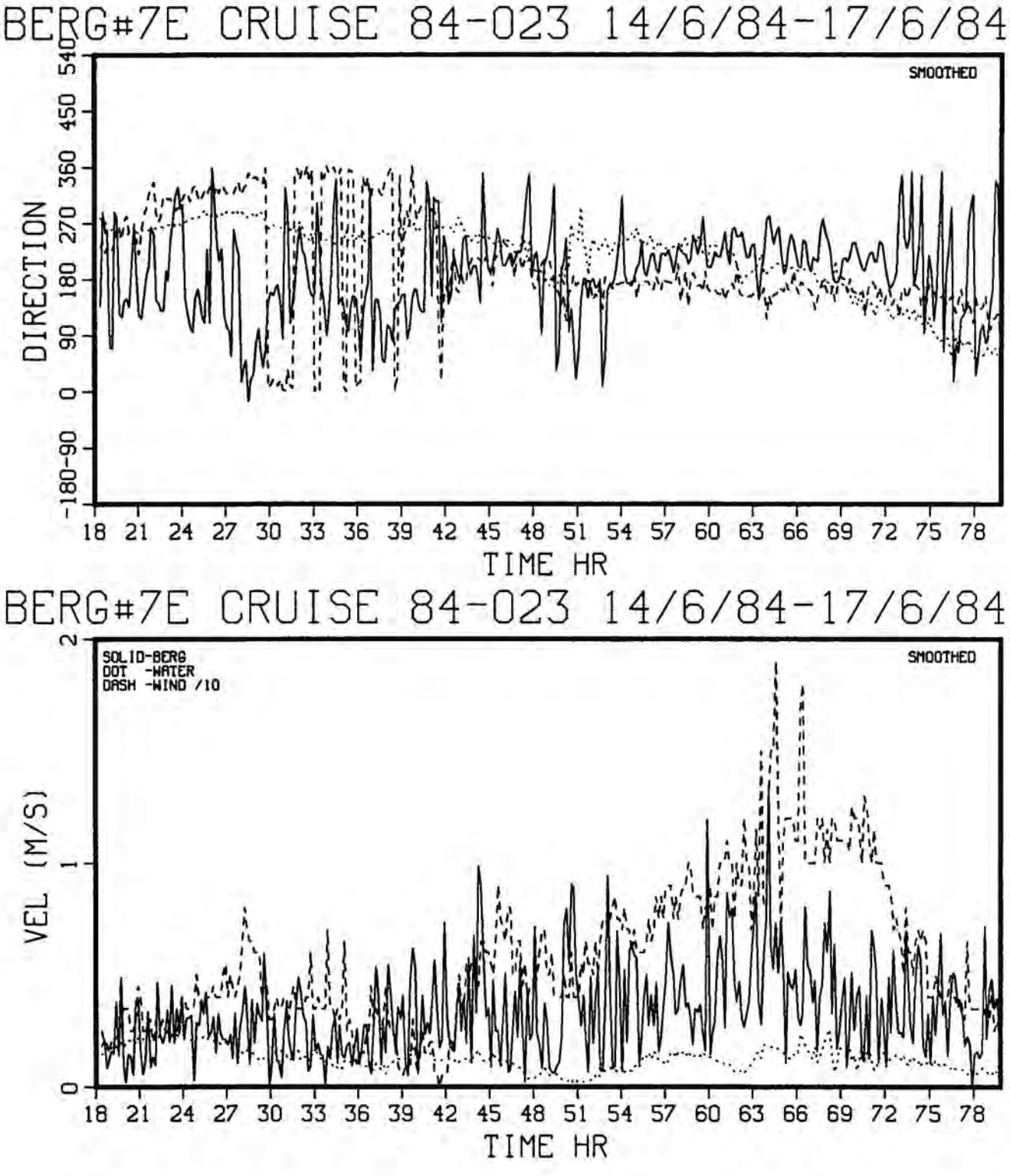

Fig. A3.11. Iceberg track 84-7E

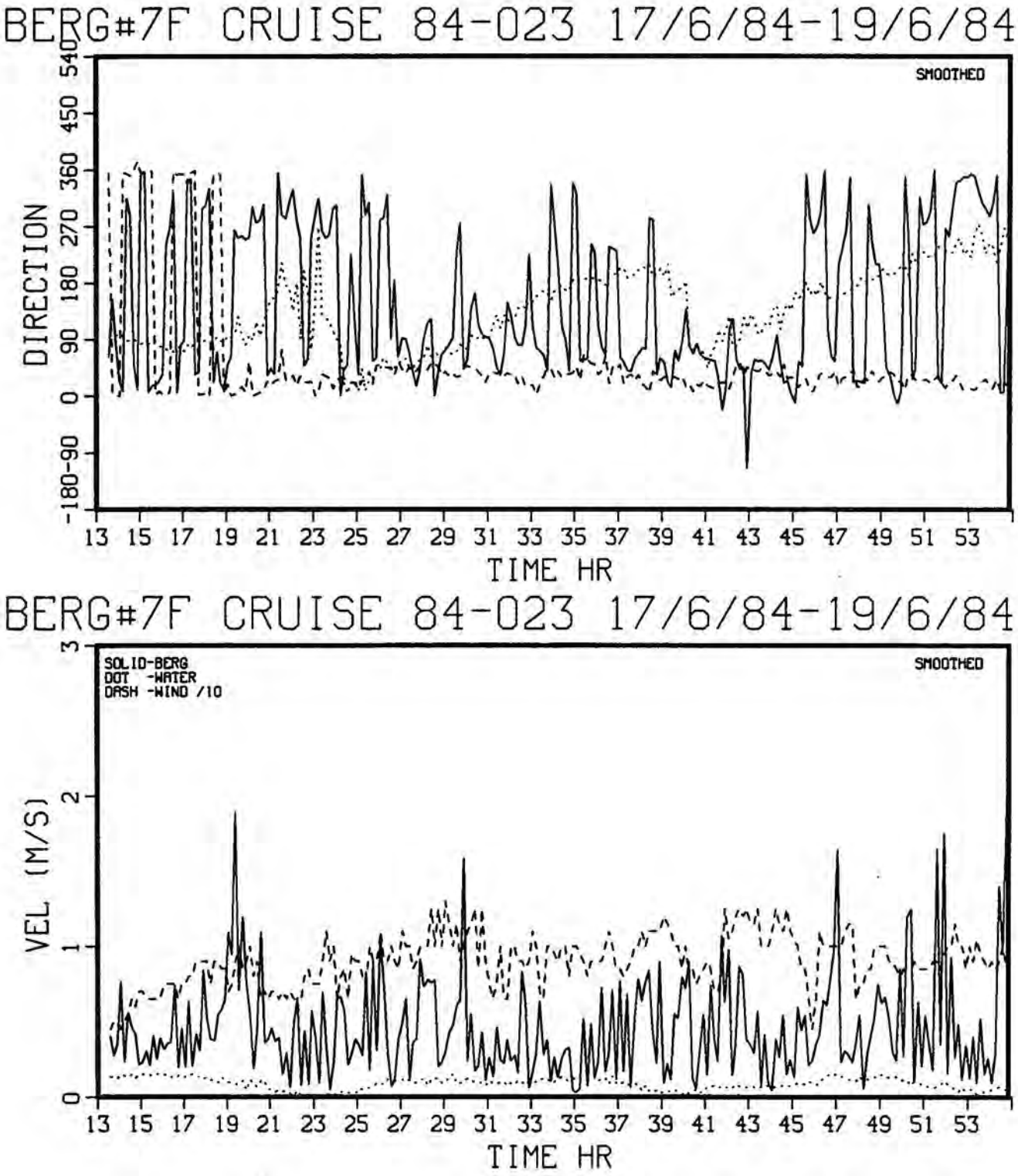

Fig. A3.12. Iceberg track 84-7F

APPENDIX 4 ICEBERGS AND SHIP TRACKS

Iceberg tracks are shown as solid lines, ship tracks as dotted lines, and radar ranges as dashed lines. Symbols mark hourly positons.

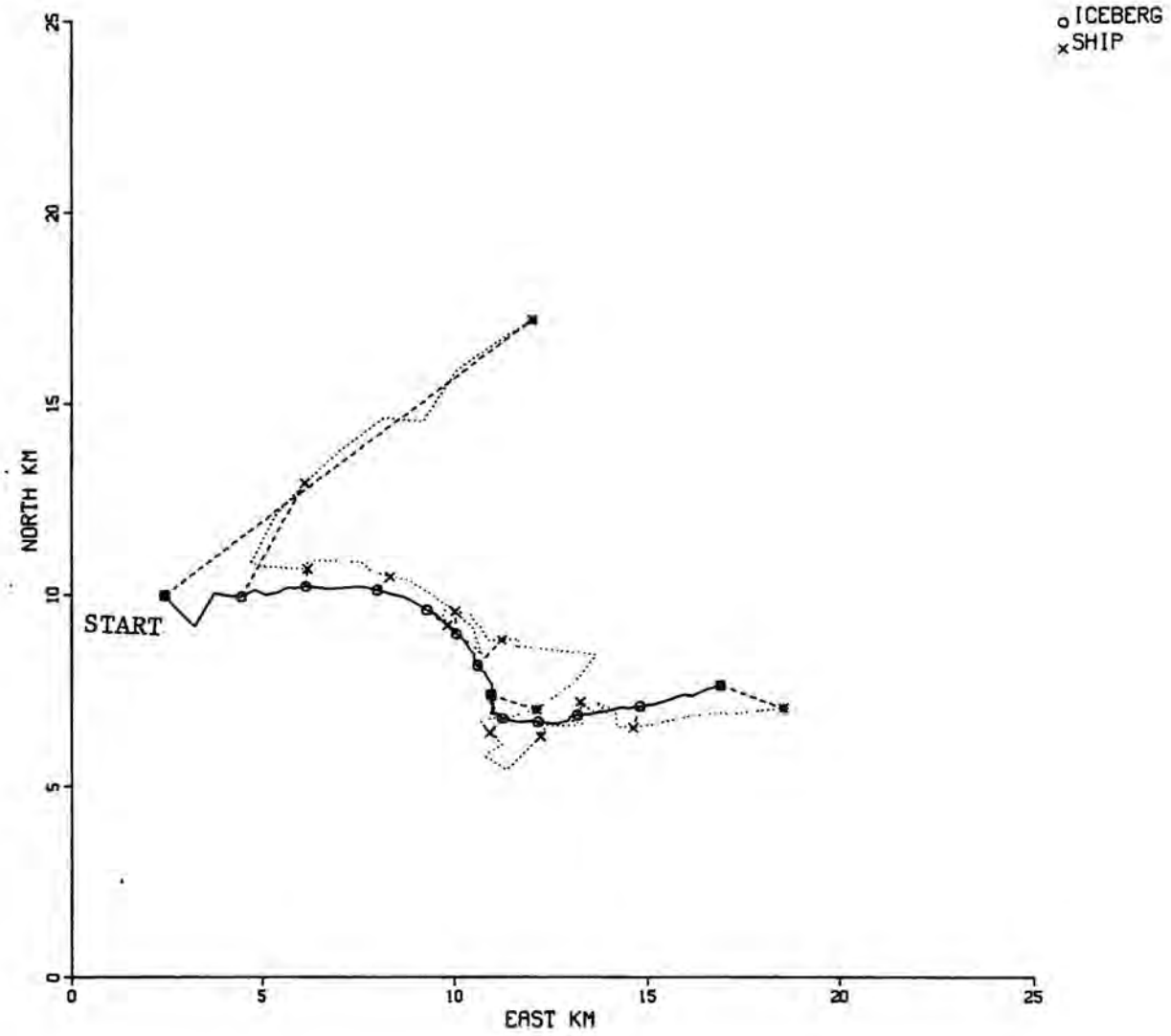

Fig. A4.1. Iceberg 83-1

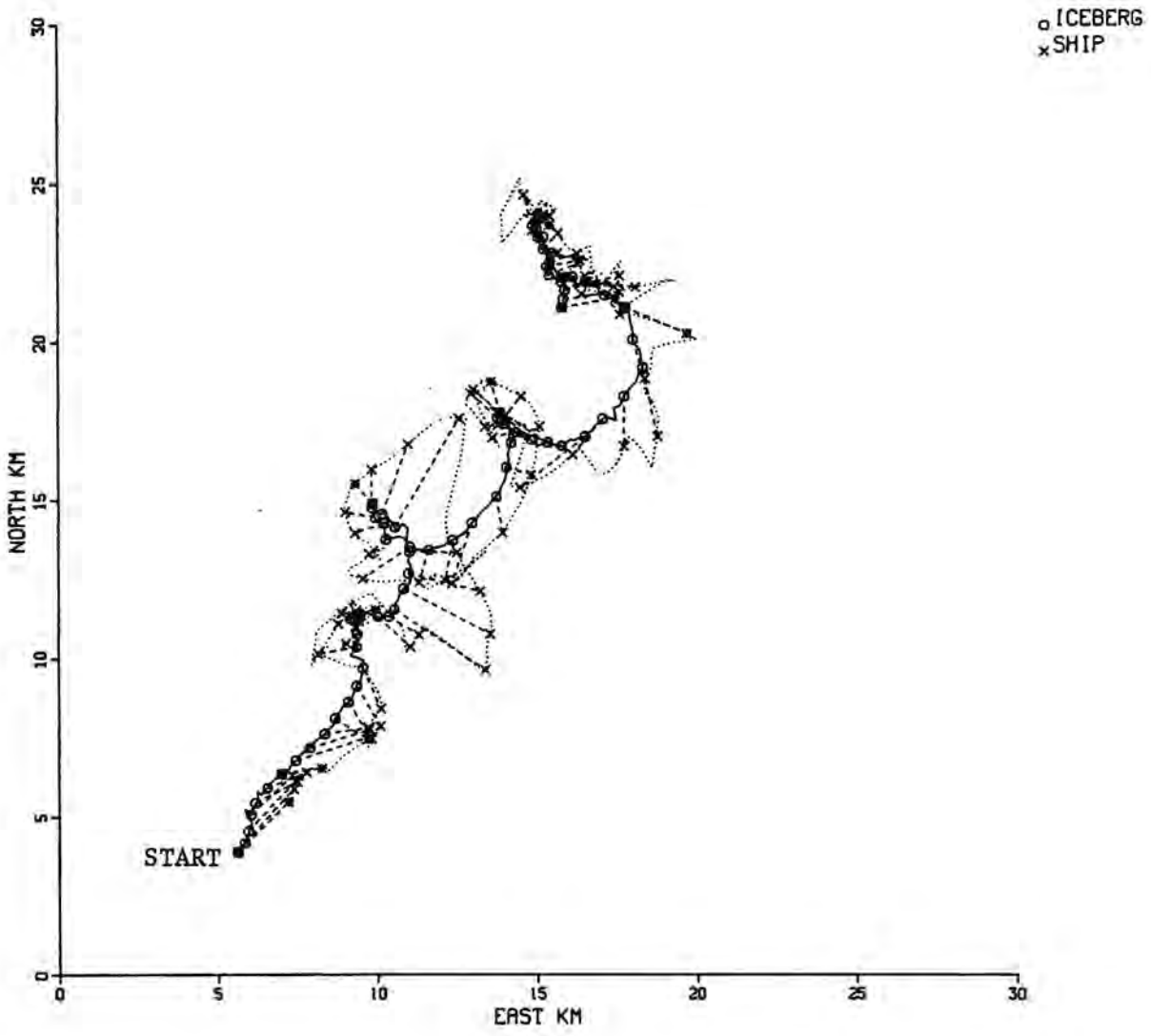

Fig. A4.2. Iceberg 83-2

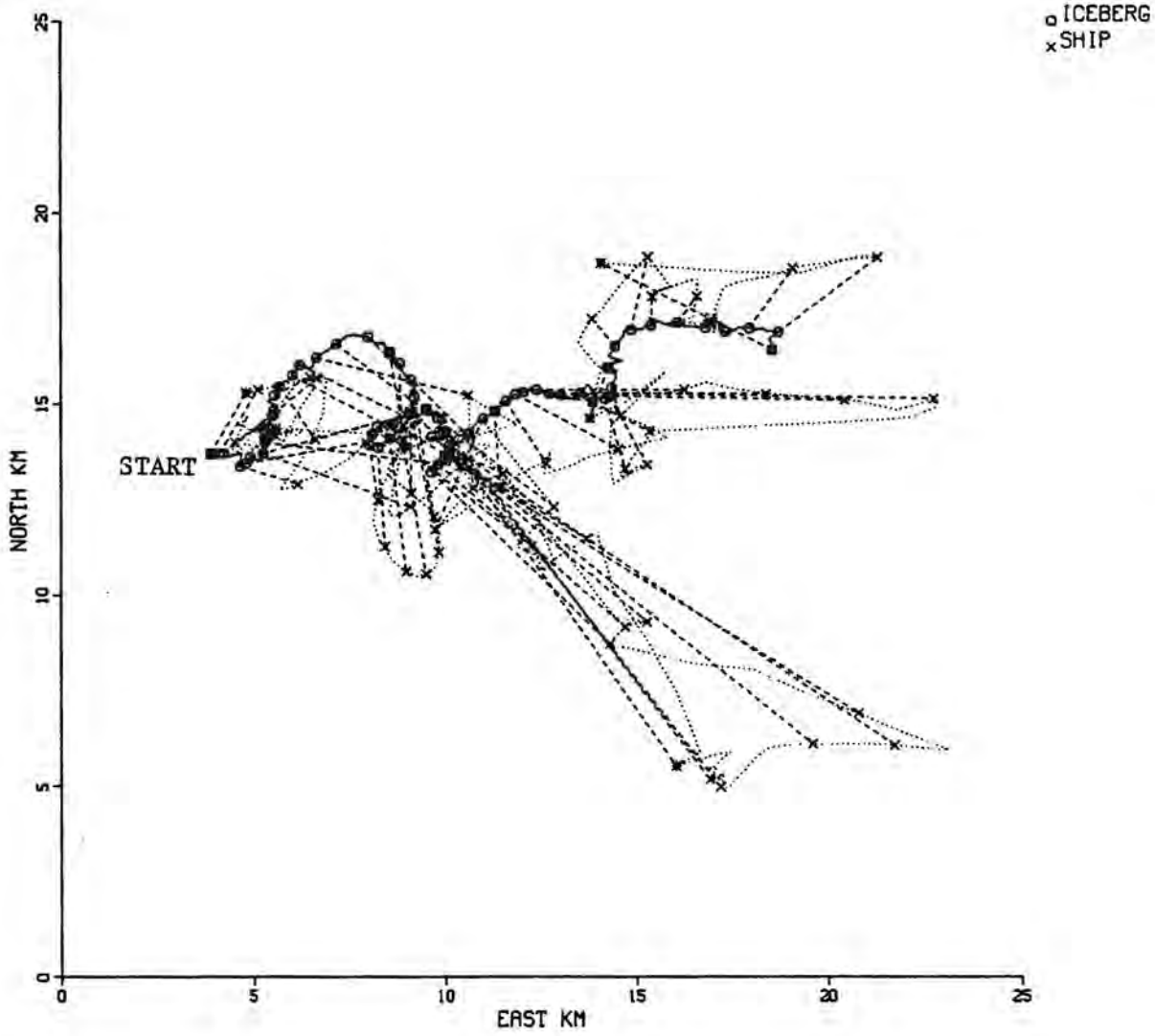

Fig. A4.3. Iceberg 83-3

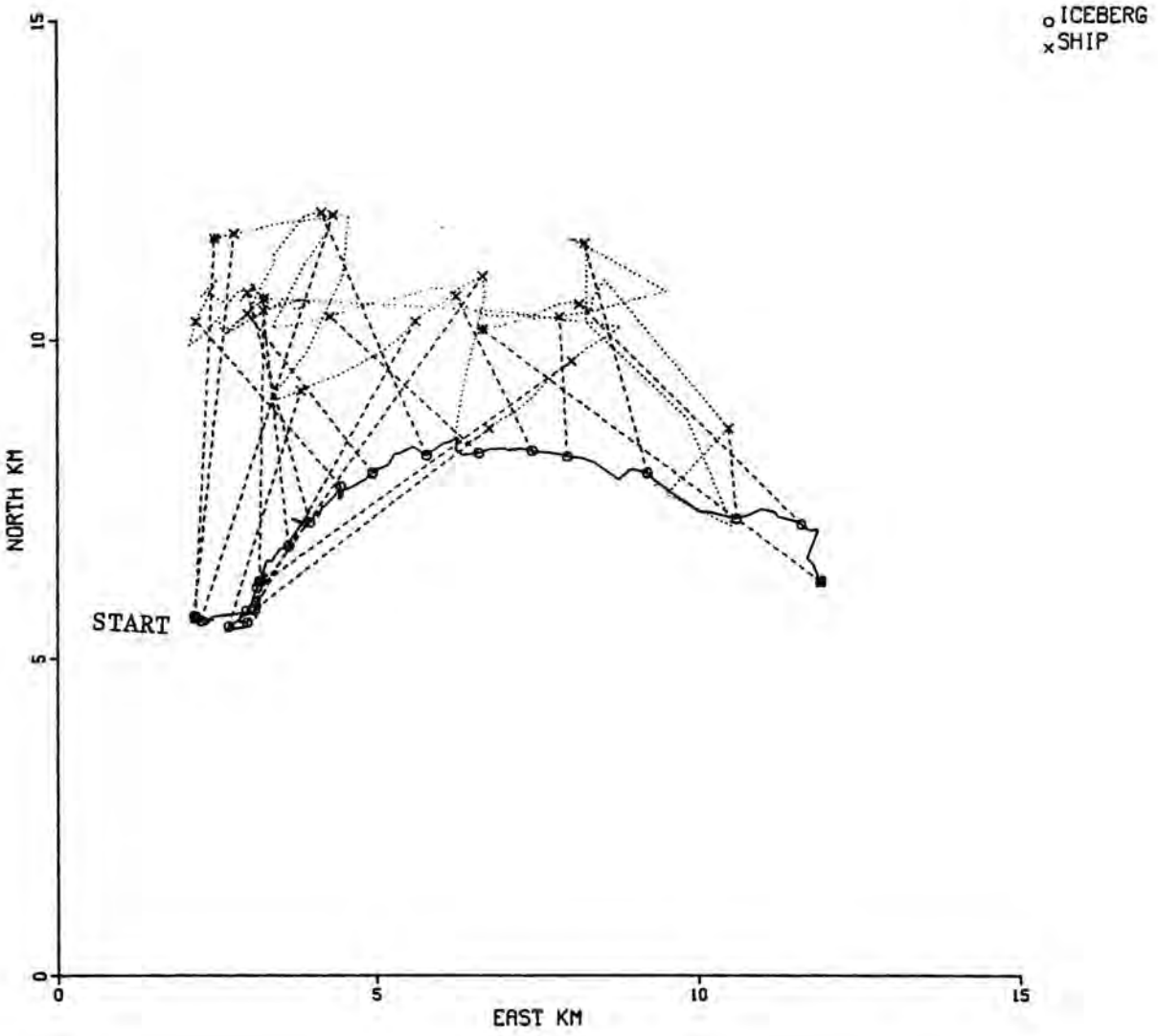

Fig. A4.4. Iceberg 83-5

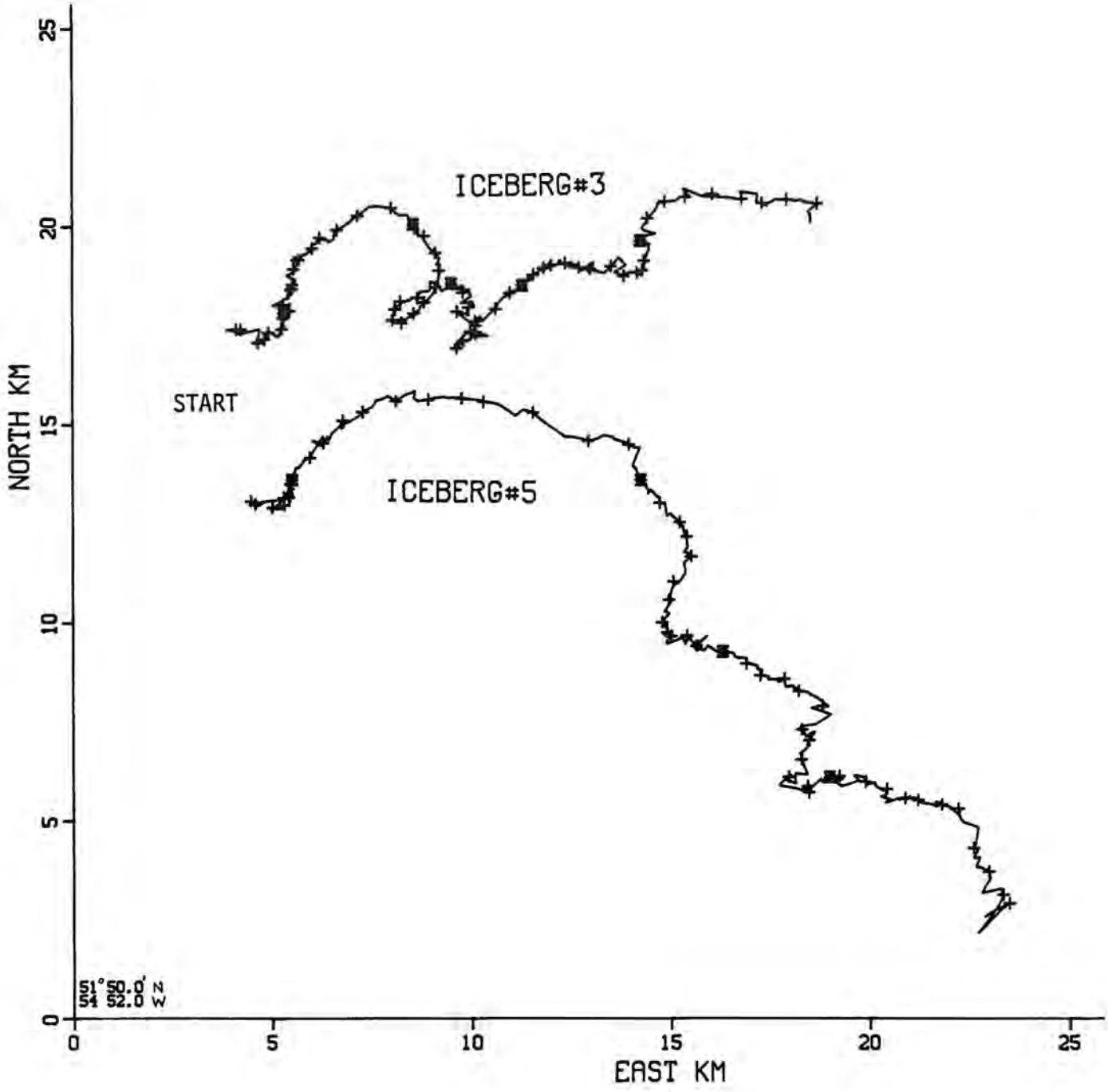

Fig. A4.5. Simultaneous tracks of Icebergs 83-3 and 83-5, ship track deleted.

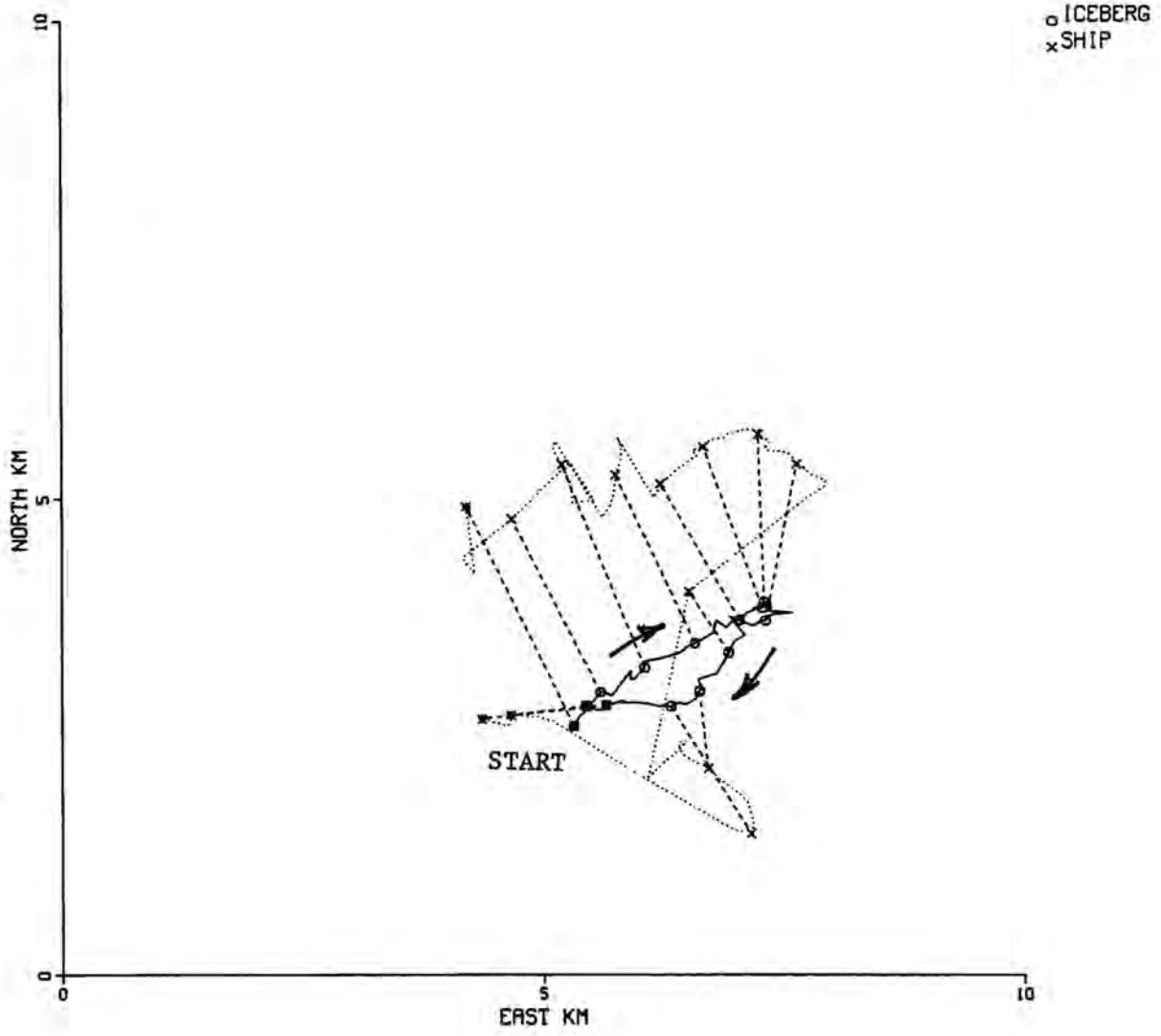

Fig. A4.6. Iceberg Track 84-5D

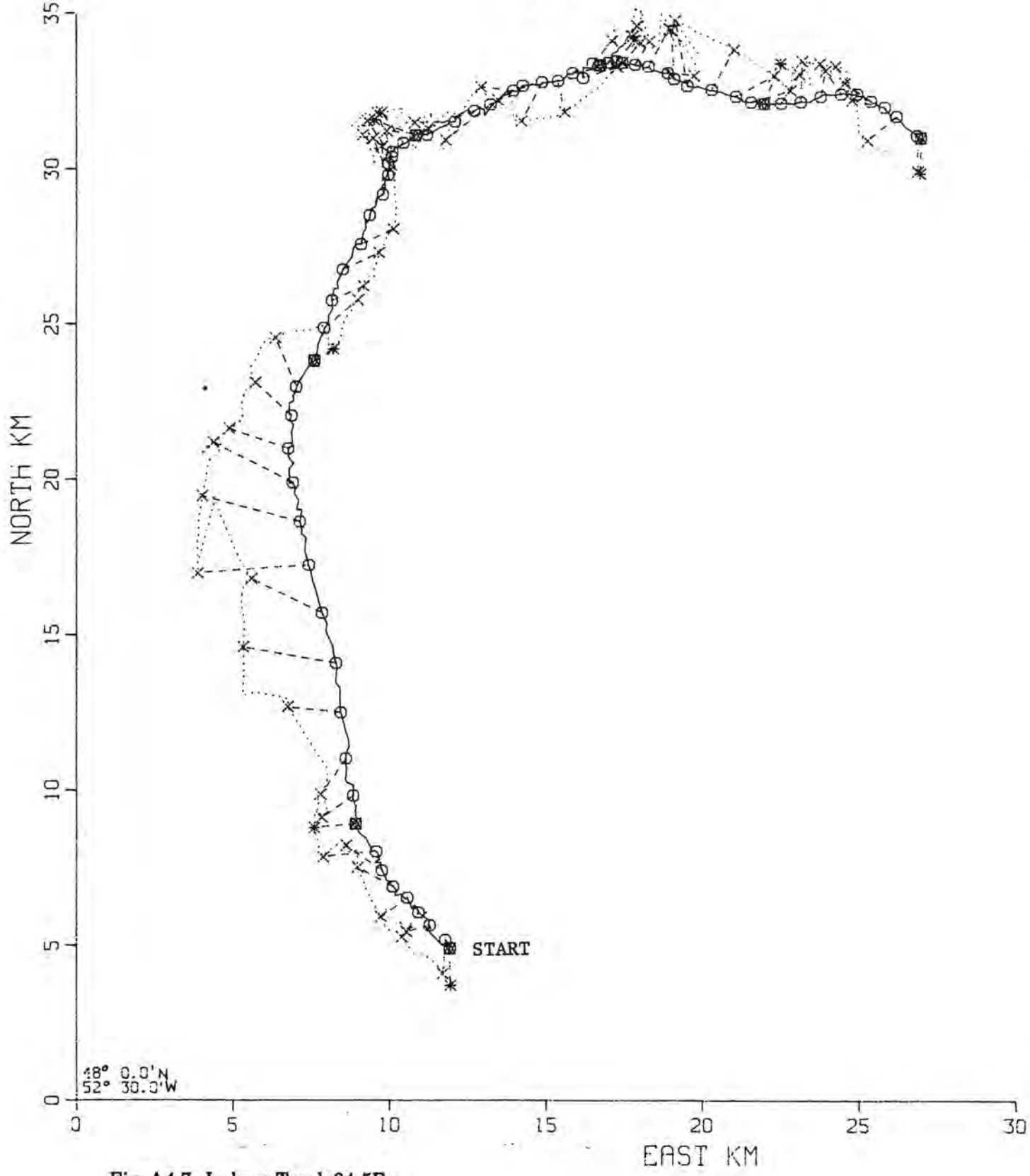

Fig. A4.7. Iceberg Track 84-5E

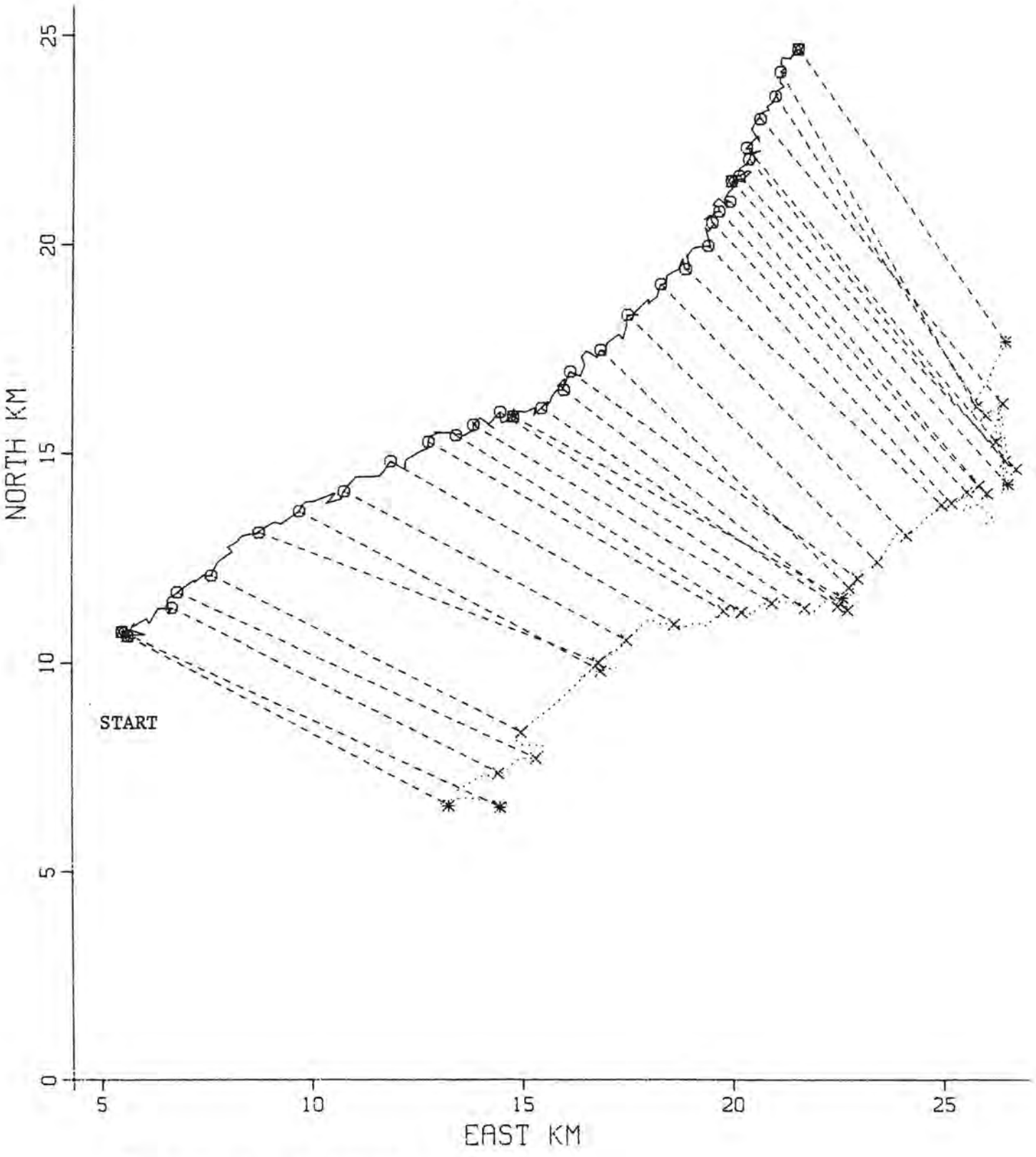

Fig. A4.8. Iceberg Track 84-5F

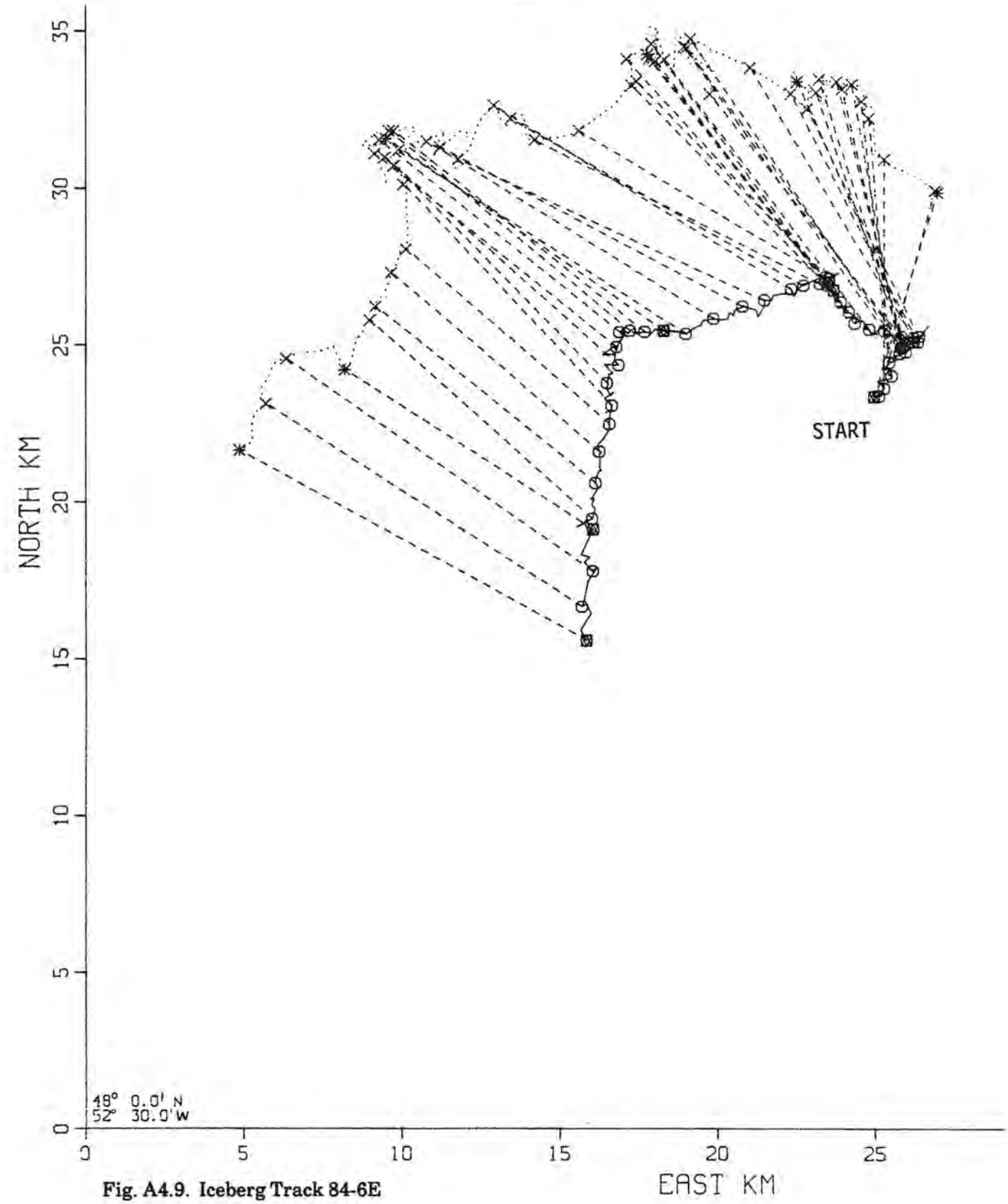

Fig. A4.9. Iceberg Track 84-6E

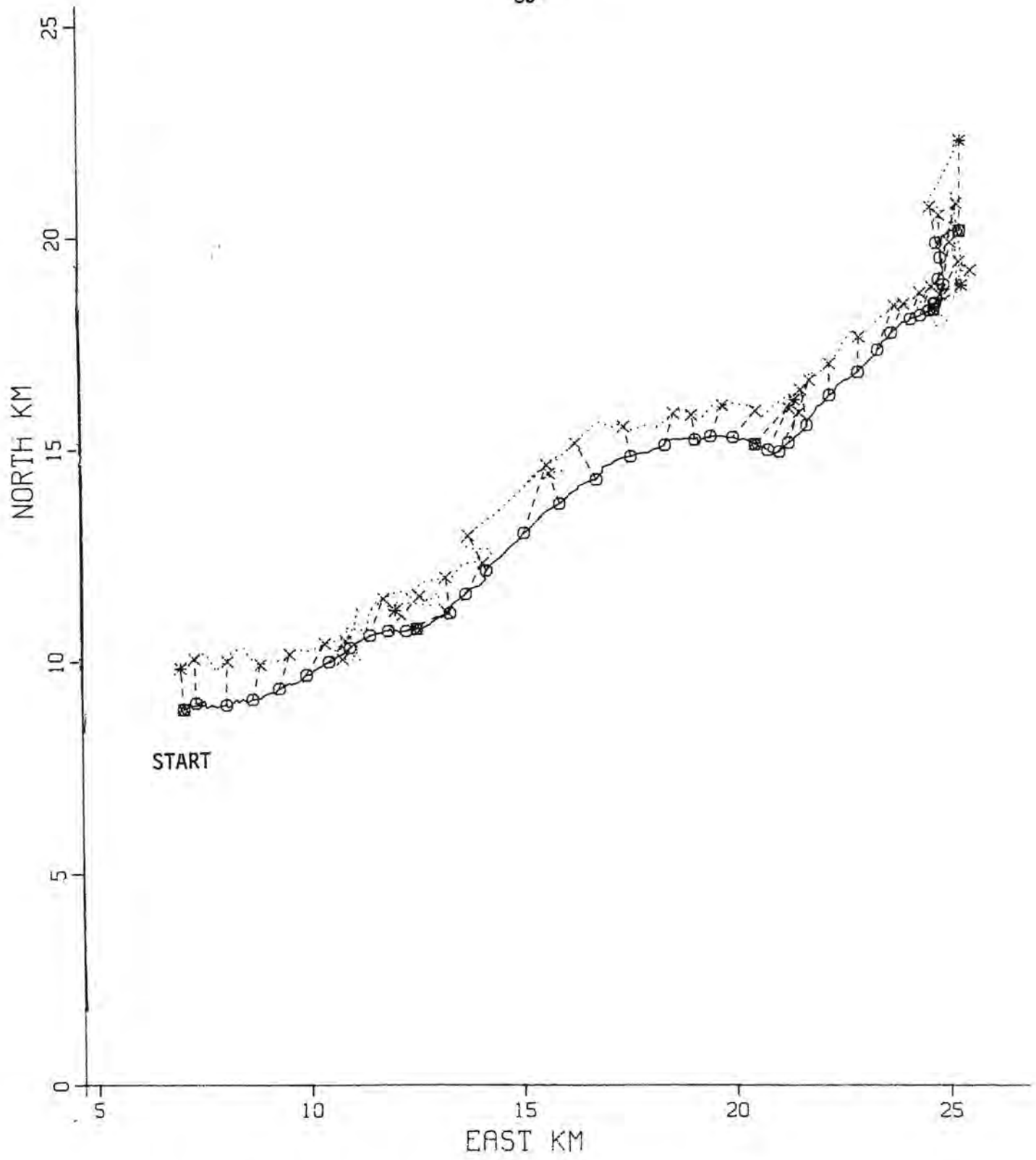

Fig. A4.10. Iceberg Track 84-6F

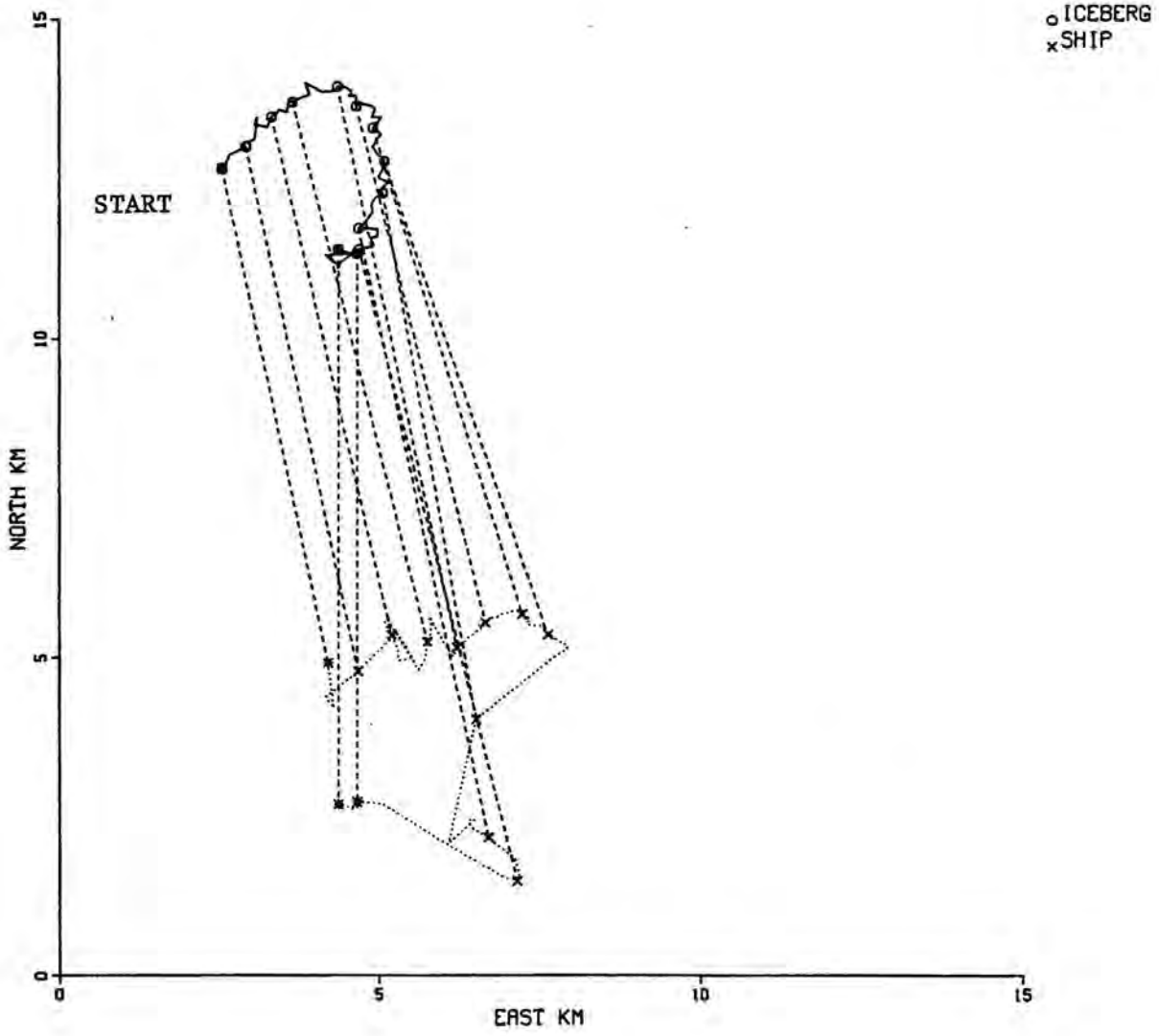

Fig. A4.11. Iceberg Track 84-7D

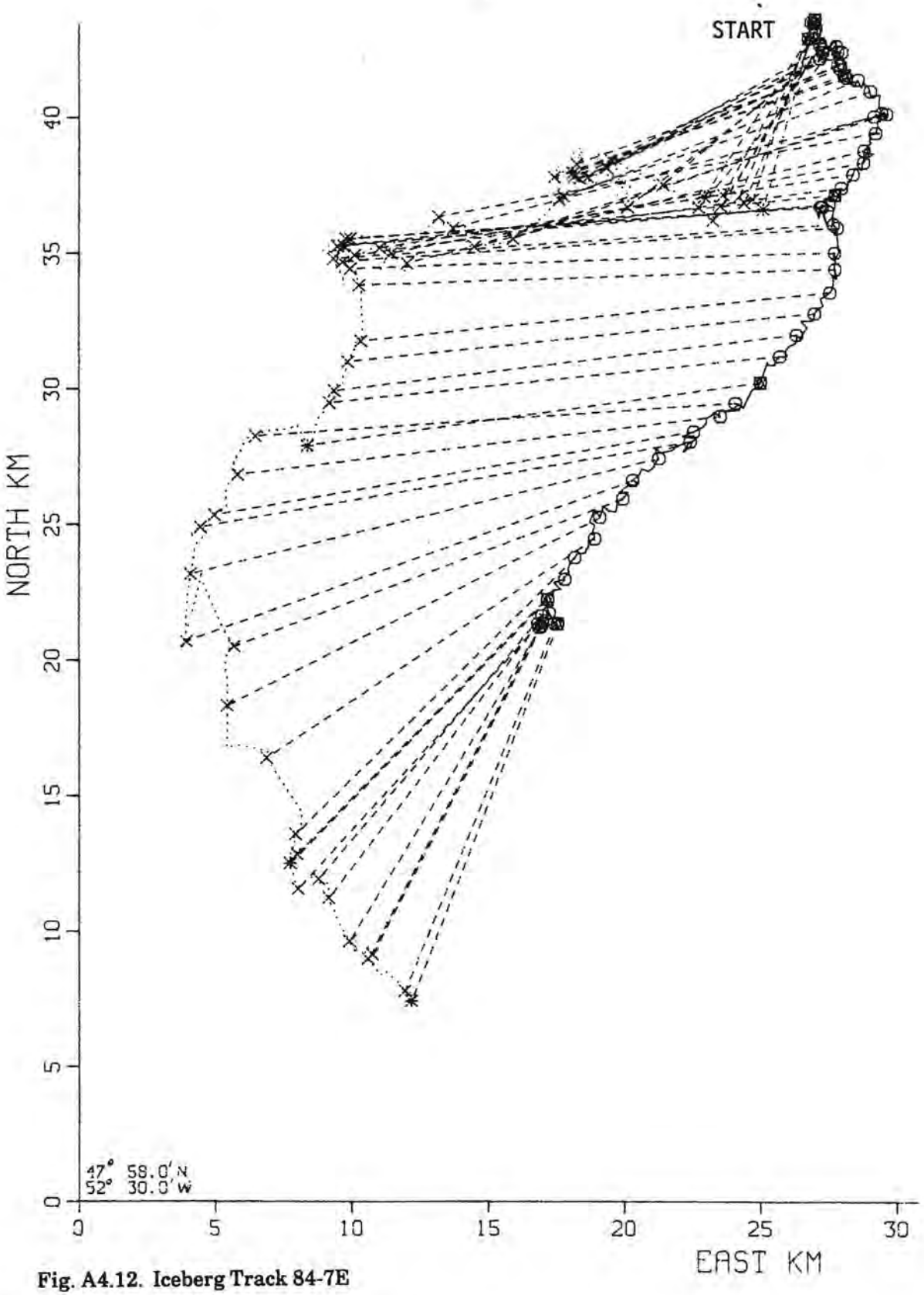

Fig. A4.12. Iceberg Track 84-7E

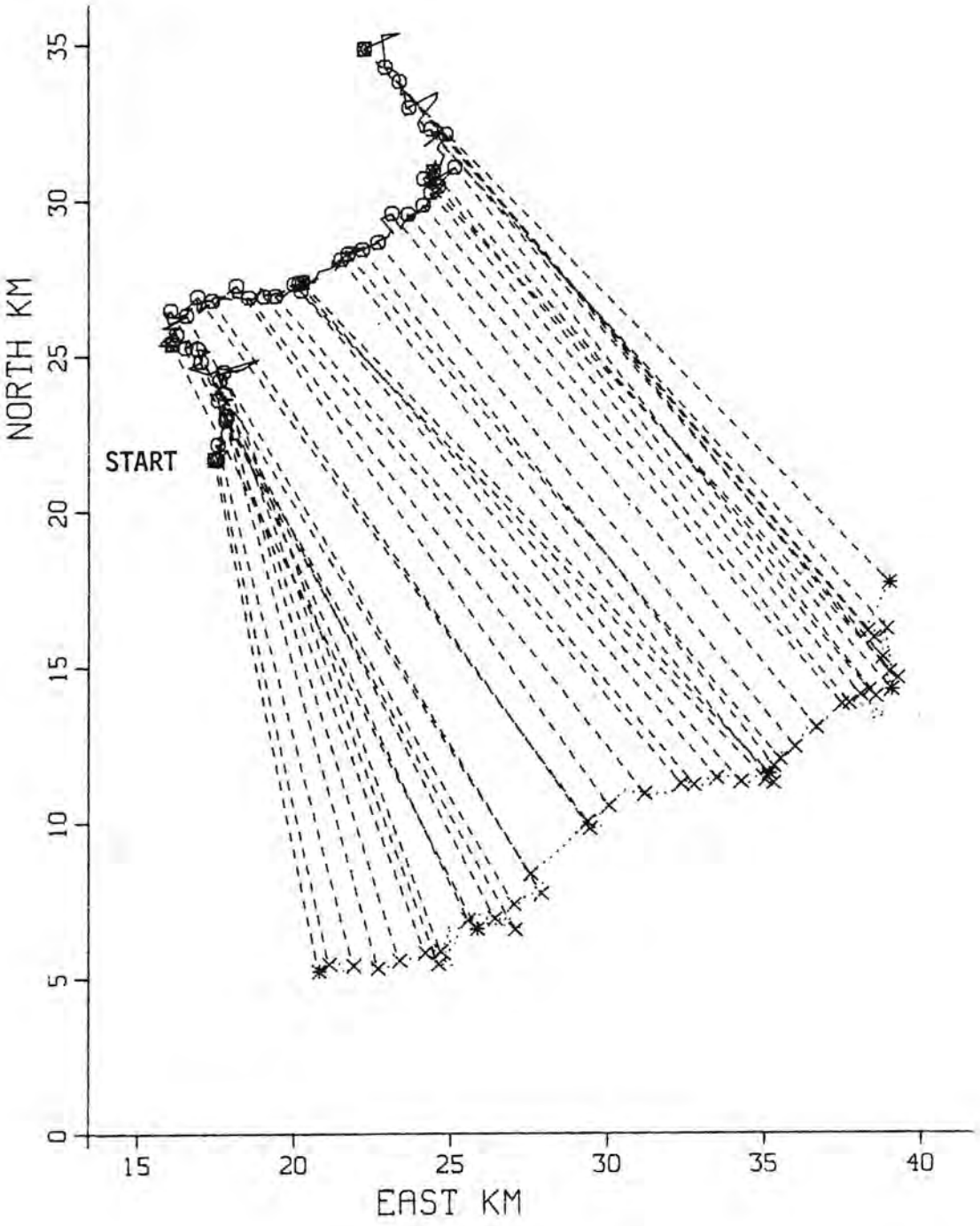

Fig. A4.13. Iceberg Track 84-7F

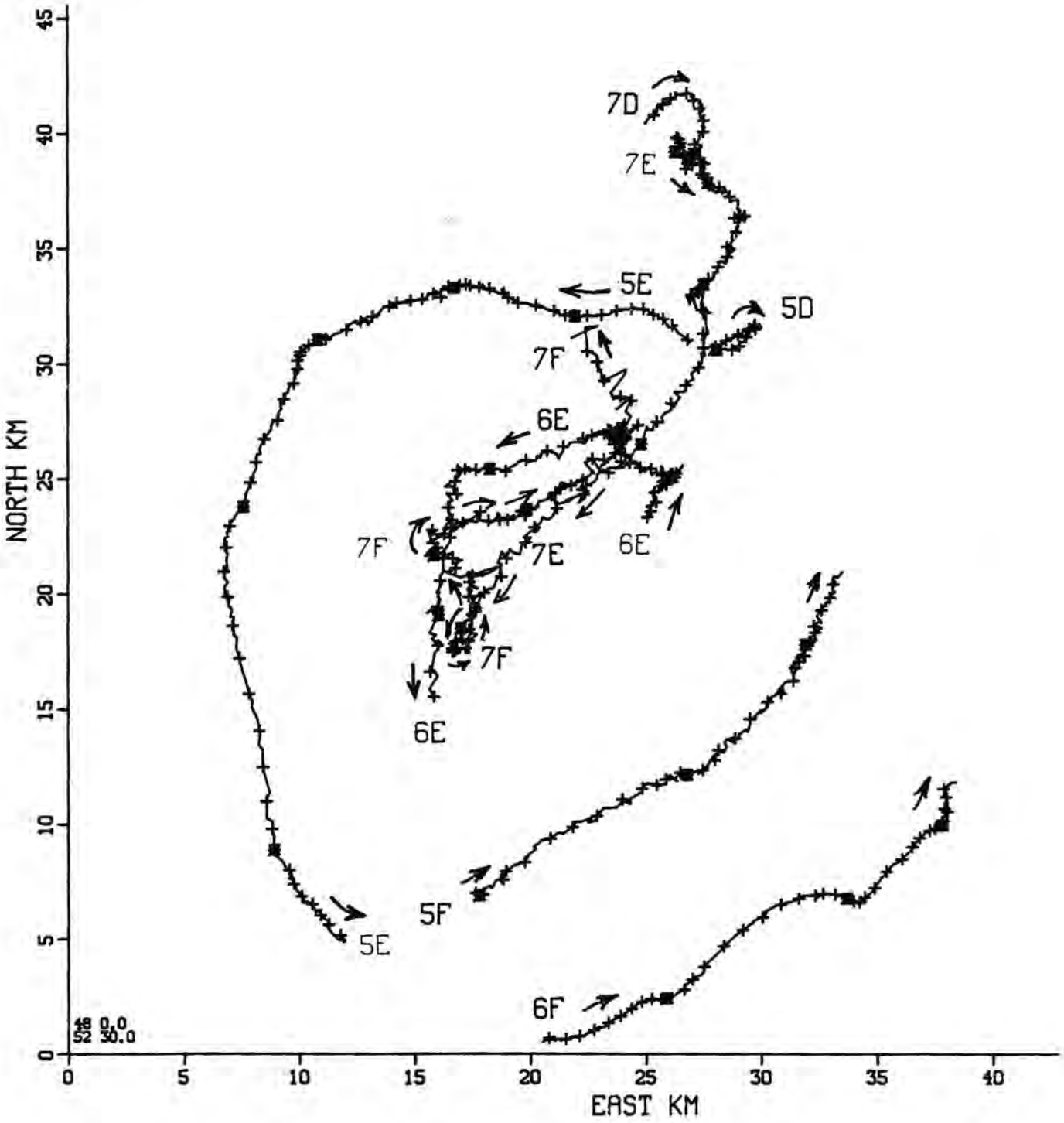

Fig. A4.14. Combined tracks of Icebergs 84-5, 84-6 and 84-7, ship track deleted.

APPENDIX 5 TEMPERATURE, SALINITY AND DENSITY STRUCTURE OF THE WATER COLUMN

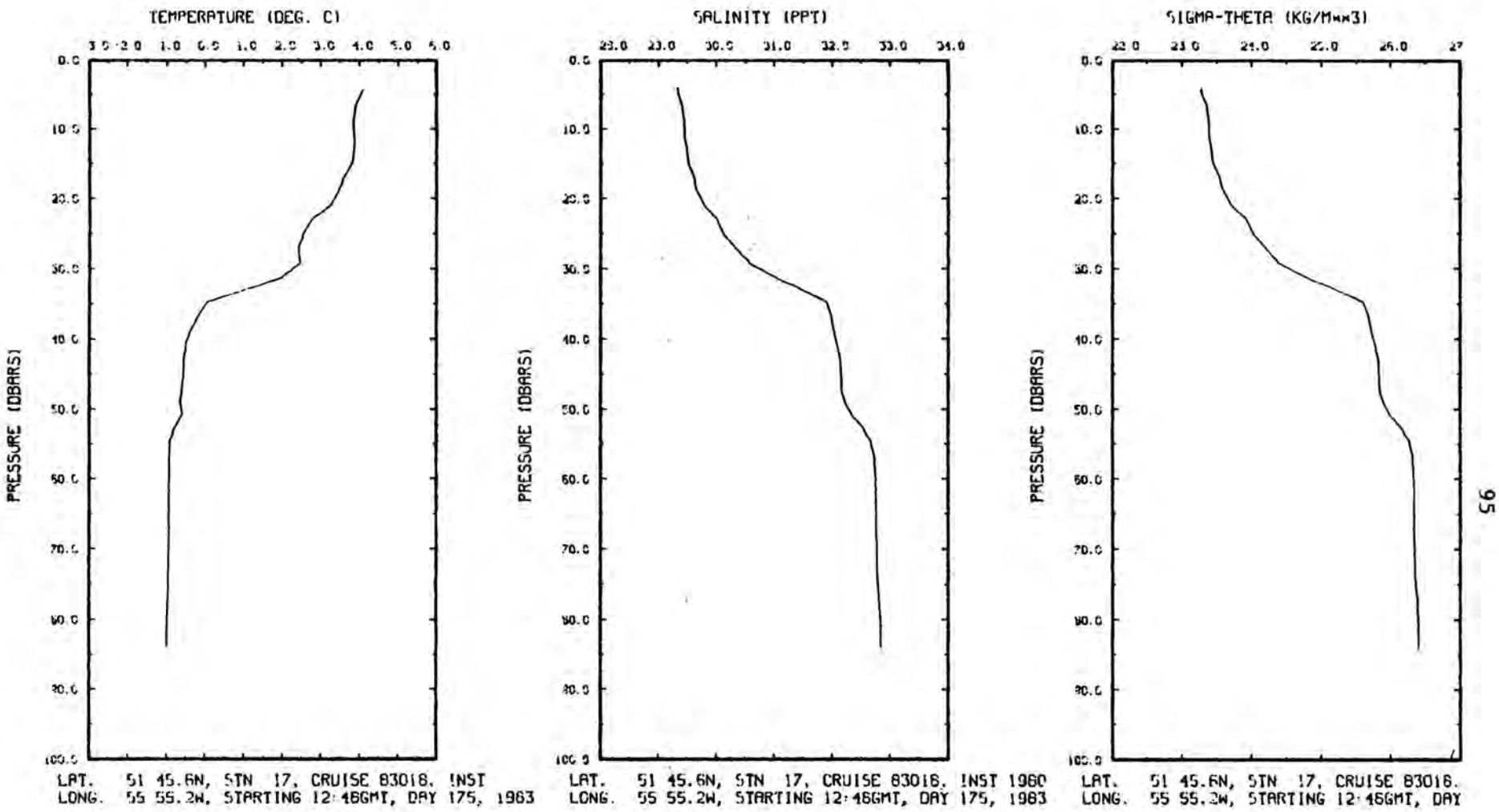

Fig. A5.1. Iceberg 83-1

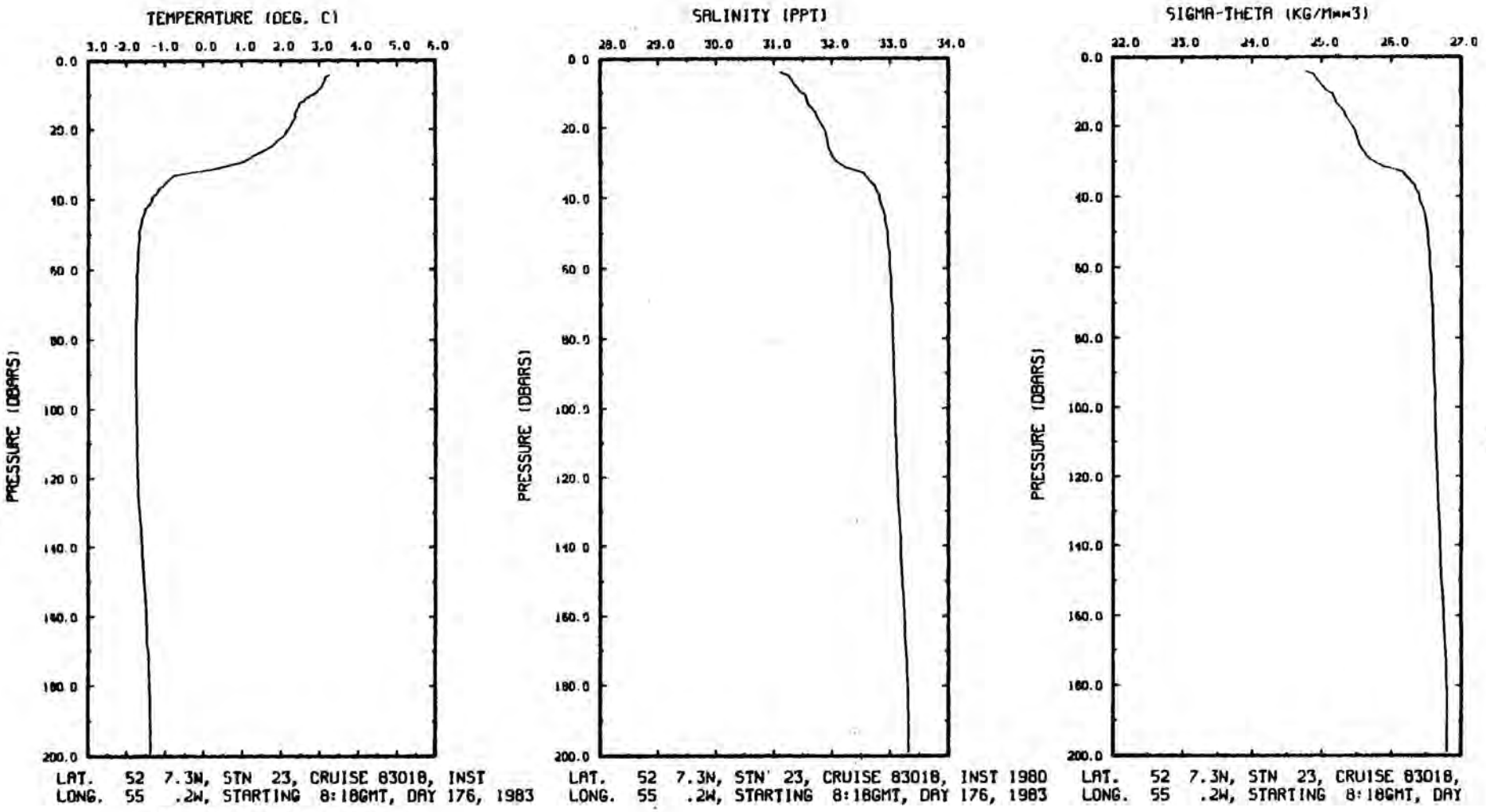

Fig. A5.2. Iceberg 83-2

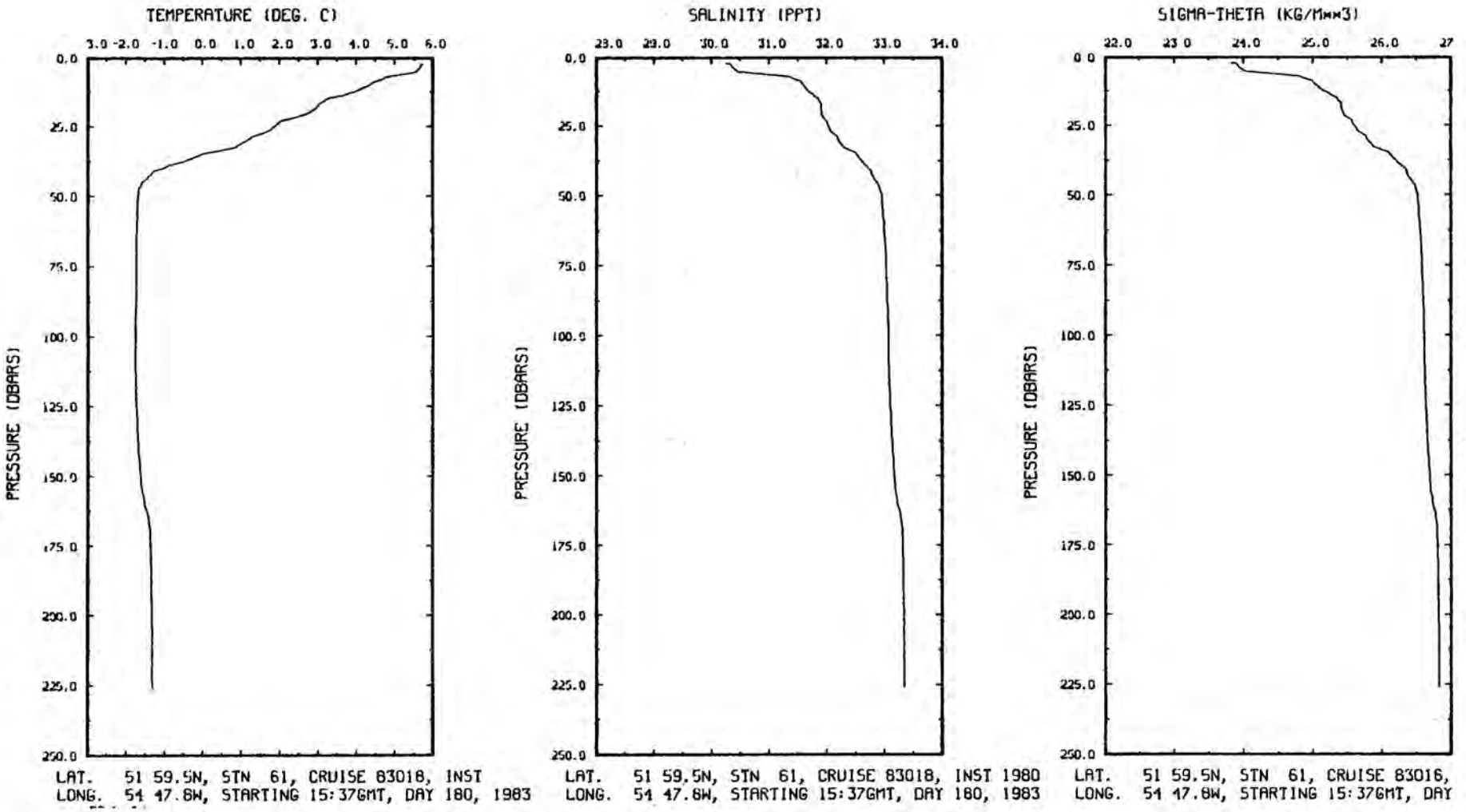

Fig. A5.3. Icebergs 83-3 and 83-5

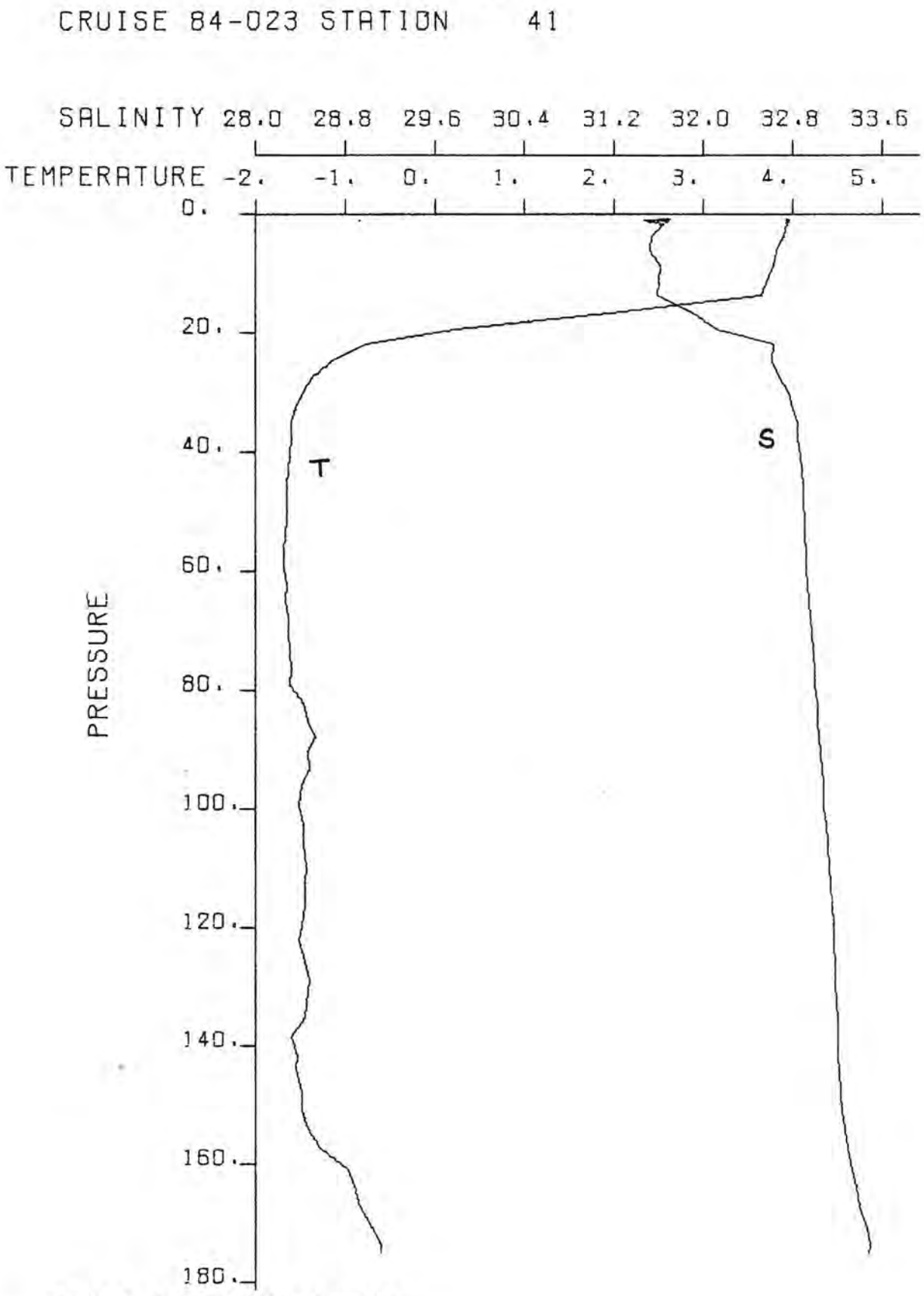

Fig. A5.4. Icebergs 84-5, 84-6 and 84-7

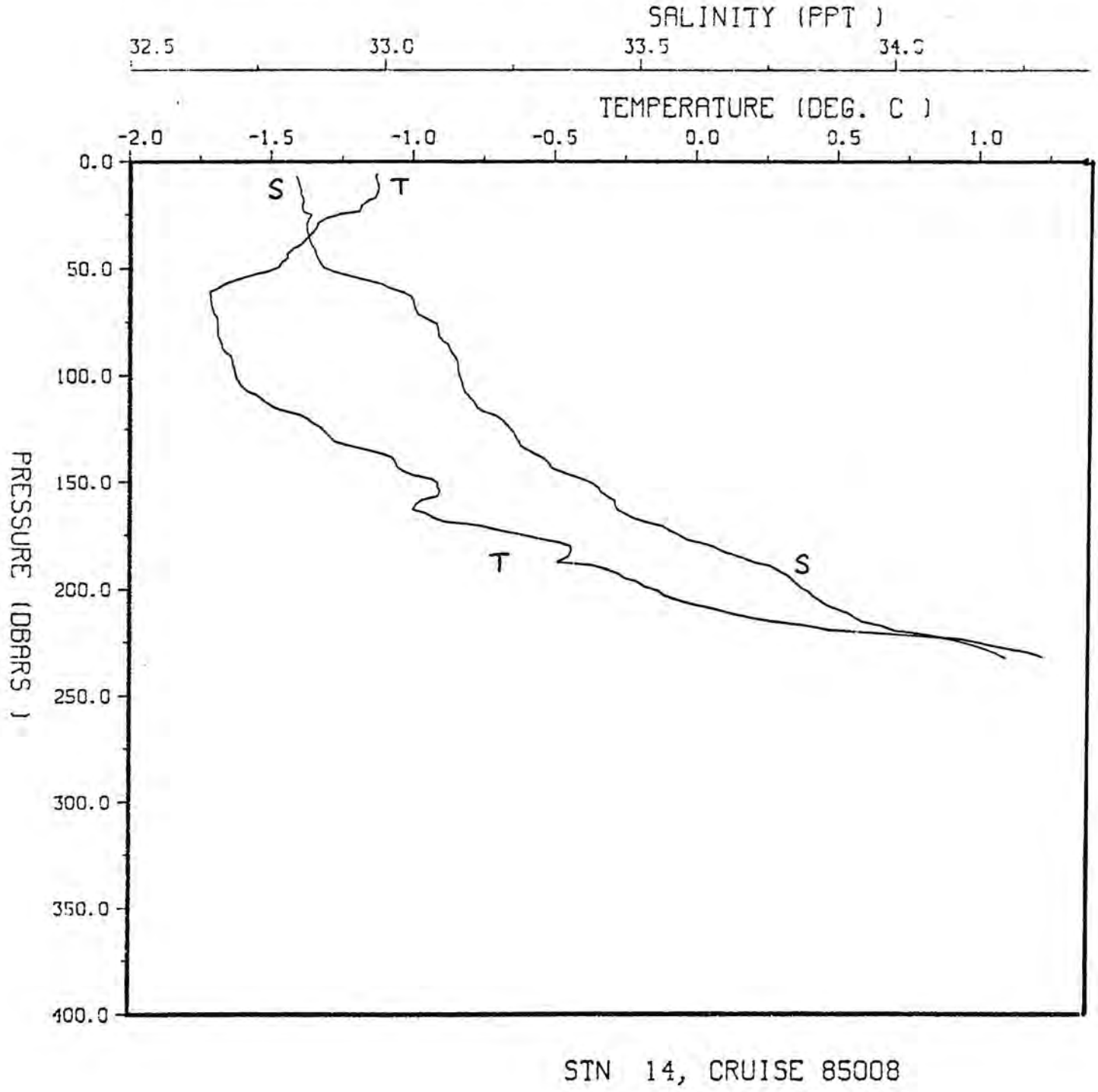

Fig. A5.5. Iceberg 85-1

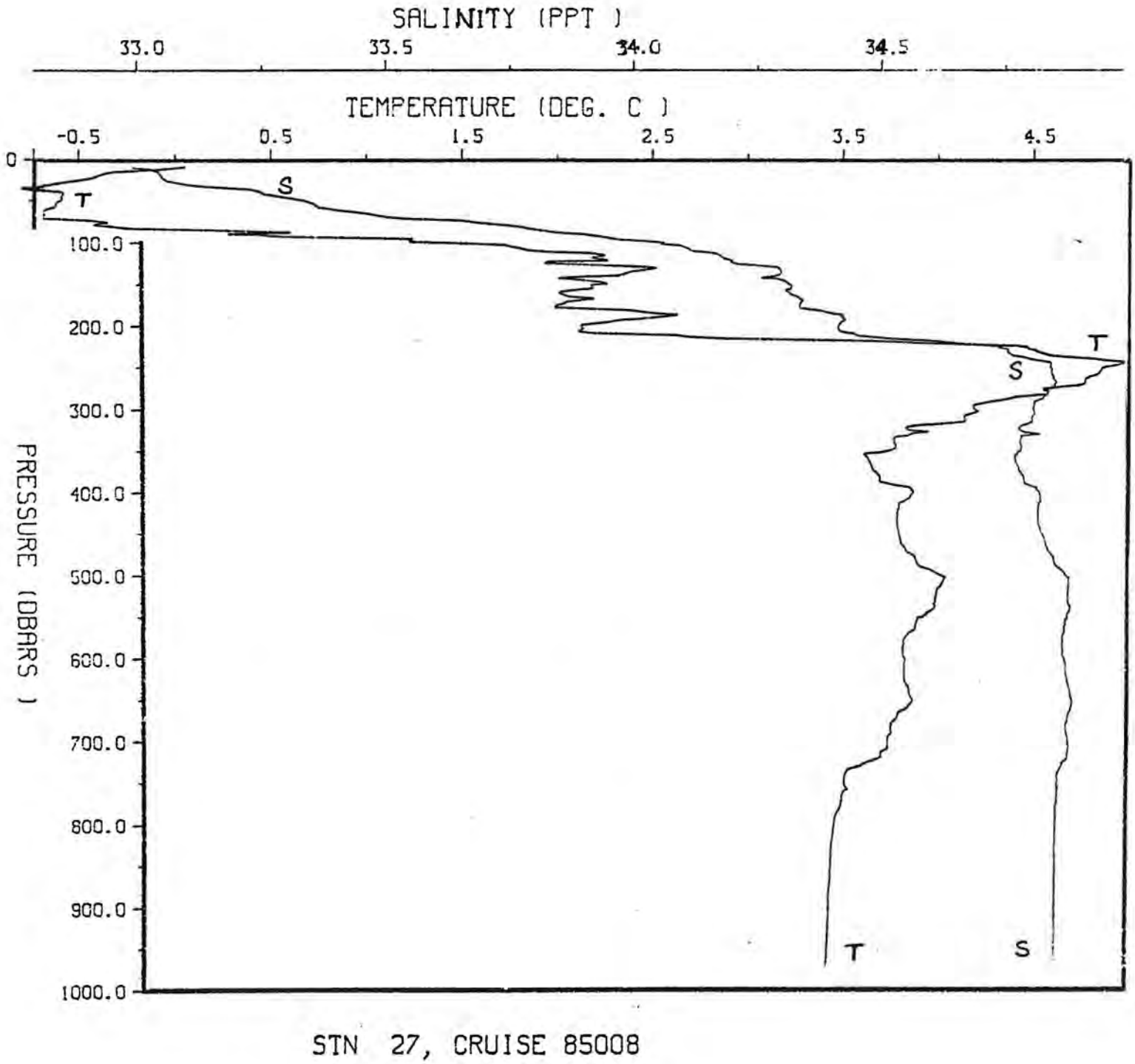

Fig. A5.6. Iceberg 85-4

APPENDIX 6 PROGRESSIVE CURRENT VECTOR PLOTS

The above figures illustrate the track of a particle travelling at the measured current velocity averaged over a particular depth layer. Symbols identify the layers: O 0-10 m, Δ 10-20 m, + 20-30 m, × 30-40 m,◇40-50 m, ∇ 50-60 m, ⊠ 60-70 m, ∗ 70-8-0 m, ⊕ 80-90 m, ⊕ 90-100 m. In 1984, currents were not measured at depths less than 27 m and data from the 27-30 m layer were used for the top three layers.

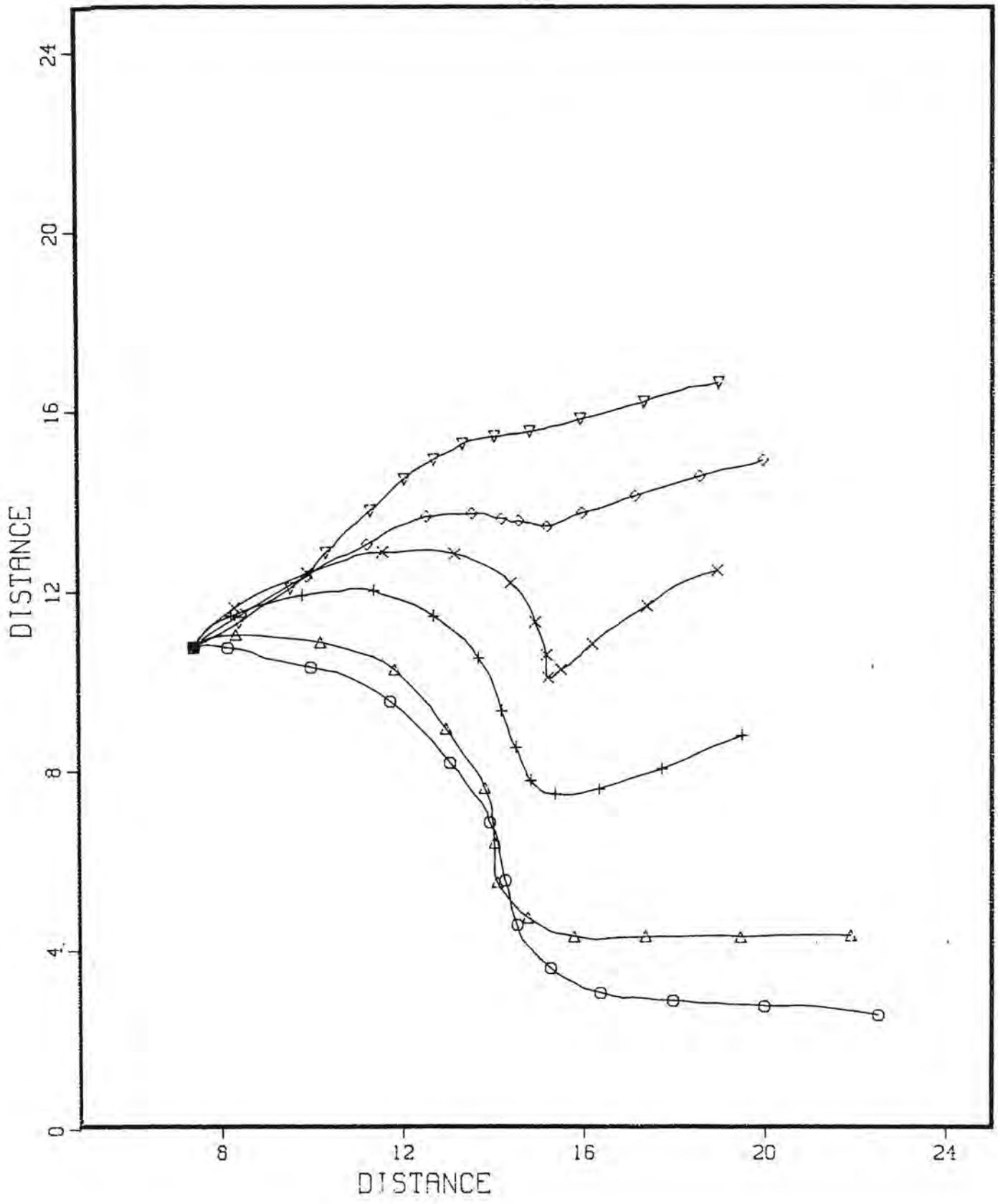

A6.1 Iceberg 83-1, hourly symbols

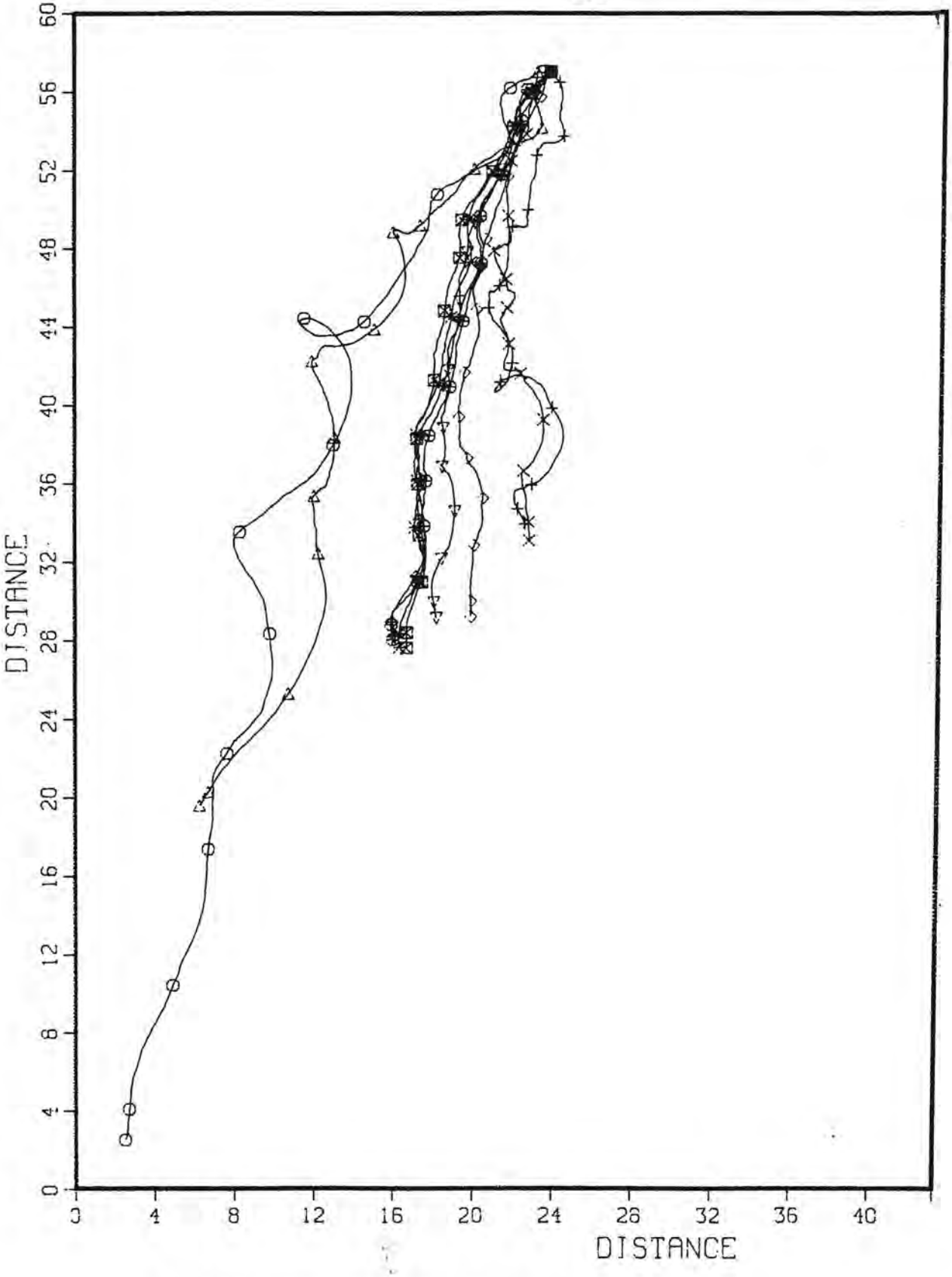

Fig. A6.2. Iceberg 83-2, six-hourly symbols

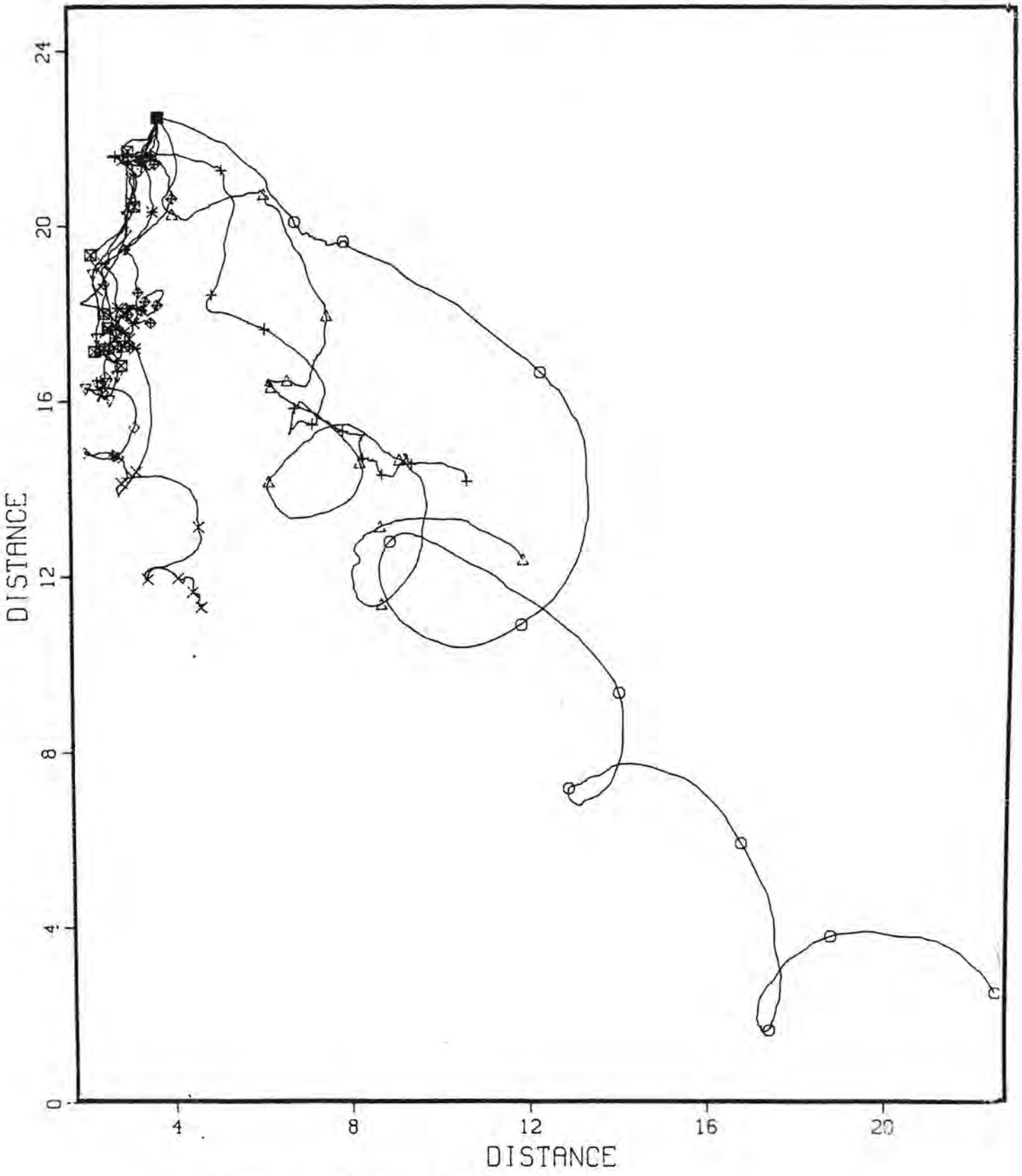

Fig. A6.3. Iceberg 83-3 and 83-5, six-hourly symbols

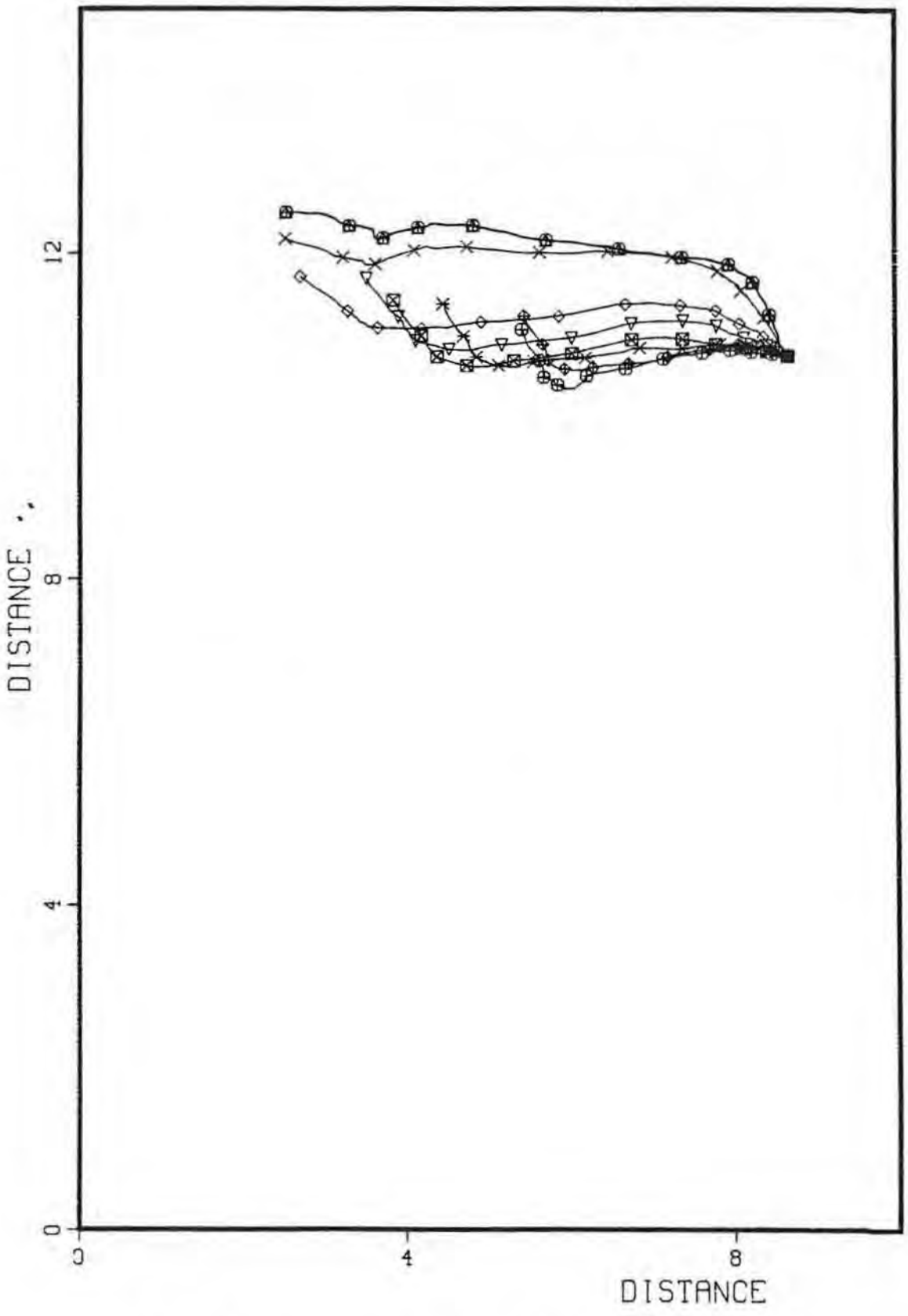

Fig. A6.4. Iceberg tracks 84-5D and 7D, hourly symbols

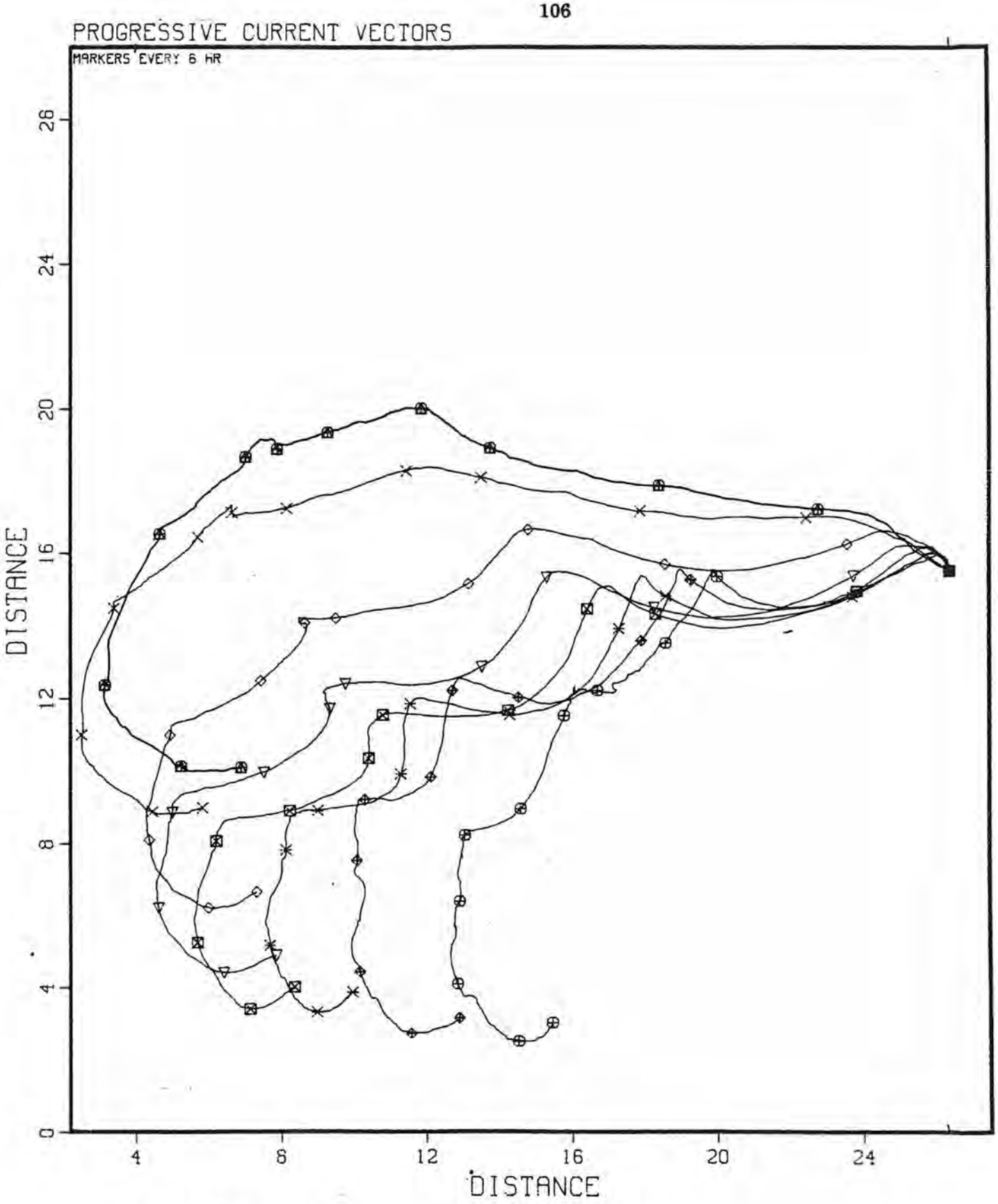

Fig. A6.5. Iceberg tracks 84-5E, 6E and 7E, six-hourly symbols

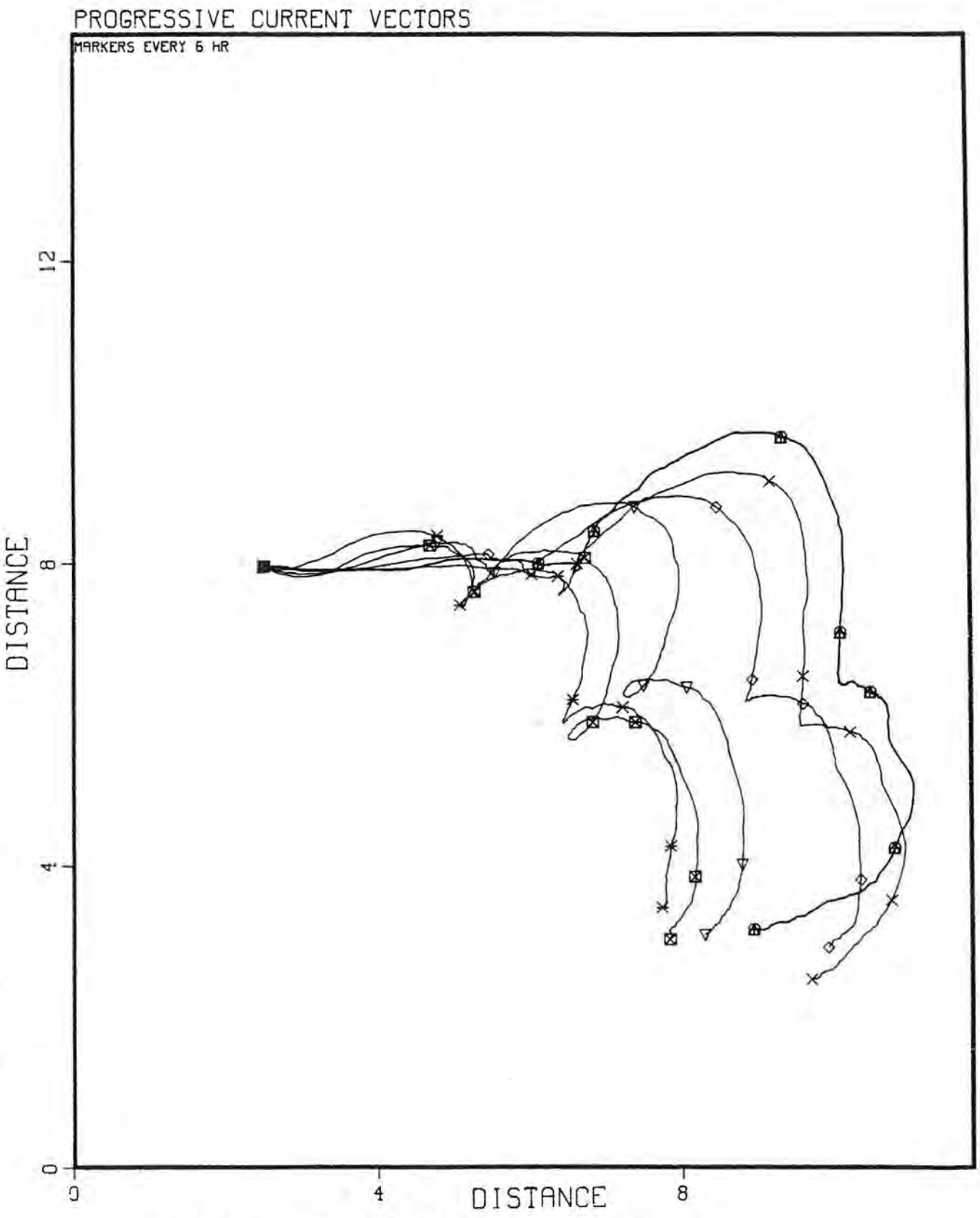

Fig. A6.6. Iceberg tracks 84-6F, 5F and 7F, six-hourly symbols

APPENDIX 7 AUTOCORRELATION OF VELOCITY

In each of these figures the upper frame shows the autocorrelations of the eastward iceberg velocity component (solid line) and of the northward component (dashed line) as a function of lag time. The lower left graph shows the complex autocorrelation of iceberg velocity, and the lower right graph shows the complex autocorrelation of either current in the 20-30 m layer, or wind, as noted in the caption. The complex autocorrelation starts at 1.0 for zero lag, and symbols mark hourly values of increasing lag.

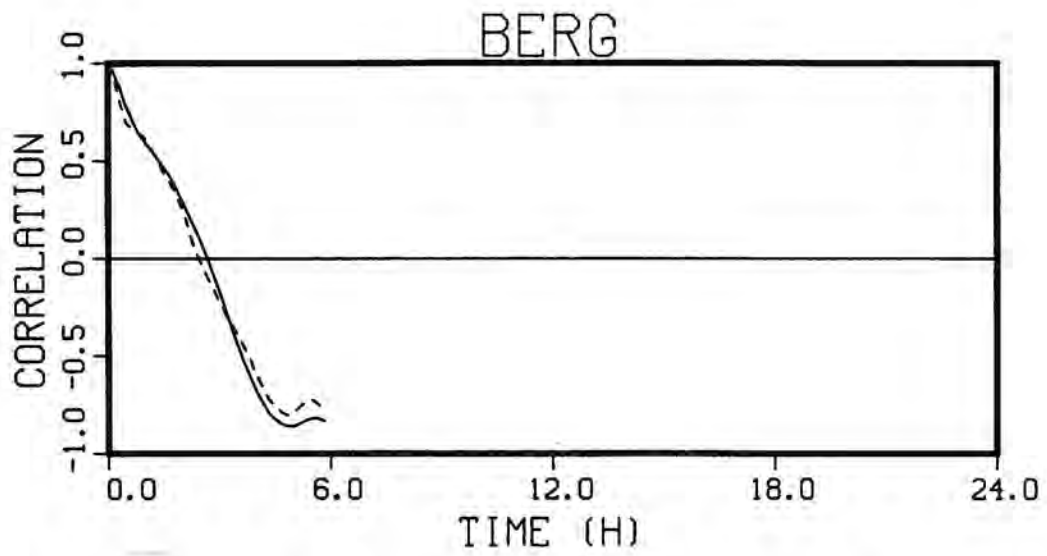

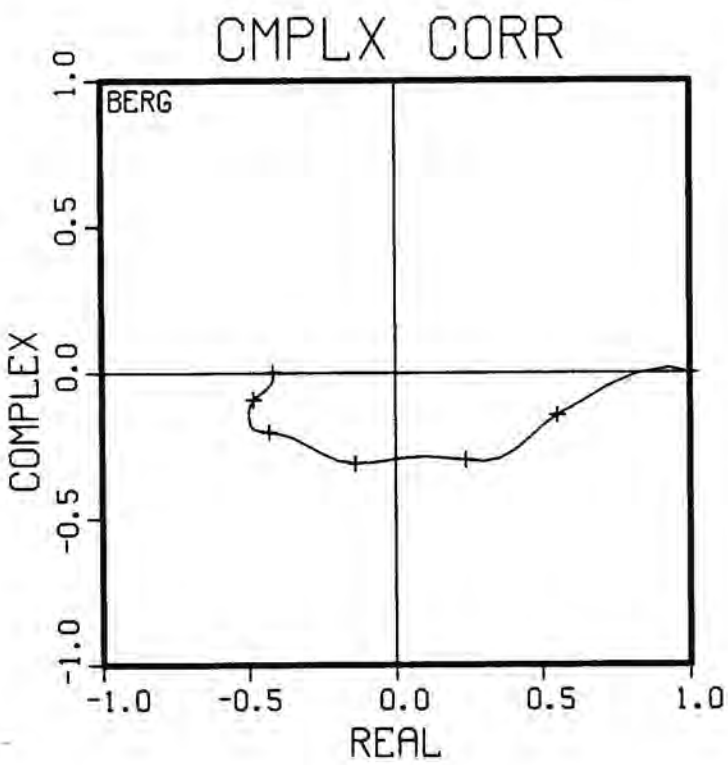

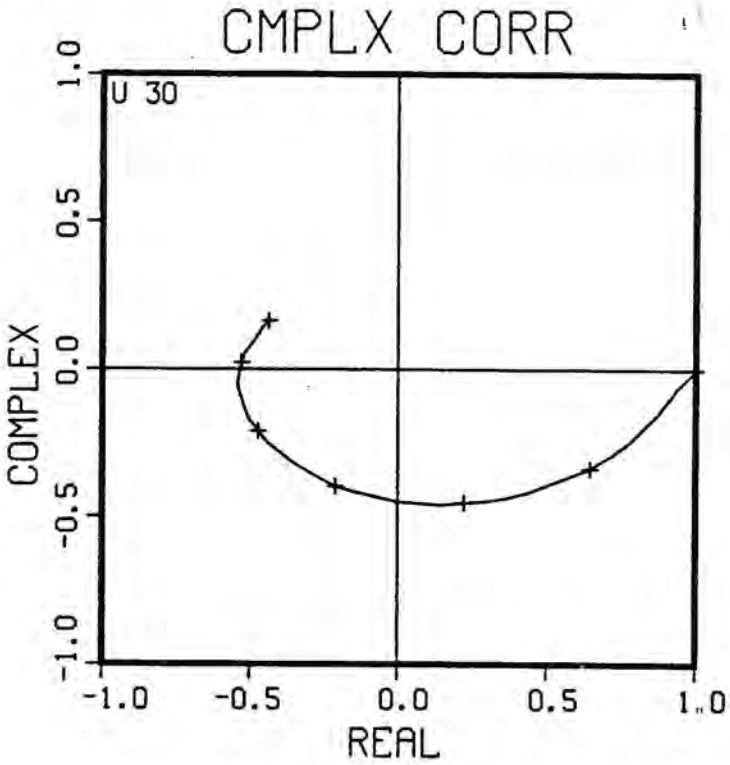

Fig. A7.1. Iceberg 83-1, autocorrelation of iceberg velocity and current

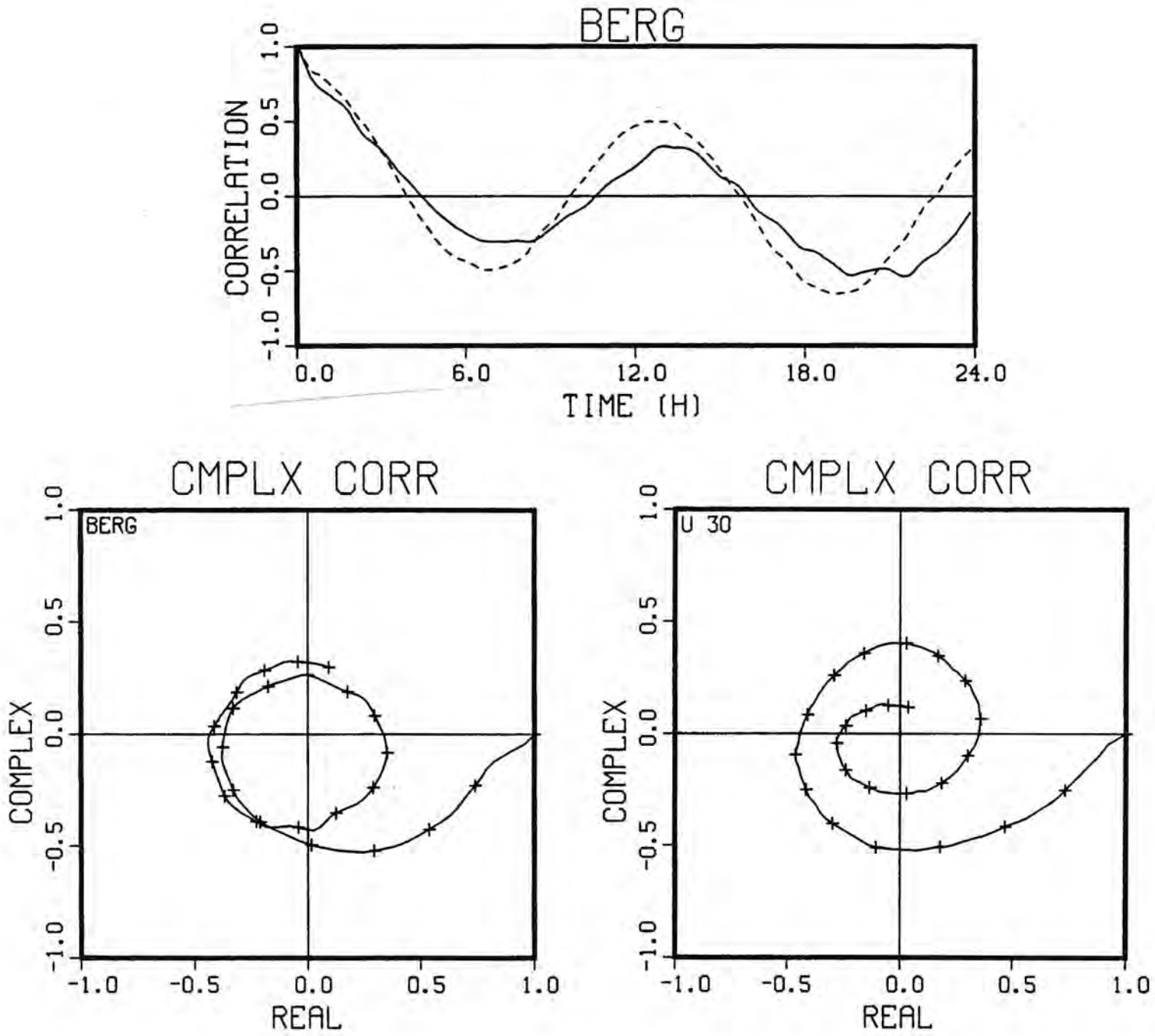

Fig. A7.2. Iceberg 83-2, autocorrelation of iceberg velocity and current

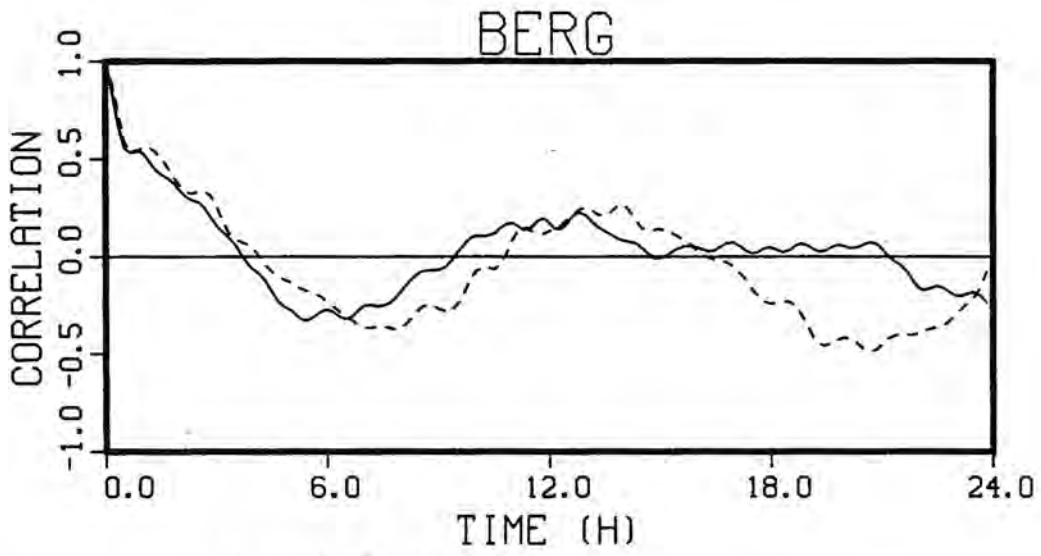

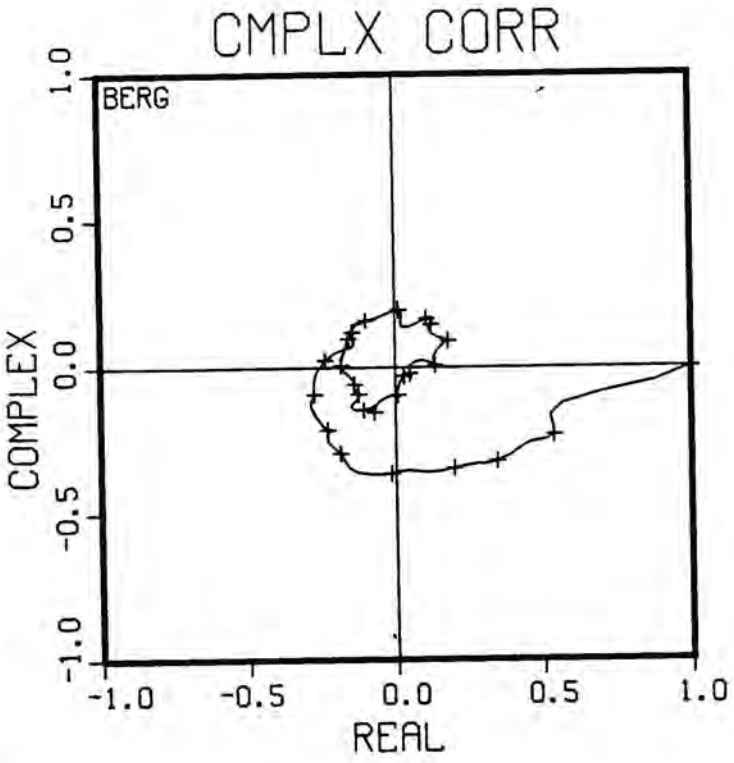

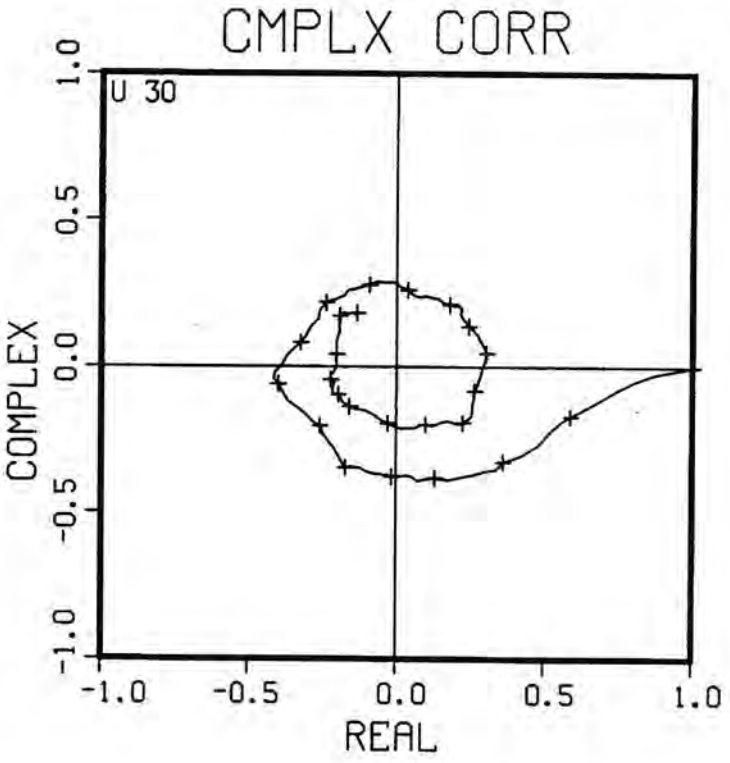

Fig. A7.3. Iceberg 83-3, autocorrelation of iceberg velocity and current

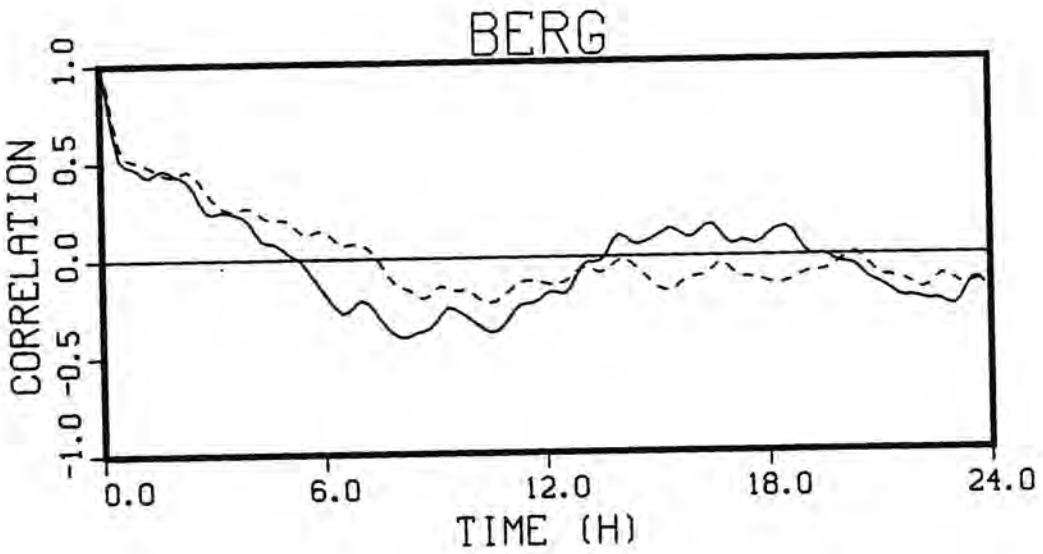

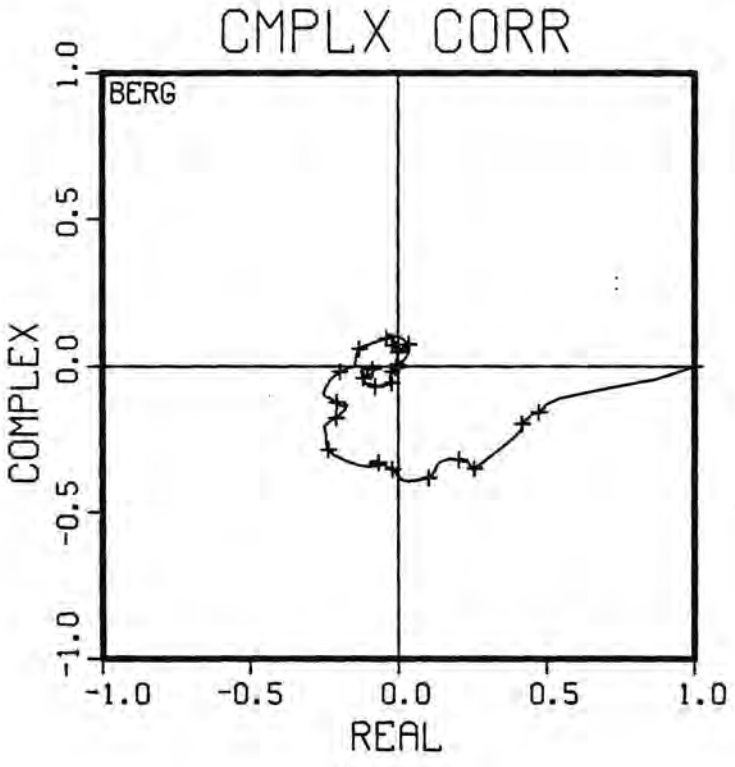

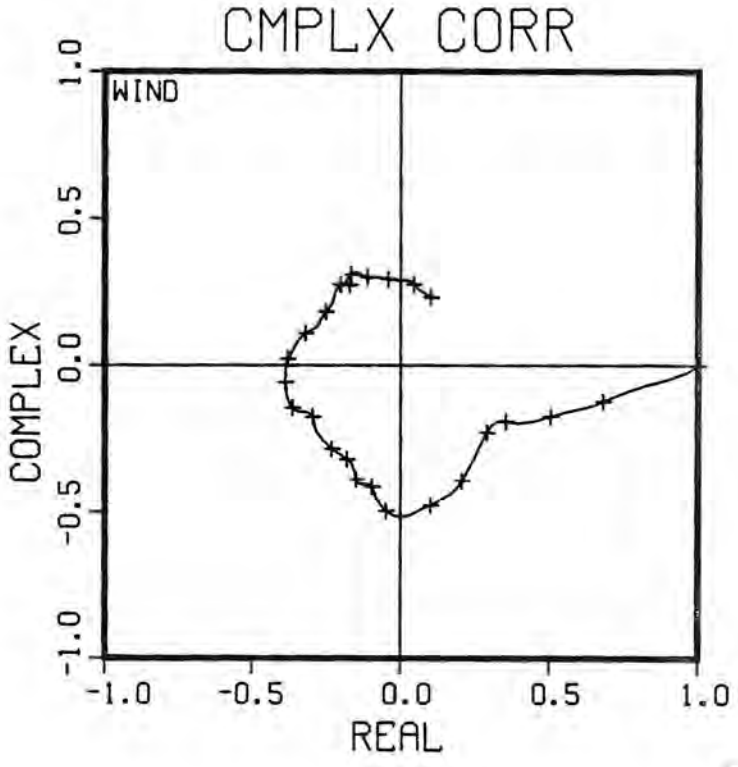

Fig. A7.4. Iceberg track 84-5 autocorrelation of iceberg velocity and wind

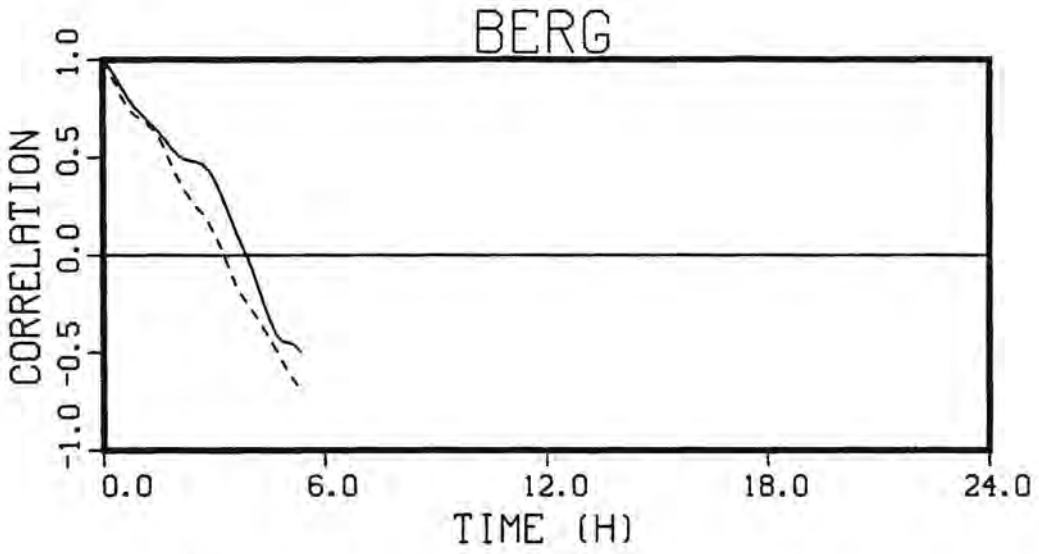

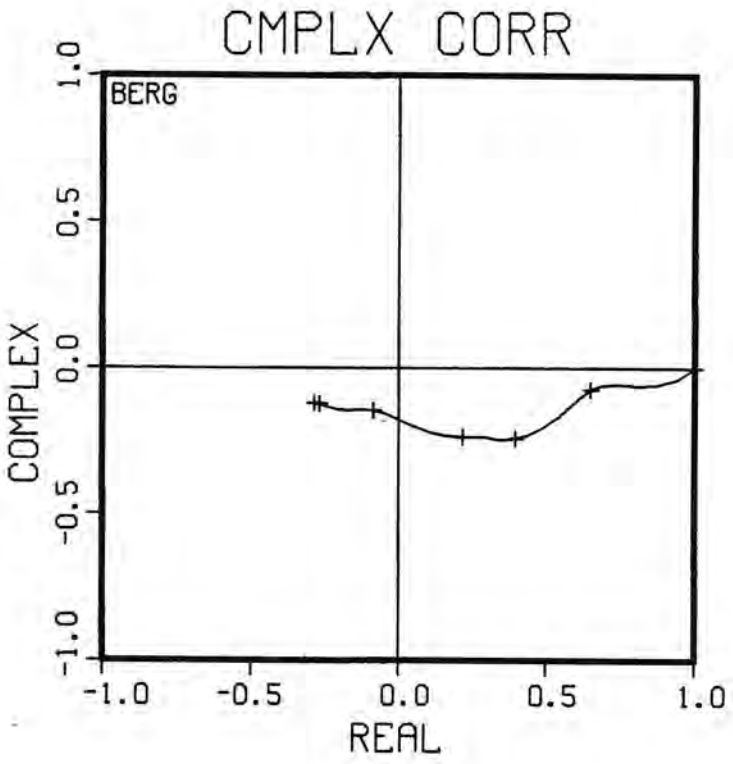

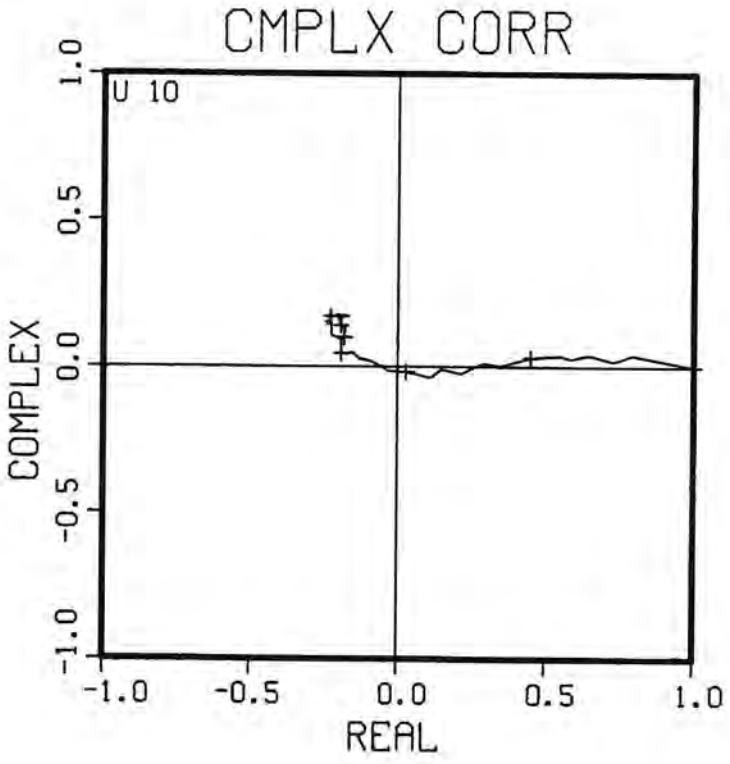

Fig. A7.5. Iceberg track 84-5D, autocorrelation of iceberg velocity and current

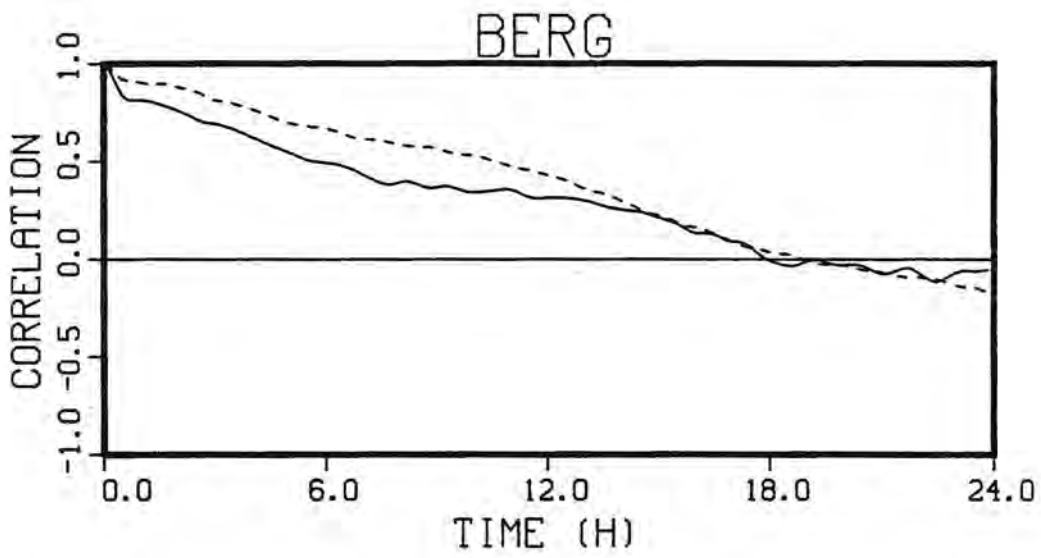

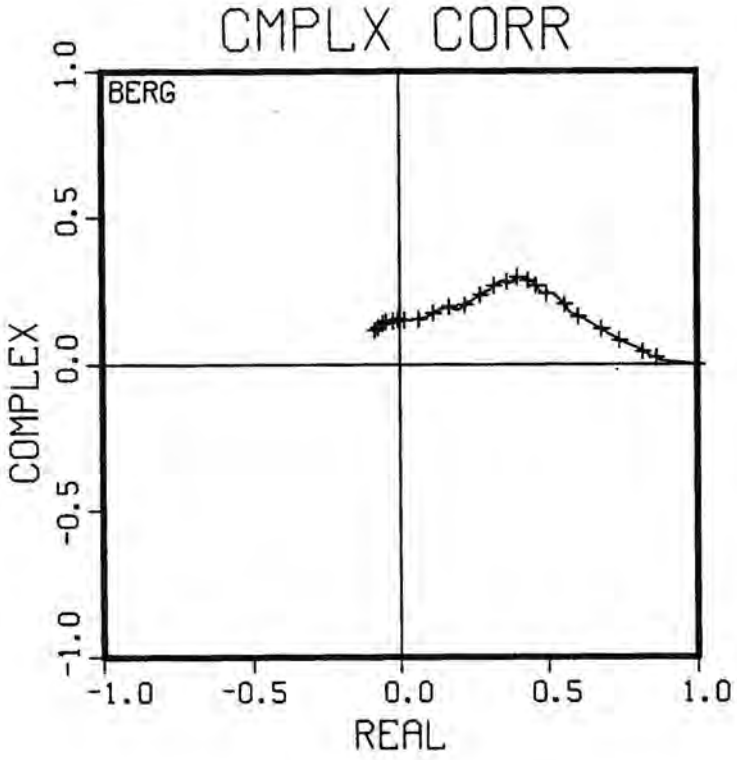

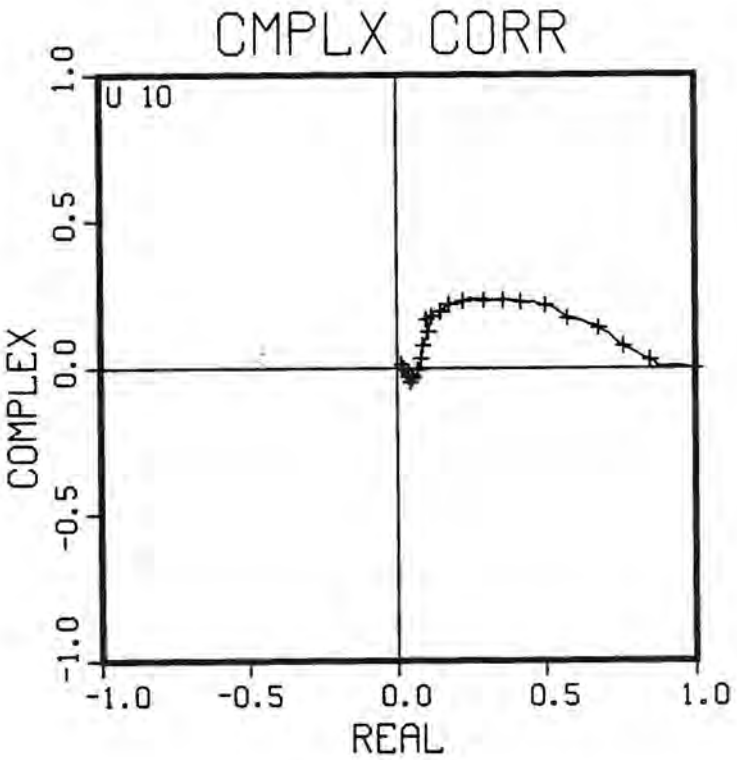

Fig. A7.6. Iceberg track 84-5E, autocorrelation of iceberg velocity and current

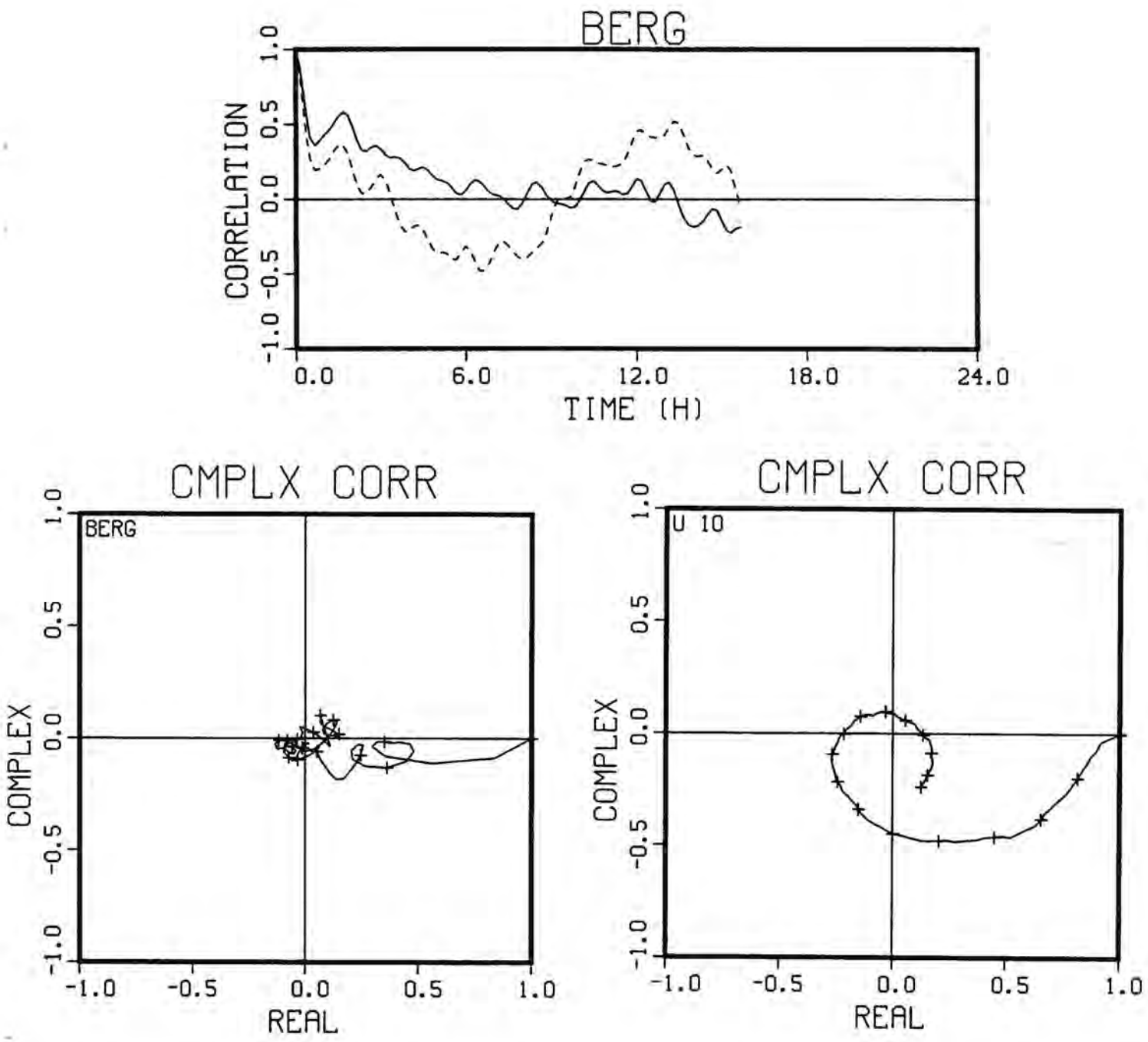

Fig. A7.7. Iceberg track 84-5F, autocorrelation of iceberg velocity and current

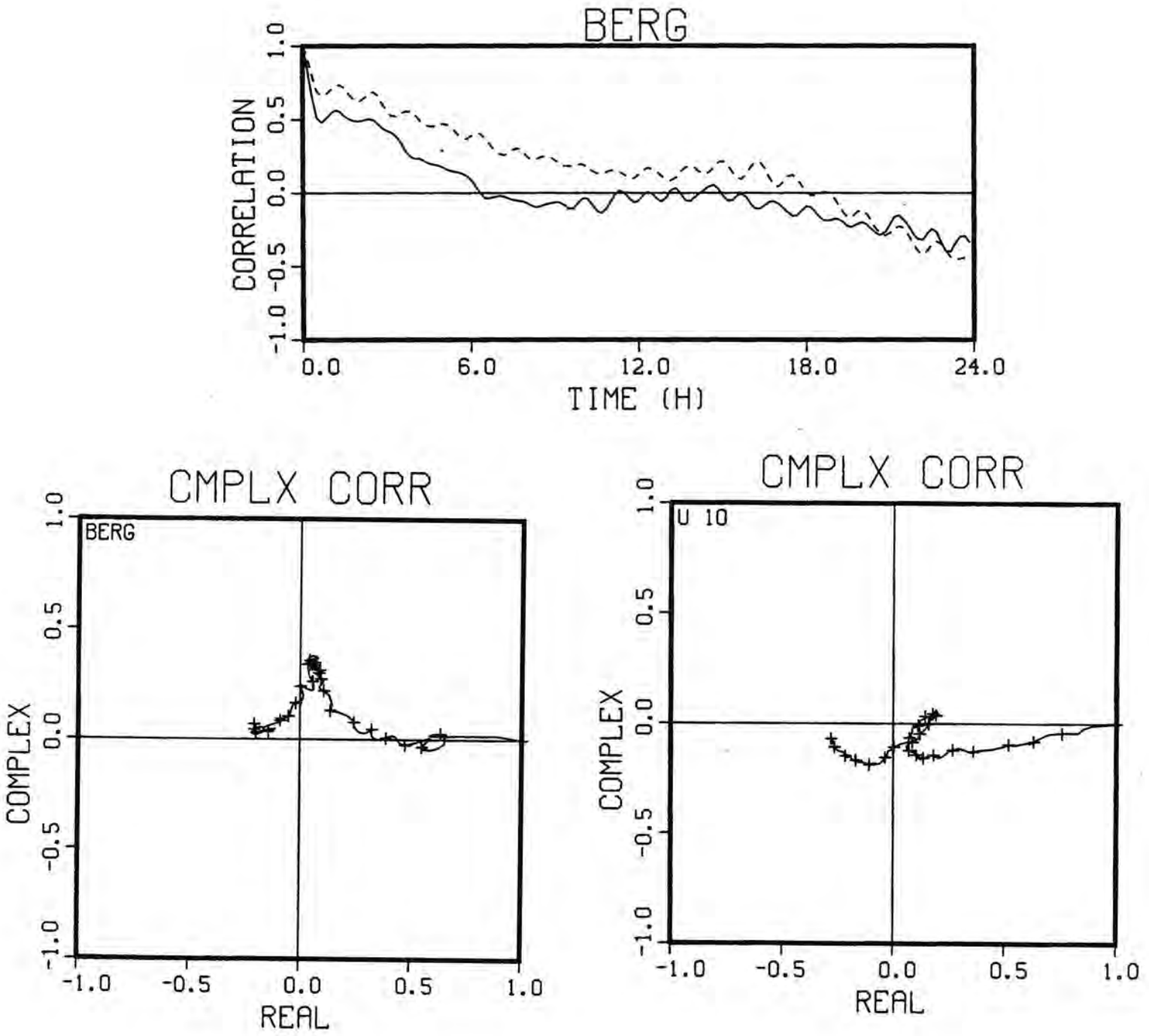

Fig. A7.8. Iceberg track 84-6E, autocorrelation of iceberg velocity and current

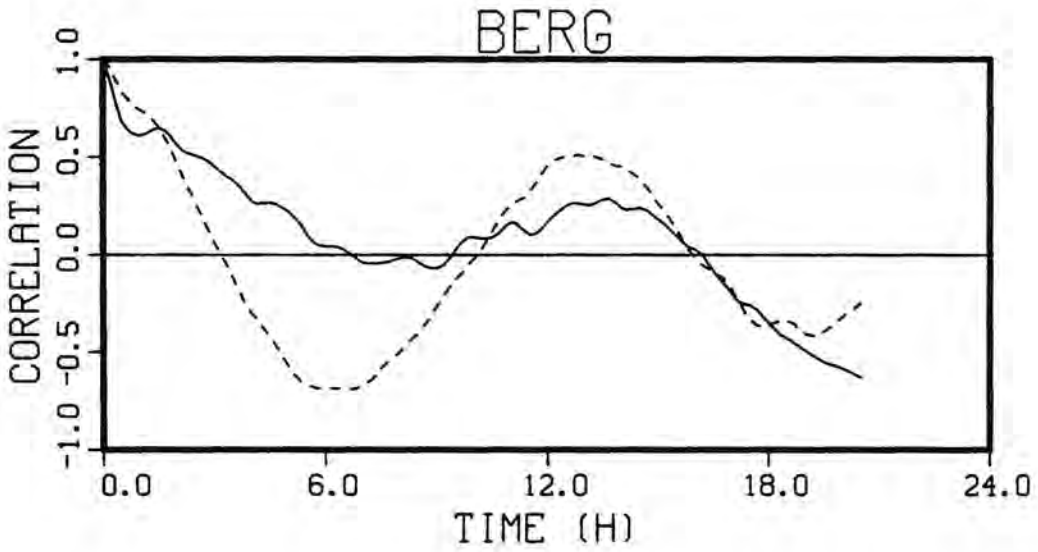

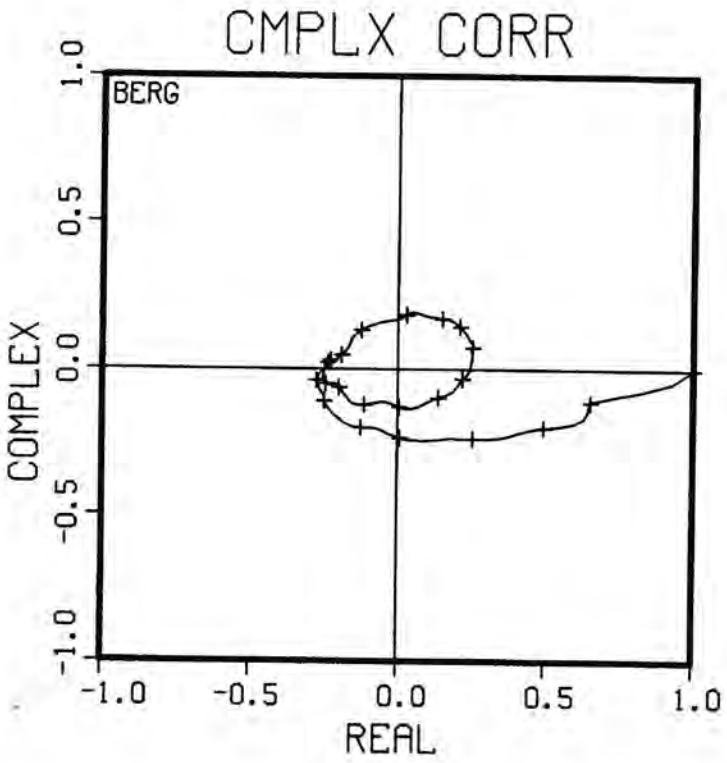

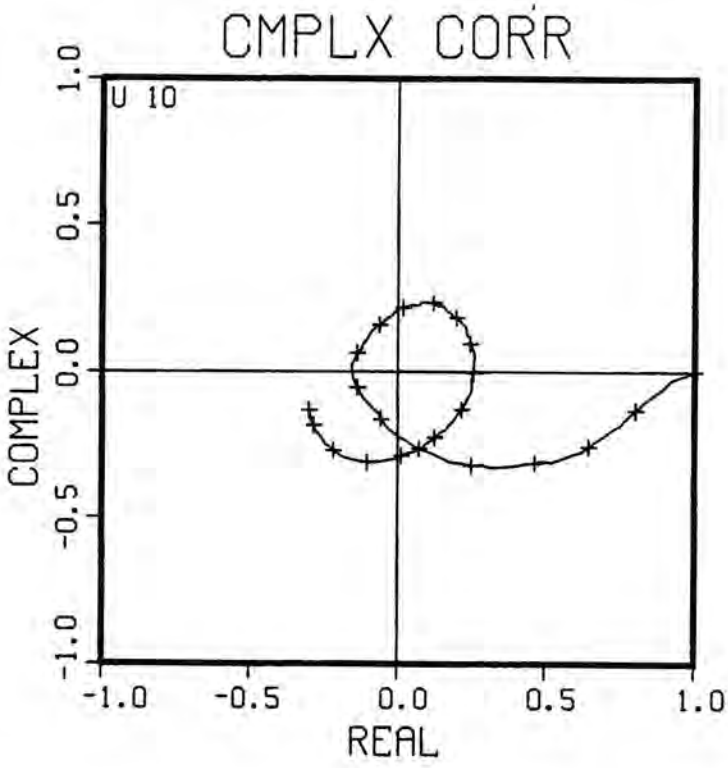

Fig. A7.9. Iceberg track 84-6F, autocorrelation of iceberg velocity and current

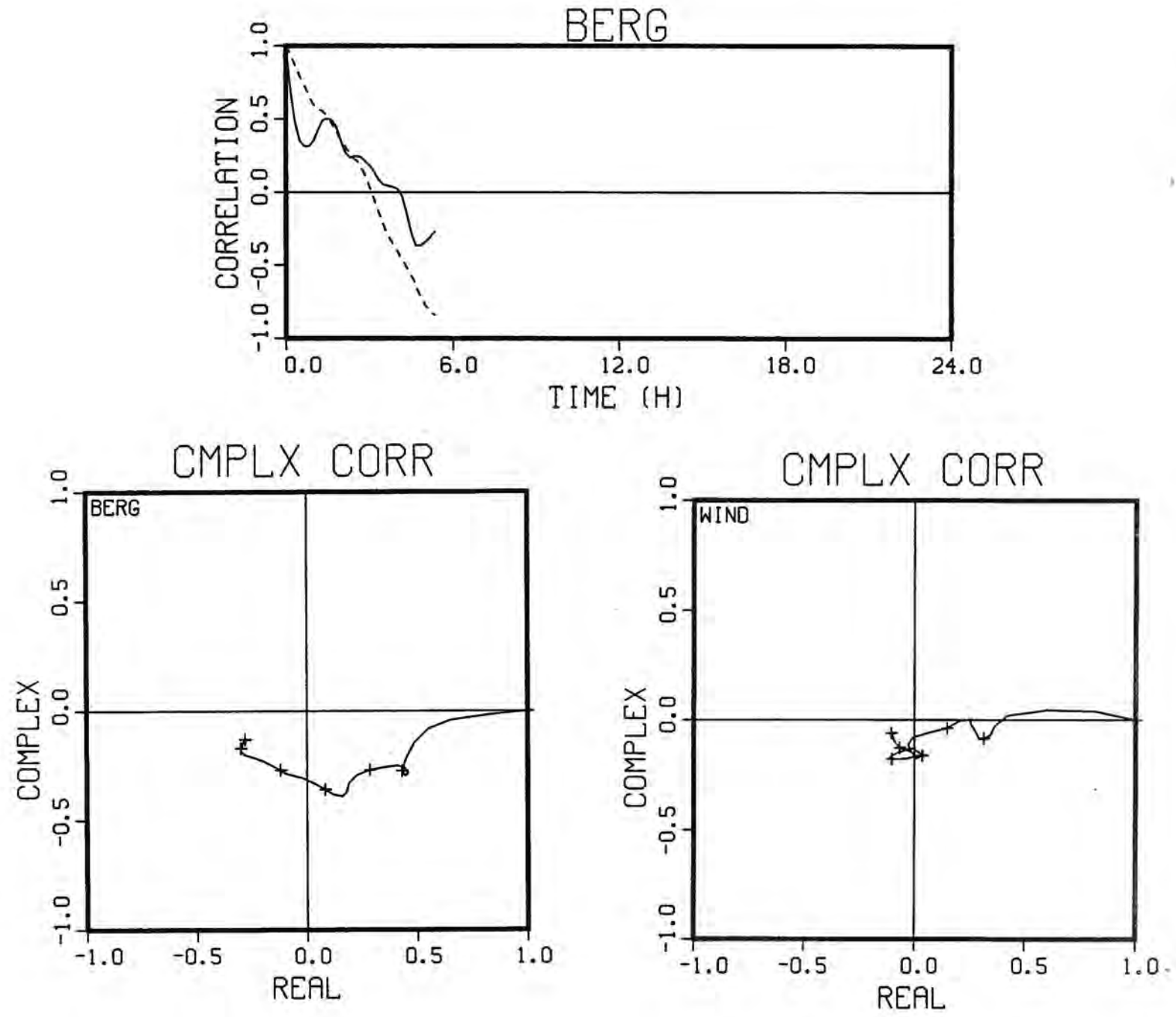

Fig. A7.10. Iceberg track 84-7D, autocorrelation of iceberg velocity and wind

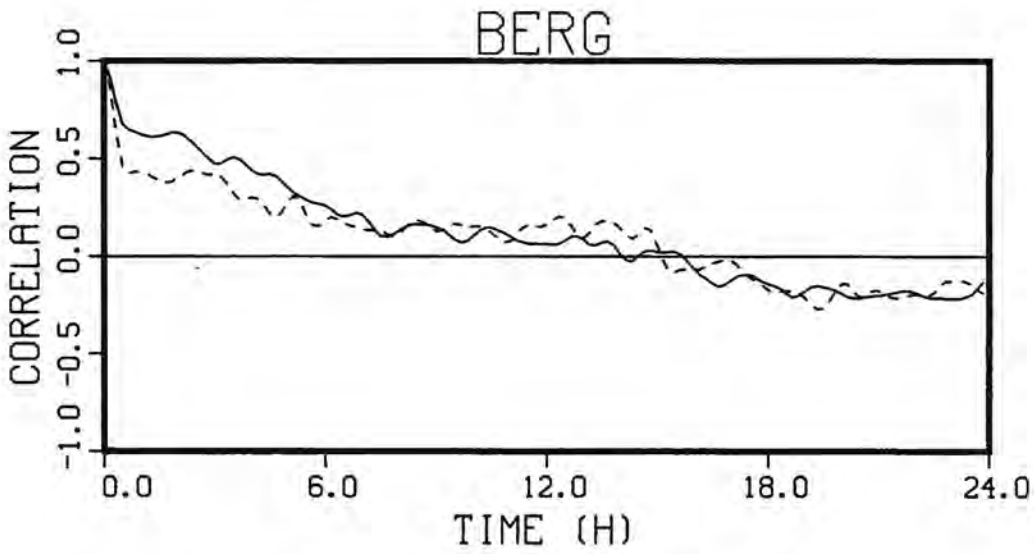

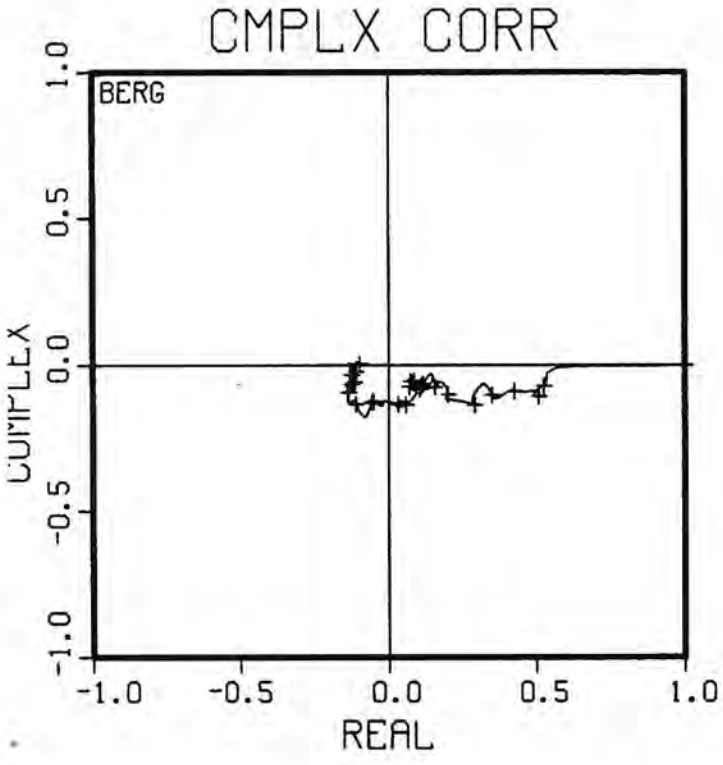

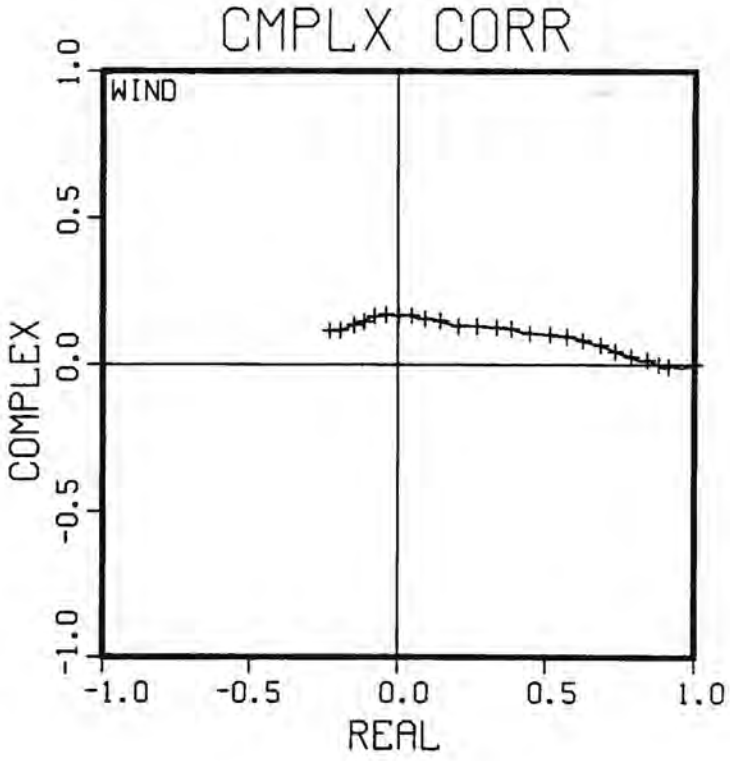

Fig. A7.11. Iceberg track 84-7E, autocorrelation of iceberg velocity and wind

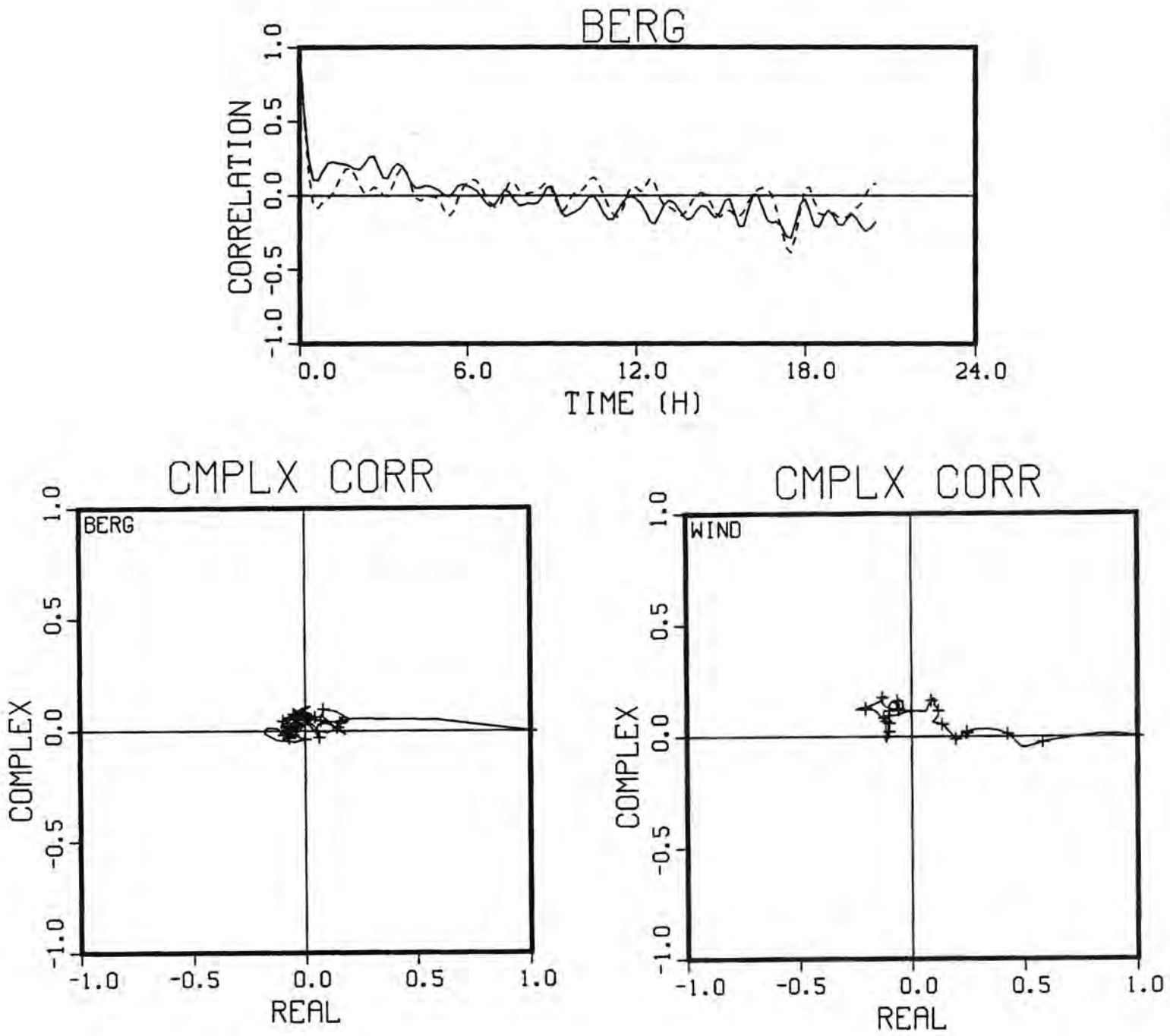

Fig. A7.12. Iceberg track 84-7F, autocorrelation of iceberg velocity and wind

APPENDIX 8 DATA FILES FOR DYNAMIC ICEBERG DRIFT MODEL

The data which have been discussed in this report may be obtained on a computer diskette by writing to the authors. For each iceberg track the first two lines (A and B) contain identification, data, location, iceberg size, and initialization instructions. The following lines (C) contain the wind, range and bearing, time, towing force, ship location, and the current profile at 10 min intervals The final line (D,not printed) contains 999 in columns 19-21. Parameters and formats are listed on the two following pages, and data for Iceberg 83-1 are reproduced here. The contents of the diskette are as follows:

	File
Program ITRACK 4 (dynamic model)	1
Iceberg 83-1	2
Iceberg 83-2	3
Iceberg 83-3	4
Iceberg 83-5	5
Iceberg track 84-5D	6
Iceberg track 84-5E	7
Iceberg track 84-5F	8
Iceberg track 84-6E	9
Iceberg track 84-6F	10
Iceberg track 84-7D	11
Iceberg track 84-7E	12
Iceberg track 84-7F	13

```
C          CARD A
C
C    NAME      CC  1-40  4A10   ICEBERG NAME, COMMENTS
C    LATC      CC 41-43  I3     LAT. OF LOWER L.H. CORNER OF PLOT (DEG)
C    CLAT      CC 44-49  F6.2   LAT. OF LOWER L.H. CORNER OF PLOT (MIN)
C                                NOTE: LATC+CLAT/60.0 SHOULD BE IN THE RANGE
C                                      40 TO 65 DEGREES.
C    LONGC     CC 50-52  I3     LONG. OF LOWER L.H. CORNER OF PLOT (DEG)
C    CLONG     CC 53-58  F6.2   LONG. OF LOWER L.H. CORNER OF PLOT (MIN)
C    RNEAST    CC 59-68  F10.3  EAST PLOT RANGE (KM)
C    RNORTH    CC 69-78  F10.3  NORTH PLOT RANGE (KM)
C    NTRACK    CC 79-80  I2     NUMBER OF TRACKS TO BE PLOTTED.
C                                (ALSO USED TO IDENTIFY DATA TYPE.)
C    DEPTH     CC 81-85  F5.2   DEPTH INTERVAL FOR CURRENT LAYERS (METERS).
C    CALIM     CC 86-90  F5.3   LARGEST CA VALUE POSSIBLE.
C                                NOT USED FOR ICE4010/STK4010.
C                                IF BLANK OR .LT.0.1, SET TO 4.0 IN ICE5010
C                                OR SET TO CA+1.1 (SEE CARD B) FOR CRUNCH.
C                                CALIM IS ROUNDED TO THE NEAREST INTEGRAL
C                                MULTIPLE OF 0.1 BY THE PROGRAM.
C                                CALIM CANNOT EXCEED CA+1.1 FOR CRUNCH.
C                                CALIM CANNOT EXCEED 4.0 IN ANY CASE.
C    CWLIM     CC 91-95  F5.3   LARGEST CW VALUE POSSIBLE.
C                                NOT USED IN ICE4010/STK4010.
C                                IF BLANK OR .LT.0.1, SET TO 5.0 IN ICE5010
C                                OR SET TO CW+1.1 (SEE CARD B) FOR CRUNCH.
C                                CWLIM IS ROUNDED TO THE NEAREST INTEGRAL
C                                MULTIPLE OF 0.1 BY THE PROGRAM.
C                                CWLIM CANNOT EXCEED CW+1.1 FOR CRUNCH.
C                                CWLIM CANNOT EXCEED 5.0 IN ANY CASE.
C
C          CARD B
C
C    V         CC  1- 5  F5.2   INITIAL ICE SPEED (M/SEC).
C    IDR       CC  6- 9  I4     INITIAL ICE DIRECTION (TOWARDS) DEG
C                                CLOCKWISE FROM NORTH.
C    LASTHR    CC 10-12  I3     TIME OF LAST OBSERVATION TO
C                                PROCESS (HOUR).
C                                LASTHR CAN BE GREATER THAN 24.
C    LASMIN    CC 13-14  I2     TIME OF LAST OBSERVATION TO
C                                PROCESS (MIN).
C              CC 15     1X     BLANK SPACE
C    CA        CC 16-20  F5.3   STARTING CA VALUE, SET TO 0.5 IF BLANK OR.
C                                .LT. 0.1.
C                                IN ICE4010/STK4010 THIS IS THE AIR
C                                DRAG COEFFICIENT (CA) VALUE USED.
C                                IN CRUNCH/ICE5010 THIS IS ROUNDED TO
C                                THE NEAREST INTEGRAL MULTIPLE OF 0.1.
C    CW        CC 21-25  F5.3   STARTING CW VALUE, SET TO 0.5 IF BLANK OR
C                                .LT. 0.1.
C                                IN ICE4010/STK4010 THIS IS THE WATER
C                                DRAG COEFFICIENT (CW) VALUE USED.
C                                IN CRUNCH/ICE5010 THIS IS ROUNDED TO
C                                THE NEAREST INTEGRAL MULTIPLE OF 0.1.
C    ISAIL     CC 26-30  I5     SAIL AREA IN AIR M**2
C    SAM       CC 31-40  E10.3  MASS IN METRIC TONNES
C    IDEVN     CC 41-44  I4     ROTATION ANGLE FOR CURRENT (CLOCKWISE)
C                                IN DEGREES.
C    KDEVN     CC 45-48  I4     ROTATION ANGLE FOR WIND (CLOCKWISE)
C                                IN DEGREES.
C    KEEL(I)   CC 49-98  10I5   KEEL AREA (M**2) AT 10 DEPTHS
C    ITIME     CC 99-102 I4     TIME STEP (SECONDS). ITIME MUST DIVIDE
C                                EVENLY INTO 600. ALL POSSIBLE VALUES OF
```

```
C                              ITIME ARE 1,2,3,4,5,6,8,10,12,15,20,24,25,
C                              30,40,50,60,75,100,120,150,200,300,600.
C                              LARGE VALUES  OF ITIME (.GE. 50) ARE NOT
C                              RECOMMENDED SINCE LARGE ERRORS OR
C                              COMPUTATIONAL INSTABILITY MAY OCCUR.
C                              DEFAULT FOR ITIME IS 24.
C    IBEGHR    CC 103-104 I2   START TIME (HOUR)  - MODEL IGNORES INPUT DATA BEFORE THIS TIME
C    IBEGMN    CC 105-106 I2   START TIME (MINUTE)
C
C         IF ISAIL OR SAM OR KEEL(1) IS 0, PROGRAM STOPS.
C
C         NEW DATA EFFECTIVE AT ELAPSED TIME NEWHR, NEWMIN.
C         INTERVAL BETWEEN OBSERVATIONS MUST BE AN INTEGRAL MULTIPLE
C         OF 10 MINUTES.
C         N.B.: PROGRAM CANNOT HANDLE MORE THAN 1000 TEN MINUTE
C               OBSERVATIONS (APPROX. 166 HOURS).
C
C          CARD C
C
C    U         CC 1-5     F5.2  WIND SPEED (M/SEC)
C    IDRU      CC 6-9     I4    WINDS FROM (DEG CLOCKWISE FROM NORTH)
C    RANGE     CC 10-14   F5.2  RANGE TO BERG (NAUTICAL MILES)
C    IBRG      CC 15-18   I4    BEARING TO BERG FROM SHIP (DEG CLOCKWISE
C                                FROM NORTH).
C    NEWHR     CC 19-21   I3    TIME (HOUR). HOURS ARE NUMBERED
C                                CONTINUOUSLY AND THEREFORE, NEWHR CAN BE
C                                .GT. 24.
C    NEWMIN    CC 22-23   I2    TIME (MIN.)
C    TOW       CC 24-28   F5.1  TOWING FORCE (METRIC TONNES)
C    IDRT      CC 29-31   I3    TOWING FORCE DIRECTION (DEG CLOCKWISE
C                                FROM NORTH).
C    LATS      CC 32-33   I2    SHIP'S LATITUDE (DEG)
C    SSLAT     CC 34-38   F5.2  SHIP'S LATITUDE (MIN)
C    LONGS     CC 39-40   I2    SHIP'S LONGITUDE (DEG)
C    SSLONG    CC 41-45   F5.2  SHIP'S LONGITUDE (MIN)
C    IWX(I),
C    IWY(I)    CC 46-125 20I4   X,Y COMPONENT CURRENT PAIRS AT
C                                10 DEPTHS (CM/S).
C    IWX(11)   CC 126-129 I4    X CURRENT COMPONENT AVERAGE (CM/S).
C    IWY(11)   CC 130-133 I4    Y CURRENT COMPONENT AVERAGE (CM/S).
C
C         CARD D
C
C         CARD D HAS ONE NUMBER (999) PLACED IN THE POSITION OF NEWHR
C         ON CARD C TO ENABLE THE PROGRAM TO DETERMINE THE END OF THE
C         SET OF DATA IN THE FILE.
C
C     999     CC 19-21          USED TO DENOTE THE END OF A DATA SET
C
C
```

```
ICEBERG #1 CRUISE 83-018 JUNE 24,1983    51 42.00 56  4.00    25.000    25.000 010.003.0005.0000.000
  .70  86 1700 1.0001.000  445   .850E+05   0   0  546  500  427  403  348   51     0    0    0    0  24 600
 2.73 202 6.47 233   5 0  0.0  05151.275553.74  20   5  16  15  15  22  11  21  21  21  20  13  18  17  19  12  26  11   0   0  13  16
 4.08 209 6.10 232  510  0.0  05151.085554.23  10   4  16  11  13  22  13  22  21  19  23  13  23  13  25  12  28   9   0   0  12  17
 4.17 239 5.20 230  520  0.0  05150.575555.41  15   1  19  10  17  22  24  23  28  19  30  15  27  13  28  11   0  -8   0   0  10  19
 5.34 213 4.32 228  530  0.0  05149.845556.17  21  -1  27   6  24  20  28  26  32  20  31  16  27  15  28  15   2  -3   0   0  11  22
 3.50 214 3.44 224  540  0.0  05149.895557.02  27  -4  35   5  31  18  34  27  35  22  31  18  27  18  28  18   5   2   0   0  12  25
 4.62 227 2.60 218  550  0.0  05149.435558.00  32  -6  43   2  38  15  39  30  39  23  32  19  27  21  27  22   8   6   0   0  13  28
 4.13 238 1.84 209   6 0  0.0  05148.975558.78  44  -5  54   0  41  17  36  23  35  23  28  21  34  19  27  19  -3  -8   0   0  10  29
 4.19 237 1.09 195  610  0.0  05148.515559.44  49 -13  49  -5  44  18  41  25  39  23  30  21  31  17  27  18   6  -6   0   0   9  31
 6.23 236  .50 155  620  0.0  05147.845559.98  42 -21  49  -5  46  12  44  22  42  26  33  24  33  18  31  22   4 -25   0   0   7  32
 3.68 221  .40 154  630  0.0  05147.795559.65  57 -11  53  -6  44  12  52  19  41  25  31  18  31  17  27  22  38  -1   0   0   9  37
 4.18 239  .30 162  640  0.0  05147.785559.30  57 -13  52  -5  43  12  48  20  44  25  35  22  31  18  31  21  38  -1   0   0   9  37
 4.11 236  .29 169  650  0.0  05147.775559.06  57 -10  54  -8  44   6  48  20  40  20  32  22  28  15  28  20  39   3   0   0   8  37
 4.55 228  .25 185   7 0  0.0  05147.765558.72  57 -13  51 -13  49   9  53  19  38  27  30  23  31  21  32  22  38  -1   0   0   9  37
 5.31 259  .41 163  710  0.0  05147.895558.72  38  -5  48 -13  43   5  47  17  38  24  28  24  27  22  20  27  -8  30   0   0  13  28
 4.57 254  .45 152  720  0.0  05147.885558.61  54 -24  51 -17  43  -1  47  15  41  21  28  26  27  20  26  24  35  -9   0   0   5  35
 5.14 266  .40 170  730  0.0  05147.885558.09  51 -25  43 -11  42  11  35  16  31   9   6  12   3  13   0   0   0   0   0   0   2  21
 3.94 271  .36 198  740  0.0  05147.855557.50  47 -28  41 -20  43   1  43   9  35  15  15  19  11  18  13   6  23  -6  18  -4   0  29
 4.77 261  .26 203  750  0.0  05147.745557.32  44 -32  39 -28  43  -8  52   2  38  22  24  27  20  22  22   4  21  -6  12  -1   0  31
 3.96 256  .26 223   8 0  0.0  05147.655556.89  43 -34  36 -36  41 -18  48  -1  38  21  31  26  24  22  26  19  35   9  35  -8   0  35
 3.87 240  .39 245  810  0.0  05147.605556.46  40 -38  33 -34  40 -12  44   6  36  26  23  32  19  24  17  20  34   4  30 -13   1  31
 3.31 226  .45 262  820  0.0  05147.465556.14  32 -33  31 -34  35 -12  44   3  38  20  27  27  15  23  13  18  21   2  22 -15   0  28
 3.51 195  .45 269  830  0.0  05147.385555.92  36 -36  32 -34  36 -13  46  -1  42  13  32  25  17  23  12  15  25 -12  13 -12  -3  29
 1.83 213  .55 279  840  0.0  05147.255555.64  35 -44  28 -43  36 -20  43  -6  32  15  24  24  11  22   6  18  19 -16   9 -10  -6  24
 3.57 247  .37 294  850  0.0  05147.105555.71  34 -43  30 -39  32 -20  41  -9  33   9  25  23  11  23   6  21   0 -15   4 -11  -6  21
 3.24 218  .36 307   9 0  0.0  05146.965555.62  31 -33  26 -36  31 -21  43 -11  36   3  27  21  11  25   6  23  15 -16   9  -8  -5  23
 4.04 217  .44 315  910  0.0  05146.835555.46  25 -38  21 -35  26 -23  35 -16  28   6  20  20   8  24   6  21  28 -17   3   0  -5  20
 4.03 233  .60 310  920  0.0  05146.695555.06  30 -42  27 -39  30 -23  40 -17  27   1  19  19  10  25  20   3  20 -13   0   4  -8  22
 5.06 218  .71 311  930  0.0  05146.555554.85  31 -36  30 -38  28 -22  34 -19  25   0  18  21   6  27  13  -4  10 -11   3   2  -8  20
 4.41 216  .35 277  940  0.0  05146.925555.04  22 -36  24 -36  27 -30  32 -20  27   0  19  17  11  24  -3  41 -30  63  -6  -9   1  12
 4.66 244  .34 169  950  0.0  05147.245555.60   8 -35  13 -36  22 -38  22 -23  25   1  23  18  11  22   6  23   3  -4   4  -5  -7  13
 4.64 249  .32 177 10 0  0.0  05147.165555.44  21 -36  16 -36  26 -36  23 -21  23   1  19  17  13  22   5  24  23   2  13  -6  -7  18
 4.16 251  .36 197 1010  0.0  05147.135555.12  13 -41  11 -36  20 -34  21 -24  24  -2  17  15  12  21   6  26  17  -6   6  -4  -8  14
 1.32 230  .34 198 1020  0.0  05147.025555.02   3 -41   1 -35  12 -33  16 -26  17  -6  17  11  13  18   8  21   9 -12   2  -4 -10   9
 1.58 206  .36 204 1030  0.0  05146.955554.89   6 -30   6 -34  12 -33  15 -27  16  -8  18  10  16  18  13  15  16  -8   2   0  -9  12
 2.15 236  .32 206 1040  0.0  05146.855554.80   6 -34   2 -30   9 -28  10 -25  15  -4  18  11  16  21   6   6  -1 -16   4  -2 -10   8
 1.61 198  .36 214 1050  0.0  05146.755554.71   8 -35   1 -32   6 -32   5 -23  12   0  20  10  15  19  22  12  12  -3  -6  -2  -8   9
 1.62 176  .50 224 11 0  0.0  05146.765554.40  11 -30   1 -28  11 -27  11 -25  12  -1  20  12  13  19  18  12  23  -2  -2   1  -7  11
 1.69 201  .69 232 1110  0.0  05146.775554.03   6 -25   0 -26   9 -23  11 -24  13  -5  20   8  12  17  13   6   9  -5  -1   0  -7   9
 2.58 237  .56 233 1120  0.0  05146.645554.08   4 -26  -2 -23   6 -18   8 -23   8  -6  19  10  16  15   4   3  -5 -19   3  -4  -9   6
 6.08 251  .63 229 1130  0.0  05146.665553.99   3 -26  -2 -25   6 -21   6 -22   9  -3  17   8  15  13  33  15  39   5  -2  -2  -5  12
 3.02 221 1.53 256 1140  0.0  05146.555552.33   8 -27   5 -22   9 -26   4 -16  11   3  12  10  15  13   0  -6  34 -30  39  -4 -10  13
 2.39 163 1.16 268 1150  0.0  05146.175552.79  12 -31   8 -21  13 -21   3 -13  11   5  17  10  18  13   6   6 -38 -40   5  -1  -9   5
 3.38 175  .67 288 12 0  0.0  05145.785553.64   9 -33  11 -22   9 -19  -2 -21   9  -5  16   8  16  13 -46 -32 -22 -19  26   2 -12   2
 3.83 219  .26 350 1210  0.0  05145.625554.54  13 -26  18 -24   9 -24  -2 -17  15  -3  18   6  16  12 -16  21 -40  24   3  -6  -3   3
 2.25 261  .12 143 1220  0.0  05146.045554.75  22 -23  18 -24   8 -22   1 -17  18  -3  24   4  19   8  13  23  24  55   3  11   1  15
 3.14 201  .15 345 1230  0.0  05145.675554.51  26 -30  21 -24  11 -23   2 -15  23  -6  21   5  19   9  -6  12 -41   3   9  -6  -7   8
 4.19 249  .17  54 1240  0.0  05145.625554.88  26 -26  20 -22   5 -19   2 -11  23  -5  20   3  20   8  21   6   4 -10   3  -1  -7  14
 5.10 252  .26  43 1250  0.0  05145.535554.77  26 -23  24 -18  13 -16   4  -4  17   0  19   2  19   8  20   1  10 -10   1  -1  -6  15
 5.58 227  .27  43 13 0  0.0  05145.465554.68  30 -25  25 -18  10 -15   6  -2  20   3  19   1  19   6  19   2   8  -4   2   1  -5  15
 3.62 253  .29  43 1310  0.0  05145.425554.56  31 -18  27 -15  17 -13   6   0  21  10  21   4  19   4  18   1   6  -5   5  -1  -3  17
 3.51 210  .34  41 1320  0.0  05145.365554.52  32 -16  25 -16  13 -13   6   2  22   9  20   4  21   9  20  -1   6  -6   2   3  -2  17
 4.39 180  .40  35 1330  0.0  05145.285554.38  31 -19  28 -10  16  -8   6   9  22  12  23   1  13   2  -6 -15   9   1  19   6  -2  16
 4.30 210  .74  51 1340  0.0  05145.145554.82  25  -6  30  -4  15  -1  11  11  19   9  22   4  26   9  10  -4   3   0   2   4   2  16
 7.01 192  .74  22 1350  0.0  05144.935554.29  33  -9  34  -6  19  -1  13  11  24   8  24   4  28  21  13  14   0  -6  -5 -11   5 -33
 5.04 204  .21 350 14 0  0.0  05145.405553.54  41 -11  39  -9  23  -2  15  10  28   8  27   5  31  34  16  32  -3 -12 -12 -27   2  20
 4.31 215  .05 325 1410  0.0  05145.565553.43  44 -10  39  -4  24  -2  19   9  30   6  28   5  32  12  21   2   6   1   2   1   2  24
 5.54 231  .05 314 1420  0.0  05145.555553.21  34   4  38   4  25   4  15  17  28  10  27   9  28  17  16   5   5   4   2   2   7  22
 3.74 197  .25 275 1430  0.0  05145.565552.79  51  -5  54   5  33   6  22  16  36  13  35   6  47  20  21   1   6  -1  10   4   6  31
```

3.91	201	.05	271	1440	0.0	05145.625552.84	49	-6	43	1	25	8	17	20	33	15	34	10	13	5	3	-1	9	2	9	-1	5	23
3.60	193	.19	300	1450	0.0	05145.585552.63	48	-2	51	2	31	5	26	22	40	11	36	11	41	19	13	5	4	-6	10	-3	6	30
4.67	237	.19	193	15 0	0.0	05145.895552.67	43	-2	52	0	28	11	24	23	36	12	35	8	18	40	-17	10	9	-24	22	-31	4	25
5.49	248	.05	210	1510	0.0	05145.765552.41	54	-8	59	0	38	12	30	24	38	12	38	10	40	3	13	-1	0	4	1	6	6	31
3.92	233	.22	266	1520	0.0	05145.745552.07	61	1	64	3	35	13	36	23	42	12	43	13	49	13	10	3	-6	2	3	15	9	33
9.44	234	.17	135	1530	0.0	05145.885552.32	54	-6	61	1	41	12	34	25	40	13	39	12	9	18	-2	-10	21	-9	28	-3	5	32
10.44	235	.09	64	1540	0.0	05145.775551.90	64	0	57	-1	44	13	38	24	41	13	42	11	59	4	10	4	-13	2	-1	13	8	34
8.57	237	.31	33	1550	0.0	05145.545551.86	60	-5	55	-6	44	15	39	24	39	11	36	10	15	-23	11	-2	10	6	16	-5	2	32
7.81	240	.31	17	16 0	0.0	05145.535551.50	67	1	61	5	48	20	39	27	42	13	42	18	44	11	6	4	-11	5	-12	8	11	32
8.42	243	.27	346	1610	0.0	05145.595550.95	69	3	66	3	44	18	36	30	44	13	57	15	23	5	-15	2	-13	12	-24	10	11	28
8.22	236	.35	313	1620	0.0	05145.685550.32	64	-5	64	1	40	21	42	24	39	6	39	11	44	9	-4	3	-17	3	-20	13	8	29
7.23	220	.50	301	1630	0.0	05145.735549.74	70	-10	72	1	47	22	43	20	36	6	32	13	50	5	3	-2	-22	2	-13	13	7	31
7.08	228	.62	295	1640	0.0	05145.725549.28	71	-9	71	-2	55	19	50	19	41	9	57	5	25	1	-8	2	-8	13	-21	1	5	33
8.88	237	.76	293	1650	0.0	05145.765548.79	80	-13	73	-1	59	24	48	13	32	13	47	10	22	3	-11	5	-13	11	-5	4	6	33
8.50	234	.95	290	17 0	0.0	05145.805548.16	73	-15	75	-8	60	19	49	13	36	10	47	4	-2	1	-13	8	-20	6	-4	-6	3	30
8.55	236	1.12	287	1710	0.0	05145.855547.64	85	-17	76	-4	62	19	41	11	32	12	54	9	17	3	-17	1	-15	9	-13	-6	3	32
8.28	225	1.34	286	1720	0.0	05145.875547.06	80	-22	71	-10	55	13	36	10	38	8	27	1	-12	3	-22	11	-21	4	21	-5	1	27
7.59	208	1.47	286	1730	0.0	05145.865546.53	76	-24	68	-12	53	15	39	13	44	5	9	0	-11	5	-16	12	-3	1	42	-2	1	30
7.18	217	1.61	285	1740	0.0	05145.885546.15	64	-15	61	-12	51	6	44	11	40	4	1	0	-13	0	-19	-3	18	0	35	3	0	28
6.63	224	1.71	285	1750	0.0	05145.915545.70	70	-20	66	-13	55	6	35	6	35	5	21	-1	-6	-1	-13	6	-4	-5	28	-5	-2	28
6.24	226	1.71	288	18 0	0.0	05145.835545.62	68	-23	69	-17	54	5	27	6	1	-9	6	-6	35	-2	44	-13	52	-11	-6	-21	-9	35
5.85	217	1.02	306	1810	0.0	05145.745546.67	64	-27	66	-16	55	4	34	11	-21	6	11	-2	40	-20	52	-27	49	-21	-40	-2	-9	31
6.26	204	.57	355	1820	0.0	05145.755547.68	59	-17	71	-11	60	3	28	15	20	22	-11	4	19	-6	30	-13	30	-20	28	-6	-3	33
4.73	219	.64	353	1830	0.0	05145.675547.43	59	-22	64	-16	57	-1	27	18	24	13	21	-3	2	0	1	-2	12	-2	26	-9	-2	29
7.76	224	.69	348	1840	0.0	05145.615547.09	50	-18	53	-16	50	-4	35	12	34	8	3	0	-9	0	-10	3	10	-1	28	-5	-2	24
8.32	222	.72	335	1850	0.0	05145.635546.70	51	-22	57	-19	51	-2	30	10	35	8	-1	-1	-16	2	-20	3	15	-3	36	3	-2	23
6.45	230	.77	332	19 0	0.0	05145.645546.31	50	-28	57	-23	50	-3	21	9	26	3	18	-6	-6	-2	-12	6	0	-3	30	-6	-5	23
4.90	238	.96	326	1910	0.0	05145.595545.93	44	-33	51	-23	47	-5	22	9	28	-5	5	-1	-6	6	-8	3	19	-8	32	-10	-6	23